Doctoral Dissertation

Study on development process of resist materials for extreme ultraviolet lithography using quartz crystal microbalance method

(極端紫外光リソグラフィに向けた
水晶振動子マイクロバランス法による
レジスト材料の現像プロセスに関する研究)

Yuko　Ito

October 2024

Graduate School of Engineering
Osaka University

Preface

The work of this thesis has been carried out under the guidance of Professor Takahiro Kozawa at Development of Beam Materials Science, SANKEN, Osaka University.

The objectives of this work are to understand the resist development process using the quartz crystal microbalance method and to gain insight into the reduction of LER and stochastic defects for the development of next-generation resists.

Yuko Ito

Contents

General introduction

Development of Lithography Technology and Resist Materials

With the development of information and communication technology (ICT), the environment for information communication and information processing using electronic devices continues to advance year by year. In the past, information sharing and communication using the information-technology (IT)-related equipment such as personal computers and servers were the mainstream. With the spread of smartphones since 2010, not only IT-related devices but also various other things have become connected to the Internet (IoT: Internet of Things), and everyone now collects, processes, and transmits massive information as a matter of course. In 2020, the introduction of telework and the promotion of ICT education led to the digitization of society as a whole in response to the outbreak of new coronavirus infections. In 2022, the release of ChatGPT (Chat Generative Pre-trained Transformer) by OpenAI led to an explosion of generative AI. As a result, the volume of data processing is expected to continue to increase, and further development of information and communication technology is desirable.

This development of information and communication technology has been supported by the development of semiconductor integrated circuits (ICs). IC integration has been progressing according to Moore's Law[1)], and today, large-scale integrated circuits with 10^{11} (100 billion) units of semiconductor elements in a single IC have been developed. Miniaturization of semiconductor devices plays an important role in achieving high integration of ICs, and lithography technology shown in **Fig. 1** is used as a microfabrication technique. Lithography is a technology that transfers a pattern by irradiating light through a mask with pattern information onto a photosensitive resin (photoresist) formed on a Si substrate. The role of the photon in lithography is to transfer pattern information and energy for inducing chemical reactions, while the role of the resist is to convert the light intensity modulation into a three-dimensional binary image for use in processing the substrate. To achieve miniaturization, the approaches from both the exposure source and resist material are necessary.

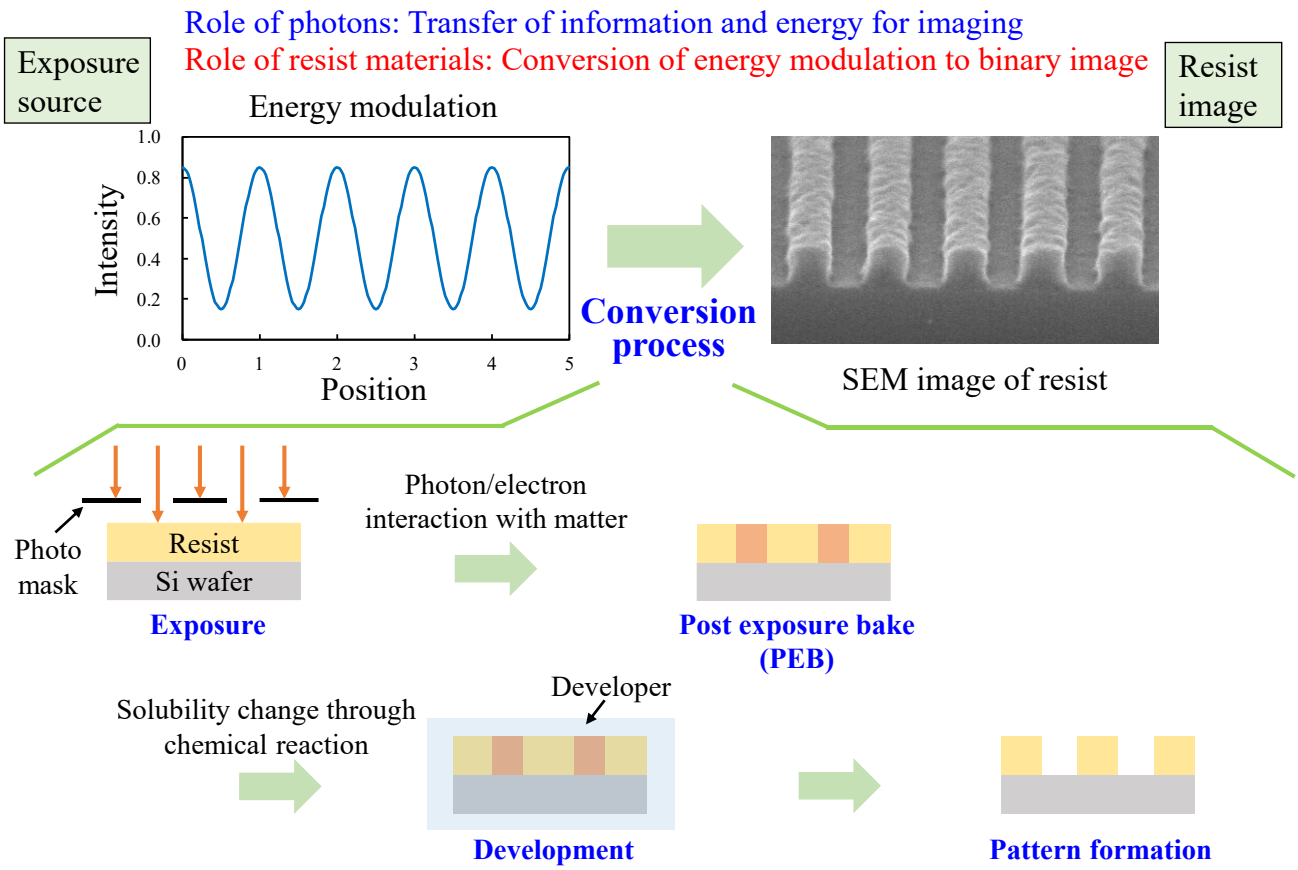

Fig. 1. Lithography process.

For exposure sources, the shortening of the wavelength of the light source and the enhancement of its performance [higher numerical aperture (NA)] have been promoted according to Rayleigh's formula shown in Eq. (1).

$$R = k_1 \frac{\lambda}{NA}, \tag{1}$$

where R is the resolution, k_1 is the process constant, λ is the wavelength, and NA is the numerical aperture. Exposure sources transitioned from mercury g-line to i-line, KrF, and ArF excimer lasers. Extreme ultraviolet (EUV) exposure tools with 0.33 NA have been applied to semiconductor manufacturing since 2019.[2] The installation of EUV exposure tools with 0.55 NA was reported at SPIE Advanced Lithography + Patterning in 2024.[3,4] The EUV exposure tool with 0.55 NA is called a high NA tool, the optical resolution of which reaches 8 nm half pitch.[5] The increase of NA has

already been planned for the further miniaturization of transistors. The next-generation exposure tool with >0.75 NA is called a hyper NA tool.[6] **Figure 2** summarizes trends in exposure sources, resist materials, and developers.

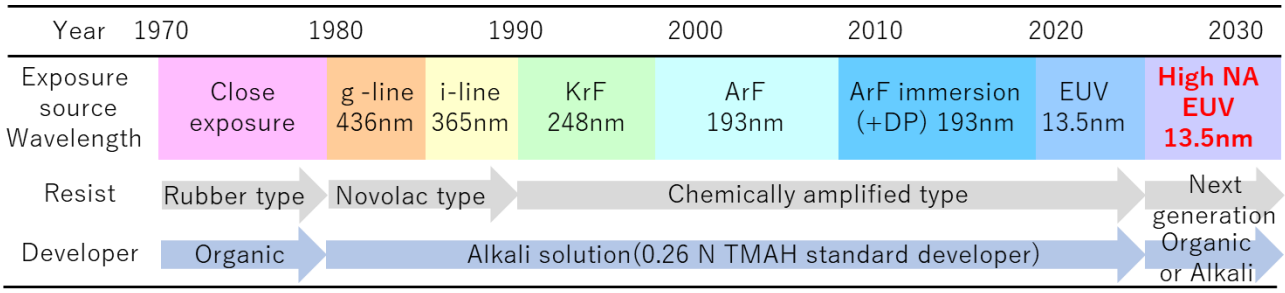

Fig. 2. Trends in lithography and resist materials.

On the other hand, resist materials are required to have high sensitivity because of productivity requirements in semiconductor manufacturing. Highly sensitive resists called chemically amplified resists (CARs)[7], which were developed during the transition period from i-line to KrF excimer lasers, are still used as mainstream resist materials. CARs generally consist of a polymer, a photoacid generator (PAG), and a quencher. When a CAR is irradiated with light, PAG decomposes to generate an acid. The energy from the photons is transferred to the resist as an acid image. At this point, the chemical change of the resist molecule that causes the difference in dissolution rate has not occurred. The acid catalyzed reaction proceeds by heating after exposure, causing a chemical change in the polymer and making it soluble. Among CARs, polarity change resist is mainly used in semiconductor high-volume production lines. The polar groups of the polymer are protected with non-polar groups in advance to make them insoluble in the alkaline aqueous developer solution, and then the polymer is made soluble by an acid-catalyzed deprotection reaction that returns non-polar groups to polar groups (**Fig. 3**).

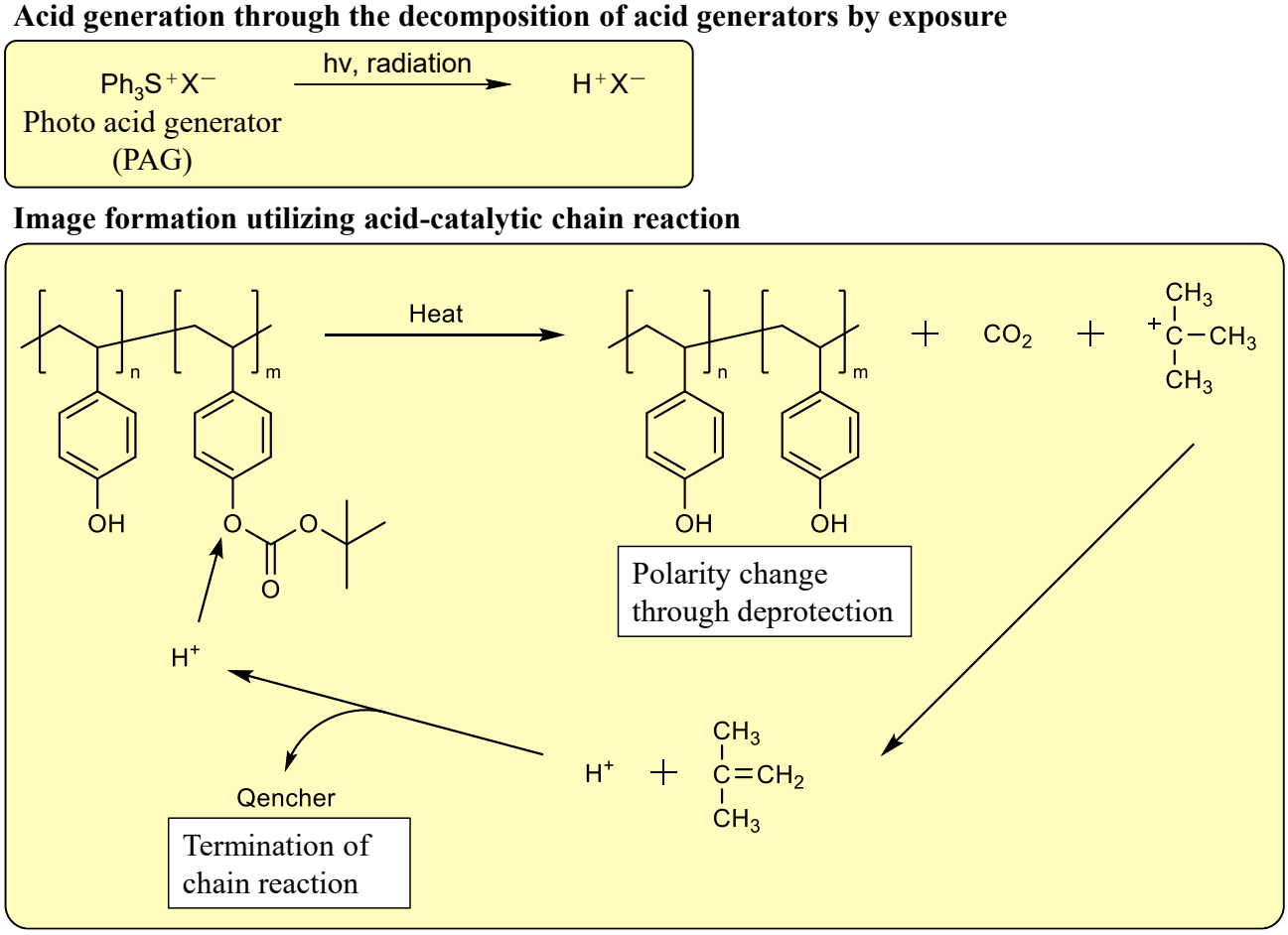

Fig. 3. Reaction mechanism of CAR.

In EUV lithography, the light source wavelength was shortened from 193 nm to 13.5 nm, and the reaction chemistry has entered the ionizing radiation chemistry. Therefore, the mechanism of acid generation in EUV resists is reported to be different from that of conventional KrF and ArF resists (**Fig. 4**).[8] Upon EUV absorption, photoelectrons are generated. The photoelectrons ionize the resist components (mainly polymers). The photoelectrons lose their kinetic energy through repeated ionization and excitation. When the photoelectrons and secondary electrons lose energy to a level at which they cannot ionize or excite molecules, they become thermalized electrons. Thermalized electrons react with the acid generator to produce negative ions. The negative ions work as a counter anion of acids. The protons are generated through the oxidation of polymer molecules.

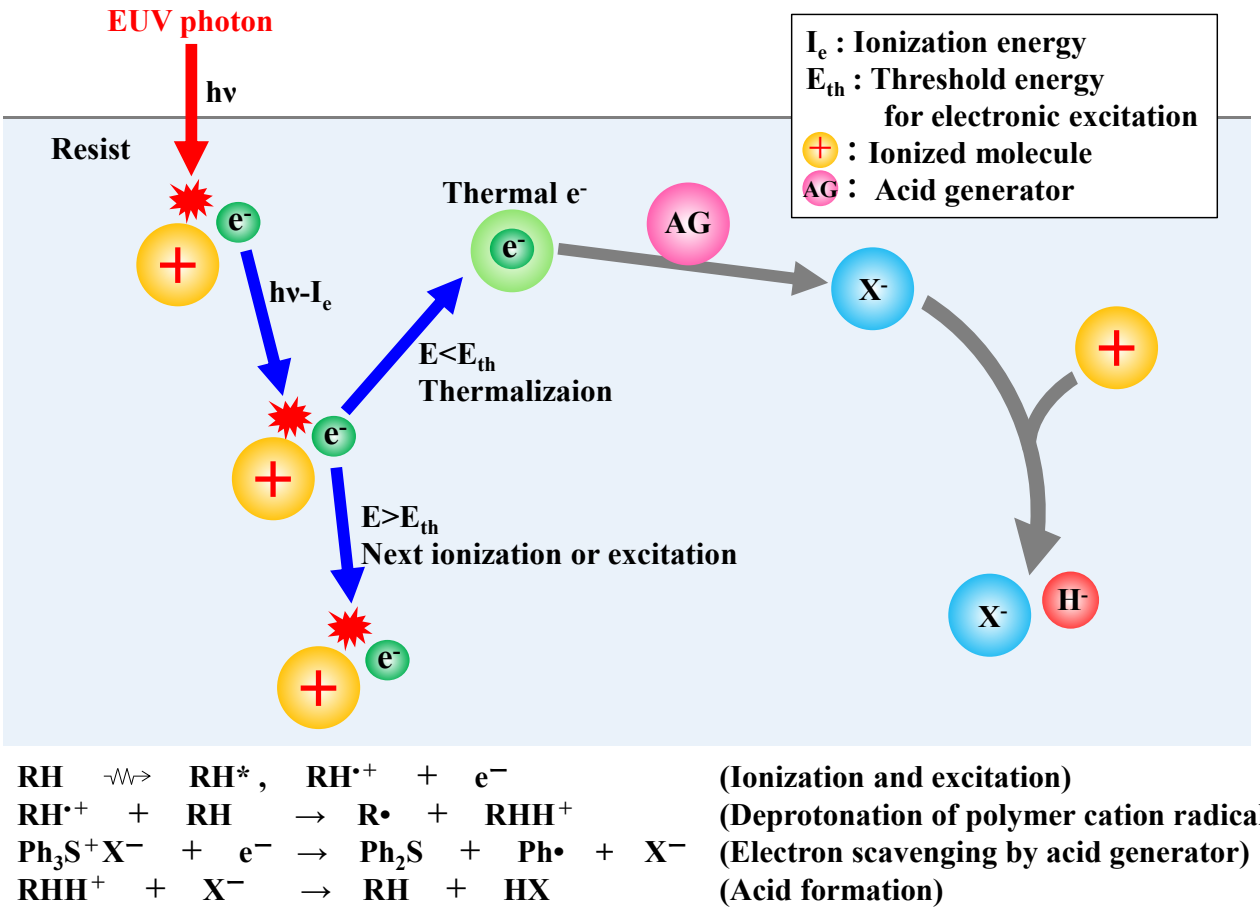

Fig. 4. Reaction mechanism of EUV resist.

CARs are also used in current EUV lithography. The standard developing solution [2.38 wt% (0.26 N) Tetramethylammonium hydroxide (TMAH) aqueous solution], which has been used since the exposure source was g-line, is still used. However, in the next generation of high NA EUV tools, the CAR development process using standard developer solutions approaches its limits from the viewpoint of optimizing resist performance. Therefore, there is a need to develop alternative developer solutions and new resist materials. As candidates for next-generation resists, not only CARs but also metal oxide resists (MORs)[9-11] and main chain scission resists[12,13] are being considered. In addition, the performance improvement is expected for CARs if the restriction imposed by the standard developer solution is removed. The next generation process is expected to be a battle between chemically amplified, metal, and main chain scission resists in alternative developer solutions. Therefore,

elucidating the development process is the most important issue in resist material development (**Fig. 5**).

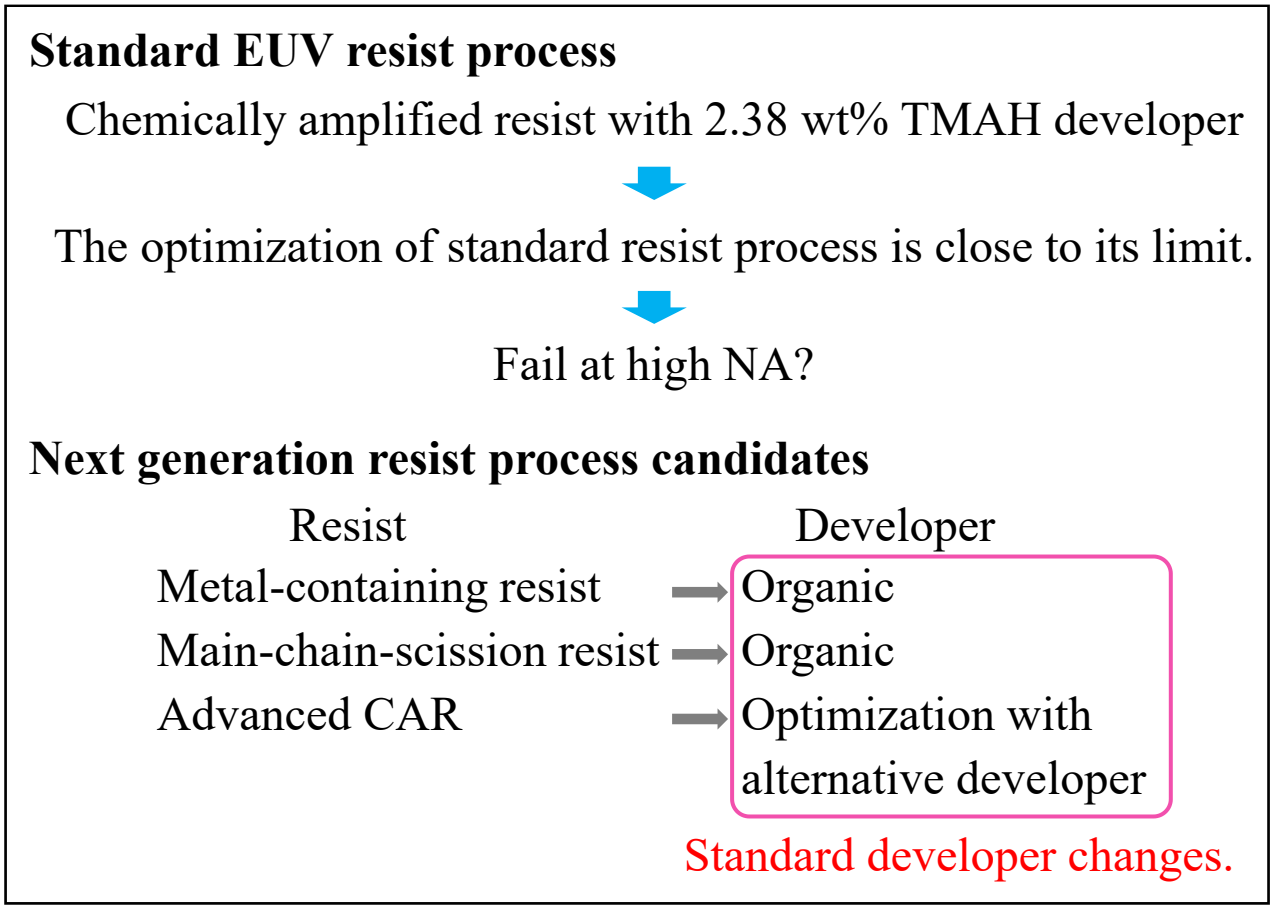

Fig. 5. Plans for Next Generation EUV Resist Processes.

LER and stochastic defects

The main performance requirements of resists are sensitivity, resolution, and line edge roughness (LER), which are trade-offs.[14] Solving the trade-off problem is the biggest challenge in resist development. In EUV lithography, the number of photons per unit irradiation dose decreased owing the high photon energy. The number of photons available for pattern formation decreased with the pattern size. As a result, stochastic defects such as LER, pinching, and bridging, as well as fluctuations in resist patterns after development, have become serious problems.[15-18] Nearly 30 years of research has already been conducted on the occurrence of LER, and almost all materials and process factors

have been reported to affect LER.[8)]

To solve these problems, our laboratory has studied the generation mechanism of LER and stochastic defects. Transient absorption spectroscopy using ultrashort pulsed electron beams from an electron linear accelerator was used to clarigy the reaction mechanism of CARs. Simulations based on the reaction mechanism were used to analyze resist images processed by an EUV lithography machine.

Figure 6 shows the mechanism of LER generation.[19,20)] The lower left graph shows the latent image (distribution of protected units) of a 22 nm pitch line-and-space pattern. The solid blue line in the graph represents the average number of protecting groups *R* on a resist polymer molecule. In CARs, latent images are formed by chemical reactions (acid-catalyzed chain reactions). Because chemical reactions, including interactions of photons and secondary electrons with molecules, are stochastic processes, the distribution of protecting groups fluctuates from place to place. The standard deviation σ of the number of protecting groups per polymer molecule is indicated by the red dotted line in the graph. In other words, the latent image shown in the **Fig. 6** is the average value in the line direction; in reality, the value fluctuates from place to place with the standard deviation indicated by the red dotted line. When the number of protective groups fluctuates, the point where the latent image intersects with the dissolution threshold in the line direction fluctuates, and the roughness appears in the resist pattern. For a typical CAR, the distribution gradient dN/dx (chemical gradient) of the protecting group after the acid-catalyzed reaction can be used to express LER by the following equation.

$$LER \approx \frac{a\sigma}{dN/dx} \tag{2}$$

Here, a is a factor related to the development and rinse process (development factor), which was estimated to be 0.68 in the example shown in **Fig. 6**. In other words, the fluctuations of $\pm 0.34\sigma$ appear as LER after development and rinsing. The LER is represented by 3σ at the line-and-space boundaries. The reason that 3σ of the protective group fluctuation directly correspond to LER is due to the nonlinear effects of the dissolution process. On the right-hand side of Eq. (2), theoretical predictions

are possible for σ and *dN*/*dx,* and the limit values of σ and *dN*/*dx* can be estimated. For the development factor, there are many unknowns, and the limit values are not yet known.

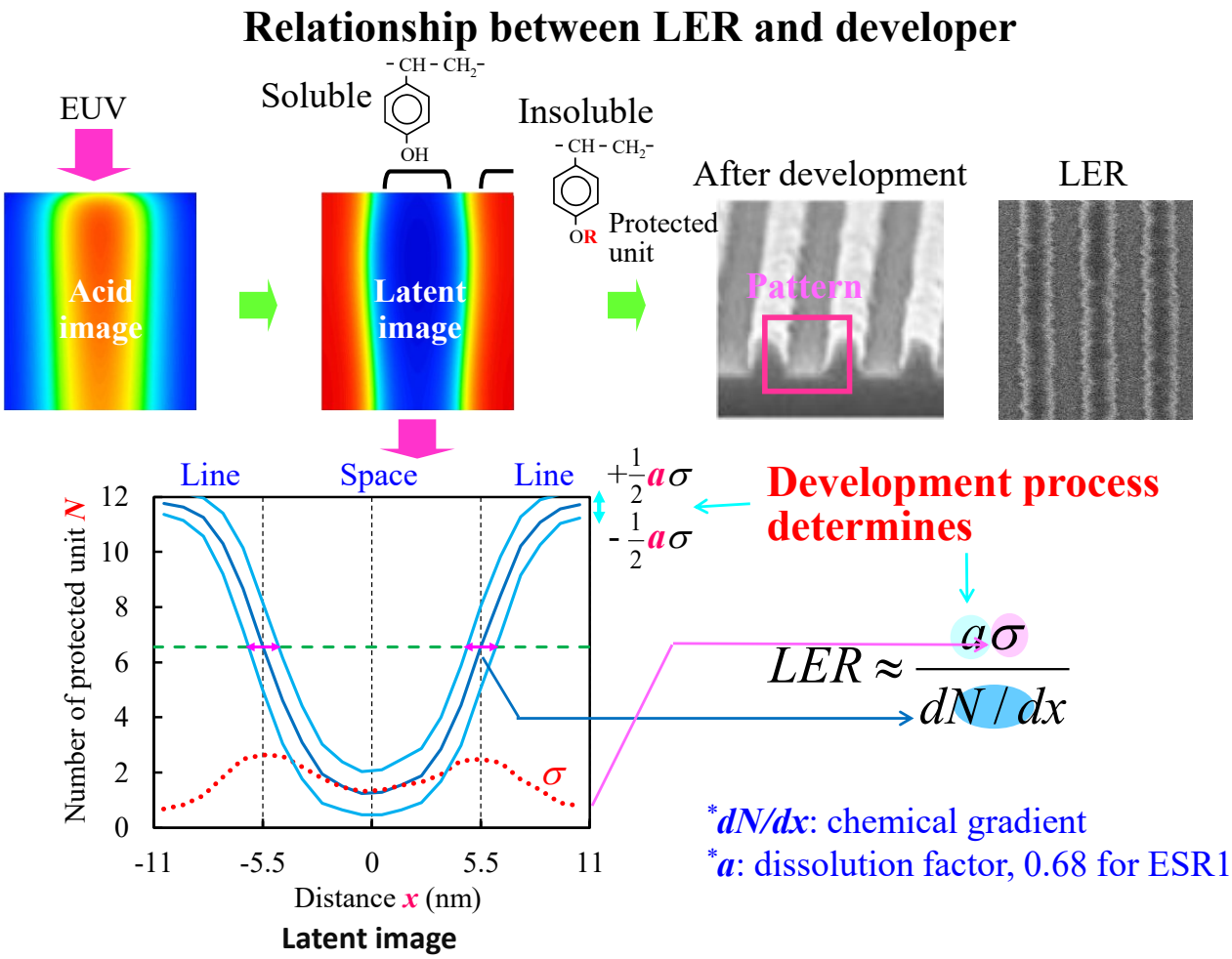

Fig. 6. Generation mechanism of LER.

Figure 7 shows the mechanism of stochastic defect generation.[21] The center graph shows the latent image (distribution of protected units) of a line-and-pattern with a pitch of 22 nm. The solid blue line in the center graph represents the average number of protective groups *R* (**Fig. 6**) on a resist polymer molecule. The number of protecting groups in the line and space areas also fluctuates with standard deviation σ because the chemical reaction is a stochastic process. If the distribution of protecting groups follows a normal distribution, the fraction of molecules below the dissolution

threshold in the line portion can be calculated by $|N_{\mathrm{L}} - N_{\mathrm{DT}}|/\sigma_{\mathrm{L}}$. On the other hand, the fraction of molecules in the space portion that exceed the dissolution threshold can be calculated by $|N_{\mathrm{DT}} - N_{\mathrm{S}}|/\sigma_{\mathrm{S}}$. Since dissolution is a collective phenomenon, the solubility of a single molecule does not determine whether it will dissolve or not. Therefore, the probability of defect formation is considered to be a complex function of $|N - N_{\mathrm{DT}}|/\sigma$. The development process determines this functional form.

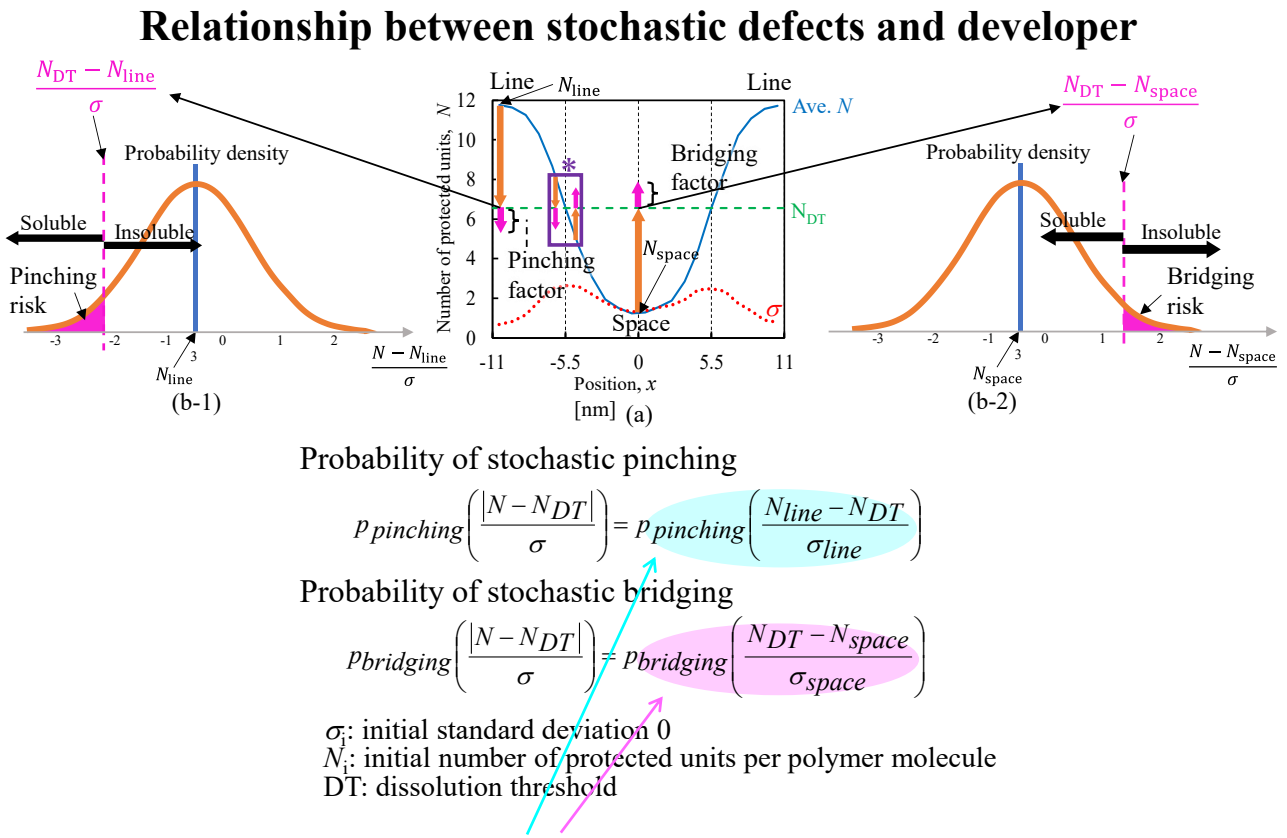

Fig. 7. Generation mechanism of stochastic defects.

From the above, elucidating the development process is the most important factor in reducing LER and suppressing stochastic defects.

Dissolution behavior of resist

Dissolution of resist films is classified into exfoliation type and dissolution type. The dissolution type is used in semiconductor manufacturing processes. When the resist thin film is immersed in alkaline developing solution, a transient swelling layer is formed due to water absorption. Subsequently, ionization (dissociation) of acidic polymers by alkali and hydration of the ionized polymers occur, and the hydrated polymers are transported to the bulk layer of the developer solution, resulting in progressive dissolution of the thin film (**Fig. 8**). When swelling and dissolution are balanced, the thickness of the transient swelling layer is constant and dissolution proceeds at a constant rate until the bottom of the transient swelling layer reaches the substrate interface.[22)] Such dissolution type is called Case II diffusion.[23-26)] Although a transient swelling layer thickness of zero is desirable for resolution improvement, roughness reduction, and defect reduction, the actual system differs greatly from this ideal condition. In a study that investigated the molecular structure dependence of resist polymers using 2.38 wt% TMAH developer solution, it was reported that the dissolution time becomes shorter and the transient swelling layer becomes smaller as the acidity of the polymer increases.[26)] It has also been reported that the dissolution behavior depends on the molecular weight and molecular weight dispersion of the resist polymer.[27,28)] However, there are many unknowns regarding the developer dependence.

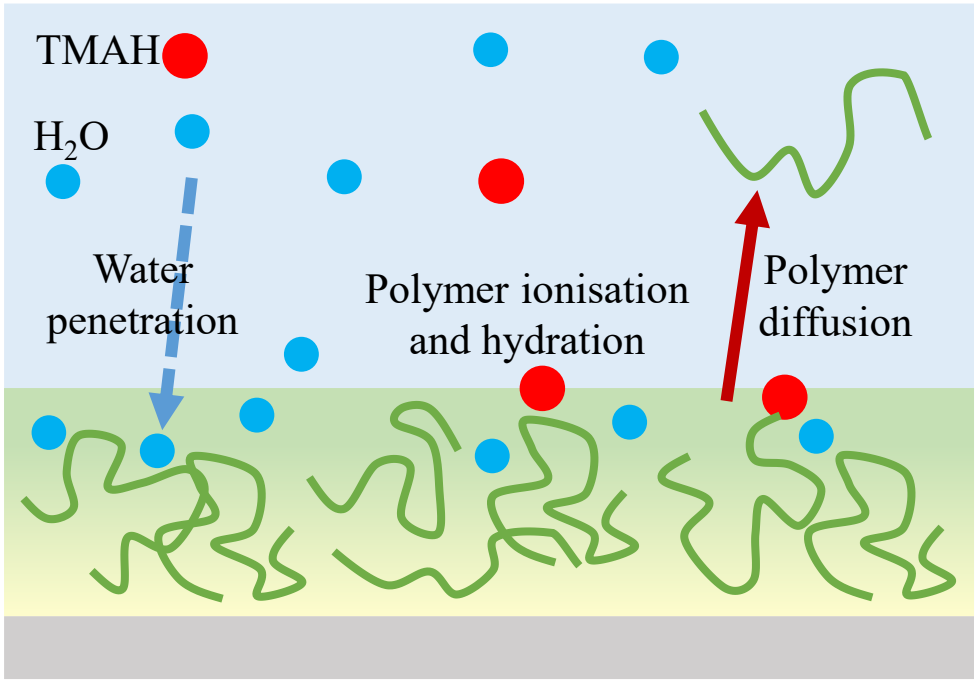

Fig. 8. Development process.

Purpose of this study

The next-generation lithography process is about to reach a turning point for the standard developer solutions that have been used for many years. In addition, the suppression of LER and stochastic defects is essential to improve resist performance, and the development process is involved in the generation of these defects. Understanding the development process is particularly important for the development of next-generation resist materials. Therefore, in this paper, the author has investigated the development process using the quartz crystal microbalance (QCM) method with the aim of reducing LER and suppressing stochastic defects for the development of next-generation resist materials.

In Chapter 1, the author worked on a detailed elucidation of the development process in TMAH aqueous solution, the standard developer solution. The relationship between the viscosity of the TMAH aqueous solution and the PHS concentration in the developer solution and the dissolution behavior of PHS resists containing an acid generator are described.

In Chapter 2, the author focused on dissolution based on the polar interaction between resist polymers and developer solutions, and examined dissolution behavior in alkaline developer solutions, which is different from TMAH. In Section 2-1, the dissolution behavior in tetrabutylammonium hydroxide (TBAH), which has longer alkyl chains than TMAH was described. In Section 2-2, the author discussed the dissolution behavior in inorganic alkali KOH and NaOH aqueous developer solutions.

In Chapter 3, the author used organic developer solutions and focused on the dissolution based on nonpolar interactions between resist polymers and developer solutions. The dissolution behavior of PHS resist in alcohol and alkyl acetate developer solutions was described.

In Chapter 4, the dissolution behavior of metal resist, which is expected to be a new resist material, in alkyl acetate developer solution.

References

1) G. E. Moore, IEEE SSCS NEWSLETTER, **38**, 8 (1965).
2) T. Itani, P. A. Gargini, P. P. Naulleau, and K. G. Ronse, Proc. SPIE **11147**, 1114701 (2019).
3) A. B. Kelleher, Proc. SPIE **PC12953**, PC1295302 (2024).
4) J. G. Garcia-Santaclara, R. Peeters, R. Ballegoij, S. Lok, J. Schoot, P. Gräupner, P. Kuerz, J. Mallmann, G. Storms, and P. Vanoppen, Proc. SPIE **12953**, 129530P (2024).
5) J. Schoot, E. Setten, K. Troost, S. Lok, R. Peeters, J. Stoeldraijer, J. Benschop, J. Zimmermann, P. Graeupner, P. Kuerz, and W. Kaiser, Proc. SPIE **11323**, 1132307 (2020).
6) I. Lee, J.-H. Franke, V. Philipsen, K. Ronse, S. D. Gendt, and E. Hendrickx, Proc. SPIE **12494**, 1249405 (2023).
7) H. Ito and C. G. Willson, Polym. Eng. Sci. **23**, 1012 (1983).
8) T. Kozawa and S. Tagawa, Jpn. J. Appl. Phys. **49**, 030001 (2010).
9) J. T. Diulus, R. T. Frederick, D. C. Hutchison, I. Lyubinetsky, R. Addou, M. Nyman, and G. S. Herman, ACS Appl. Nano Mater. **3**, 2266 (2020).
10) S. T. Meyers et al., Proc. SPIE **11609**, 116090K (2021).
11) C. Luo, C. Xu, L. Lv, H. Li, X. Huang, and W. Liu, RSC Adv. **10**, 8385 (2020).
12) A. Shirotori, M. Hoshino, M. Fujimura, S. F. Yeh, H. S. Suh, D. D. Simone, G. Vandenberghe, and H. Sanuki, Proc. SPIE **12498**, 1249807 (2023).
13) K. Morita, Y. Tanaka, Y. Tanaka, and M. Asai, Proc. SPIE **12498**, 1249815 (2023).
14) G. M. Gallatin, Proc. SPIE **5754**, 38 (2005).
15) M. D. Smith, J. Biafore, and C. Fang, Proc. SPIE **8682**, 868203 (2013).
16) G. M. Gallatin, P. P. Naulleau, and R. L. Brainard, Proc. SPIE **8322**, 83221C (2012).
17) W. Gao, A. Philippou, U. Klostermann, J. Siebert, V. Philipsen, E. Hendrickx, T. Vandeweyer, and G. Lorusso, Proc. SPIE **8322**, 83221D (2012).
18) C. A. Mack, Proc. SPIE **8325**, 83251K (2012).
19) T. Kozawa, J. J. Santillan, and T. Itani, Appl. Phys. Express **6**, 026502 (2013).
20) T. Kozawa, Jpn. J. Appl. Phys. **61**, 106502 (2022).
21) K. Azumagawa and T. Kozawa, Jpn. J. Appl. Phys. **60**, SCCC02 (2021).
22) N. Maeda, A. Konda, K. Okamoto, T. Kozawa, and T. Tamura, Jpn. J. Appl. Phys. **59**, 086501 (2020).
23) C. Y. Hui and K. C. Wu, J. Appl. Phys. **61**, 5129 (1987).
24) N. L. Thomas and A. H. Windle, Polymer **23**, 529 (1982).
25) C. Y. Hui, K. C. Wu, R. C. Lasky, and E. J. Kramer, J. Appl. Phys. **61**, 5137 (1987).
26) A. Tsuneishi, S. Uchiyama, and T. Kozawa, Jpn. J. Appl. Phys. **57**, 046501 (2018).
27) A. Nakajima, K. Watanabe, K. Matsuoka, T. Kozawa, Y. Komuro, D. Kawana, and A. Yamazaki, Jpn. J. Appl. Phys. **59**, 036505 (2020).
28) N. Tanaka, K. Watanabe, K. Matsuoka, K. Azumagawa, T. Kozawa, T. Ikeda, Y. Komuro, and D.

Kawana, Jpn. J. Appl. Phys. **60**, 066503 (2021).

Chapter 1

Dissolution kinetics of PHS resists in TMAH aqueous solutions

1-1. Introduction

In current EUV lithography, polarity change-type resists are used among chemically amplified resists (CARs). Poly(4-hydroxystyrene) (PHS) is a typical backbone polymer for the EUV resists. PHS molecules are soluble in the 2.38 wt% TMAH developer. In the alkaline solution, the hydroxyl groups of PHS dissociate. The ionized PHS molecules are hydrated and transported to the bulk of the solution. The resist materials are prepared by protecting the hydroxyl groups with nonpolar groups. Sufficiently protected PHS molecules are insoluble in 2.38 wt% TMAH solution. Protected PHS molecules are deprotected by exposure and heat treatment in the presence of an acid generator, resulting in a change in solubility and the formation of a pattern. A phenolic hydroxyl group also plays an important role in the acid generation upon exposure to EUV.[1–3] Therefore, the phenol unit is essential to the chemically amplified EUV resists. It is important to understand the dissolution dynamics of phenol units.

The development processes of resist films have been investigated by visible and infrared reflectance spectroscopy[4], high-speed atomic force microscopy (AFM)[5-7], and a quartz crystal microbalance (QCM) method.[4, 8–13] However, more detailed studies are needed to obtain knowledge that will lead to the development of next-generation resists.

In this chapter, the dissolution behavior of PHS resists in 2.38wt% TMAH aqueous solutions were investigated using the QCM method. First, only PHS was measured to understand the basic dissolution behavior. The relationship between the viscosity of a 2.38 wt% TMAH solution containing PHS and the PHS concentration was determined. Further measurements were performed by adding triphenylsulfonium-nonaflate (TPS-nf) as an acid generator to PHS. The effects of acid generator addition and acid generator decomposition are discussed in terms of surface free energy.

1-2. Experimental and analysis methods

1-2-1. Materials

PHS (M_w = 11000) and propylene glycol monomethyl ether acetate (PGMEA) were purchased from

Sigma-Aldrich. TPS-nf was purchased from Midori Kagaku and used as an acid generator. A 2.38 wt% TMAH aqueous developer (Tokyo Ohka Kogyo NMD-3) and pure water were used in the QCM experiment. The molecular structures of PHS, TPS-nf, and TMAH are shown in **Fig. 1-1**. Probe solutions for contact angle measurement, namely, diiodomethane, hexadecane, and ethylene glycol, were purchased from Tokyo Chemical Industry, Sigma-Aldrich, and Wako, respectively.

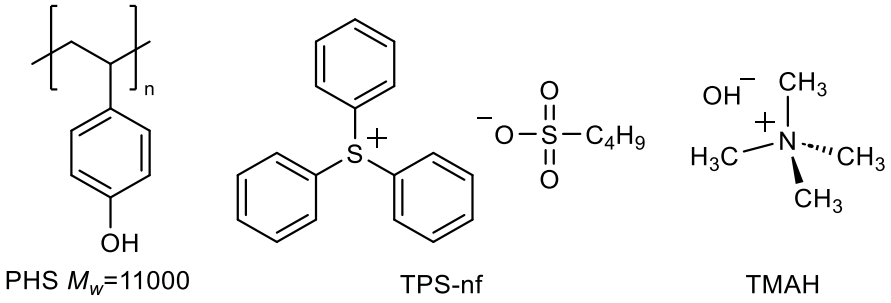

Fig. 1-1. The molecular structures of PHS, TPS-nf, and TMAH

1-2-2. QCM measurement

The PHS powders were dissolved in PGMEA and the concentration was adjusted to prepare films with thicknesses of approximately 30, 60, 110, and 310 nm. The PHS films spin-coated on QCM substrates were prebaked at 90 °C for 90 s. The dissolution kinetics of PHS films was measured using a QCM-based development analyzer (Litho Tech Japan RDAQz3). The films were developed in the 2.38 wt% TMAH aqueous developer (or distilled water) at 23 °C and then rinsed in water. The film thicknesses before and after development were measured using an ellipsometer (Meiwafosis FS-1).

The PHS films with TPS-nf also prepared. The PHS powder and TPS-nf were dissolved in PGMEA and their concentrations were adjusted to prepare films with a thickness of approximately 300 nm. The concentration of TPS-nf in the film after prebaking was 0.2 molecules nm^{-3} (estimated from the film density and the weight ratio). The PHS films with TPS-nf spin-coated on QCM substrates were prebaked at 90 °C for 90 s. The PHS films were exposed to 254 nm wavelength light (AS ONE Handy UV Lamp SLUV-6) in the exposure dose range of 0–100 mJ cm^{-2}. The exposure dose was

measured by a UV intensity meter (ORC UVM03A). The PHS films were baked at 90 °C for 60 s after their exposure to UV light to keep the same process condition as a typical resist process although the catalytic chain reaction was not induced in the samples used in this study. The absorption coefficient of the PHS films was 1.38 μm^{-1}. The reflectance of gold is 0.28 at the wavelength of 254 nm.[14] Thus, the absorbed UV light dose at the surface was 1.13 mJ cm^{-2} against the UV light exposure dose of 1 mJ cm^{-2}. The dissolution kinetics of PHS films was measured using a QCM-based development analyzer. The films were developed in the TMAH developer and water at 23 °C, and then rinsed in water. The film thickness before and after development was measured using an ellipsometer.

QCM measurement provides a weight change of resist on Au electrodes sandwiching the quartz crystal by detecting the resonance frequency of the quartz crystal. The decrease and increase in weight should correspond to the swelling and dissolution of the polymer, respectively. The change in frequency obtained by measurement can be converted to the change in weight in accordance with Sauerbrey's equation:[15]

$$\Delta f = -\frac{2{f_0}^2}{A\sqrt{\rho_q \mu_q}}\Delta m. \tag{1-1}$$

Here, Δf, f_0, Δm, A, ρ_q, and μ_q are the frequency change, the resonant frequency of the unloaded QCM substrate, the mass change of the material on the substrate, the piezoelectrically active crystal area, the density of quartz, and the shear modulus of the quartz used as the AT-cut crystal, respectively. In this equation, it is assumed that the material observed on the substrate is rigid. However, the transient swelling layer is not rigid, which we should take into consideration.

1-2-3. Impedance measurement

The PHS powders were dissolved in the 2.38wt% TMAH developer by applying ultrasonic agitation. The concentrations of PHS monomer units were adjusted within a 0–0.5M range. Hereafter, the concentration of PHS monomer units is simply called PHS concentration for convenience. The

solutions were left to stand for 1 d. If dissolution residue was observed, the solution was regarded as "saturated." The dissolution residue in saturated solution was removed using a polytetrafluoroethylene filter with a 0.45 μm pore size. The QCM substrate was set in the cup-shaped folder. The PHS solutions were dropped onto QCM substrate using a Pasteur pipette until the QCM output became constant. The impedance was measured at 23 °C using the QCM digital controller (Stanford Research Systems QCM200).

The water and ethylene glycol were mixed in arbitrary ratios. The impedance of the mixed solutions was measured, in a similar way to the case of the developer.

1-2-4. Surface free energy

The polymer powder and TPS-nf were dissolved in PGMEA and their concentrations were adjusted to prepare films with a thickness of approximately 300 nm. The films spin-coated on Si substrates were prebaked at 90 °C for 90 s. The concentration of TPS-nf in the film after prebaking was 0.2 molecules nm−3 PHS films without TPS-nf were also prepared. The PHS films were exposed to 254 nm wavelength light in the exposure dose range of 0–100 mJ cm^{-2}. The PHS films without TPS-nf were not exposed to 254 nm wavelength light. The reflectance of Si substrates is 0.68 at the wavelength of 250 nm.[16] Thus, the absorbed dose at the surface was 1.30 mJ cm^{-2} against the exposure dose of 1 mJ cm^{-2}. The contact angles were measured using a contactangle meter (Kyowa Interface Science DMe-211). Water, diiodomethane, hexadecane, and ethylene glycol were used as probe liquids. The volume of liquid droplets was 1 μl. The size of the liquid needle was 22 G. The static contact angles were measured during the period of 1–21 s at intervals of 1 s after droplet landing. The static contact angle was evaluated by a θ/2 method. The measurement was repeated 10 times and the obtained values were averaged.

Using the observed contact angles, we calculated surface free energies and their components. Surface free energy is often used to evaluate the wettability at the interface between solid and liquid.

The relationships among the contact angle of a liquid droplet on the solid surface θ, the surface tension of the solid γ_S, the surface tension of the liquid γ_L, and the interfacial tension between the solid and the liquid γ_{SL} are expressed as (Young's equation)

$$\gamma_S = \gamma_L \cdot \cos\theta + \gamma_{SL}. \quad (1\text{-}2)$$

When a liquid is in contact with a solid, the surface free energy can be expressed, using the work of adhesion W_{SL}, as (Dupré's equation)

$$\gamma_S + \gamma_L = W_{SL} + \gamma_{SL}. \quad (1\text{-}3)$$

Using Eqs. (1-2) and (1-3), we derive the Young–Dupré equation as

$$W_{SL} = \gamma_L(1 + \cos\theta). \quad (1\text{-}4)$$

Some theoretical formulas of surface free energy are known. The separation of surface energy into its components depends on the formulas. In this study, surface free energy was evaluated using the following theoretical equations to obtain the fundamental knowledge about the water intake of resist films.

1-2-4-1. Owens, Wendt, Rabel, and Kaelble (OWRK) method[17, 18)]

W_{SL} is expressed by dividing the surface free energy into the dispersion component γ^d and polar component γ^p.

$$\gamma = \gamma^d + \gamma^p, \quad (1\text{-}5)$$

$$W_{SL} = 2\sqrt{\gamma_S^d \cdot \gamma_L^d} + 2\sqrt{\gamma_S^p \cdot \gamma_L^p}. \quad (1\text{-}6)$$

The relationship between θ and the surface free energy is derived from Eqs. (1-4) and (1-6) as

$$\sqrt{\gamma_S^d \cdot \gamma_L^d} + \sqrt{\gamma_S^p \cdot \gamma_L^p} = \gamma_L(1 + \cos\theta)/2. \quad (1\text{-}7)$$

The components of surface free energy are evaluated using two distinct probe liquids. The surface tensions of probe liquids used in the OWRK method and their components are listed in **Table 1-1**.[17, 18)]

Table 1-1. Surface tensions of probe liquids used in OWRK method and their components.

	γ_L^d (mJ m^{-2})	γ_L^p (mJ m^{-2})	γ_L (mJ m^{-2})
Water	21.8	51.0	72.8
Diiodomethane	48.5	2.3	50.8
Hexadecane	27.6	0.0	27.6

1-2-4-2. Kitazaki–Hata method[19)]

W_{SL} is obtained by dividing the surface free energy into the dispersion component γ^d, polar component γ^p, and hydrogen bonding component γ^h.

$$\gamma = \gamma^d + \gamma^p + \gamma^h, \tag{1-8}$$

$$W_{SL} = 2\sqrt{\gamma_S^d \cdot \gamma_L^d} + 2\sqrt{\gamma_S^p \cdot \gamma_L^p} + 2\sqrt{\gamma_S^h \cdot \gamma_L^h}. \tag{1-9}$$

The relationship between θ and the surface free energy is derived from Eqs. (1-4) and (1-9) as

$$\sqrt{\gamma_S^d \cdot \gamma_L^d} + \sqrt{\gamma_S^p \cdot \gamma_L^p} + \sqrt{\gamma_S^h \cdot \gamma_L^h} = \gamma_L(1 + \cos\theta)/2. \tag{1-10}$$

The components of surface free energy are evaluated using three distinct probe liquids. The surface tensions of probe liquids used in the Kitazaki–Hata method and their components are listed in **Table 1-2**.[19)]

Table 1-2. Surface tensions of probe liquids used in Kitazaki–Hata method and their components.

	γ_L^d (mJ m^{-2})	γ_L^p (mJ m^{-2})	γ_L^p (mJ m^{-2})	γ_L (mJ m^{-2})
Water	29.1	1.3	42.4	72.8
Diiodomethane	46.8	4.0	0.0	50.8
Hexadecane	27.6	0.0	0.0	27.6

1-2-4-3. Acid-base method[20)]

Surface free energy is divided into the Lifshitz–van der Waals (LW) component γ^{LW} and acid–base component γ^{AB}, which is divided into the acid component γ^+ and base component γ^-.

$$\gamma = \gamma^{LW} + \gamma^{AB}, \tag{1-11}$$

$$\gamma^{AB} = 2\sqrt{\gamma^+ \cdot \gamma^-}. \quad (1\text{-}12)$$

The relationship between W_{SL} and the components of surface free energy is expressed as

$$W_{SL} = 2\sqrt{\gamma_S^{LW} \cdot \gamma_L^{LW}} + 2\sqrt{\gamma_S^+ \cdot \gamma_L^-} + 2\sqrt{\gamma_S^- \cdot \gamma_L^+}. \quad (1\text{-}13)$$

The relationship between θ and the surface free energy is derived from Eqs. (1-4) and (1-13) as

$$\sqrt{\gamma_S^{LW} \cdot \gamma_L^{LW}} + \sqrt{\gamma_S^+ \cdot \gamma_L^-} + \sqrt{\gamma_S^- \cdot \gamma_L^+} = \gamma_L(1 + \cos\theta)/2. \quad (1\text{-}14)$$

The components of surface free energy are evaluated using three distinct probe liquids. The surface tensions of probe liquids used in the acid–base method and their components are listed in **Table 1-3**.[20)]

Table 1-3. Surface tensions of probe liquids used in base method and their components.

	γ_L^{LW} (mJ m^{-2})	γ_L^+ (mJ m^{-2})	γ_L^- (mJ m^{-2})	γ_L^{AB} (mJ m^{-2})	γ_L (mJ m^{-2})
Water	21.8	25.5	25.5	51.0	72.8
Hexadecane e	27.5	0.0	0.0	0.0	27.5
Ethylene glycol	29.0	1.9	47.0	19.0	48.0

1-3. Results and discussion

1-3-1. The kinetics (temporal change) of viscosity and PHS concentration during development

Figure 1-2 shows the relationship between PHS concentration C_{PHS} and the impedance change of developer ΔZ. The baseline was set at the impedance of pure developer (287 Ω), namely, $\Delta Z = Z - 287$. The solutions plotted at 0.3 and 0.4M concentrations in **Fig. 1-2** were saturated with PHS. Therefore, the PHS concentrations of these solutions are neither 0.3 nor 0.4 M. The data of unsaturated solutions were fitted by a linear approximation. The best fitted equation was,

$$\Delta Z = 201 C_{PHS}. \quad (1\text{-}15)$$

All the impedance change data of the saturated solutions were averaged to be 55.8 Ω (the horizontal dashed line in **Fig. 1-2**). Using Eq. (1-15), the PHS concentration of the saturated solutions was calculated to be 0.28 M. This value is reasonable because the TMAH concentration was 0.26M

and the PHS is not dissolved in pure water.[11)]

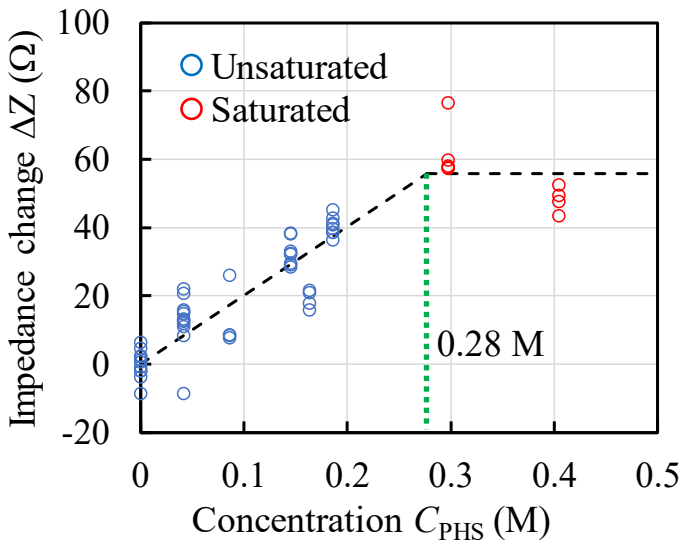

Fig. 1-2. Relationship between PHS concentration and impedance change. The impedance of developer was 287 Ω (a base line). The black dashed line is a fitting curve.

Using the mixture solution of water and ethylene glycol, the relationship between impedance of QCM circuit Z and viscosity η was investigated, as shown in **Fig. 1-3**. The viscosities of the mixture solutions were obtained by interpolating the reported data[21)] in terms of temperature and mixture ratio. The viscosities of pure water and ethylene glycol are 0.94 and 19.8 mPa s at 23 °C, respectively.[21)] The relationship was well fitted with a second-order polynomial (the dashed line in **Fig. 1-3**). The best fitted equation was,

$$\eta = 6.81 \times 10^{-6} Z^2 + 4.67 \times 10^{-3} Z - 0.987. \quad (1\text{-}16)$$

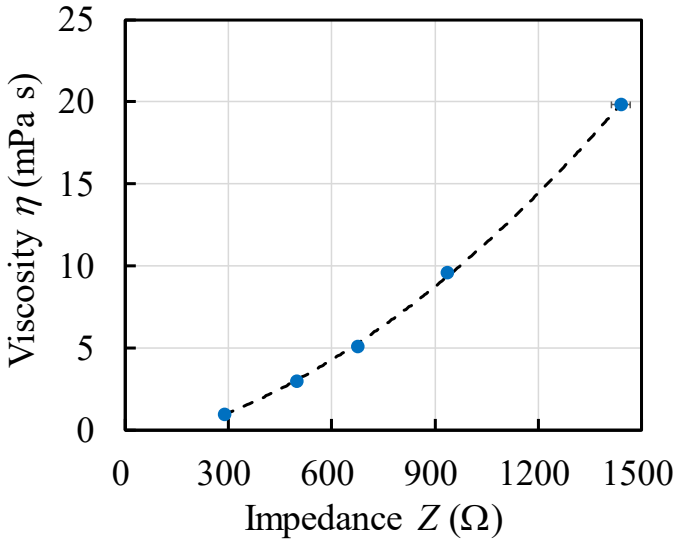

Fig. 1-3. Relationship between impedance and viscosity, obtained by using mixture solution of water and ethylene glycol. The dashed line is a fitting curve.

The dissolution kinetics of PHS films was measured using the QCM method. Using Eq. (1-15), the impedance chart was converted to the temporal change of PHS concentration during development, as shown in **Fig. 1-4(a)**. Similarly, the impedance chart was converted to the temporal change of viscosity using Eq. (1-16), as shown in **Fig. 1-4(b)**. Note that Z = ΔZ+287 (the impedance of pure developer). The QCM method provides not only an impedance chart, but also a frequency chart, simultaneously. The corresponding frequency chart is shown in **Fig. 1-4(c)**, which indicates the weight loss of PHS films during development.[15] The frequency change is inversely proportional to the mass change on the QCM substrate. The maximum concentrations during development were 0.10, 0.15, 0.23 and 0.30 M for PHS film thicknesses of 28, 59, 110 and 310 nm, respectively. For film thicknesses of 28, 59 and 110 nm, the PHS concentration did not exceed the TMAH concentration during development. The PHS concentration increased with the development time. The maximum PHS concentration also increased with the PHS film thickness. The early kinetics (the time profile before the development time of 0.12 s) of PHS concentration for the PHS film with 110 nm thickness agreed with that for the PHS film with 310 nm thickness within the PHS concentration range of 0–0.23 M, as shown in **Fig. 1-4(a)**. The early kinetics of PHS concentrations for the PHS films with thicknesses of

28 and 59 nm seems to agree with that for the PHS film with 310 nm thickness within the corresponding PHS concentration range, although they are close to the time resolution of QCM apparatus. These facts suggest that the diffusion of PHS molecules is slightly slower than the dissolution of PHS molecules (the supply of PHS molecules from solid layer to the developer). The viscosity increased approximately from 0.93 to 1.46 with development time, as shown in **Fig. 1-4(b)**. The diffusion constant of solutes in solution is generally inversely proportional to the viscosity. Therefore, the increase in viscosity indicates the decrease in diffusion speed of PHS molecules. The frequency data of PHS film with a thickness of 310 nm within 0.1 s after immersion were fitted with a linear approximation and the fitting curve was extrapolated to 0.5 s, as shown in **Fig. 1-4(c)**. The rising rate of frequency (the loss of film weight) for the PHS film with a thickness of 310 nm decreased with the development time due to the decrease in diffusion constant and the decrease in pH owing to the neutralization.

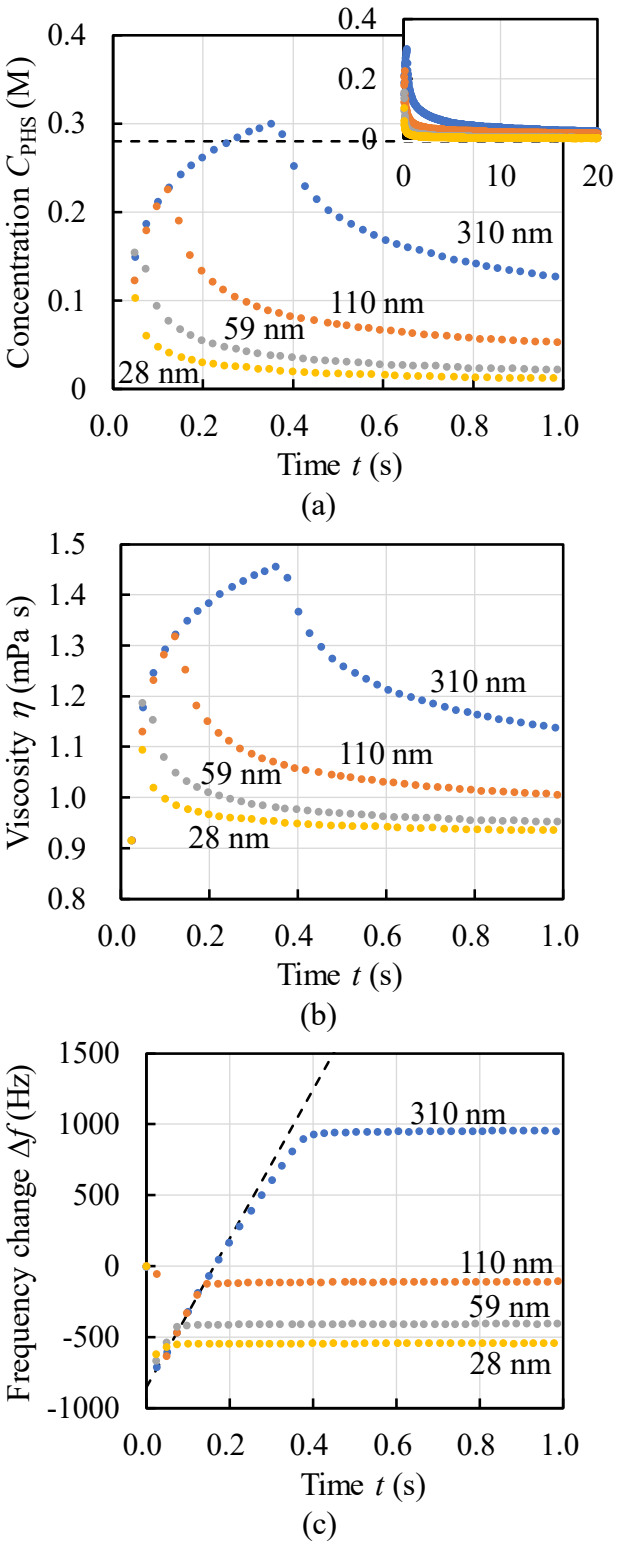

Fig. 1-4. Dissolution kinetics of PHS films in 2.38 wt% TMAH developer: (a) PHS concentration chart near dissolution front, (b) viscosity chart, and (c) frequency chart. The horizontal and vertical axes of inset in (b) are time in s and PHS concentration in M, respectively. The numerical values in nm in the graphs are the initial thicknesses of PHS films. The dashed line in (c) is a fitting curve.

1-3-2. The swelling kinetics of the PHS films with TPS-nf

The swelling kinetics of the PHS films with TPS-nf was measured in water using QCM after their exposure to UV light. The exposure doses were changed from 0 to 100 mJ cm^{-2} in steps of 10 mJ cm^{-2}. The development time was 180 s. The obtained QCM charts are shown in **Fig. 1-5**. Upon insertion of the QCM substrate into the developer, the frequency immediately dropped by approximately 660 Hz owing to the increase in the viscosity of its surroundings. The frequency immediately after the drop was set to 0 (base value) and the frequency change was plotted in the graph. The base values were evaluated by dropping the QCM substrates without PHS films into the developer. As indicated by Eq. (1-1), the decrease in the frequency indicates the increase in the film weight. For all the PHS films, the decrease in the frequency, namely, swelling, was observed. The swelling was caused by the penetration of water into the films. With the addition of TPS-nf, the water intake became slow, as shown in **Fig. 1-5**. It was reported that the film density increased upon the addition of acid generators such as TPS-nf.[22–24] The decrease in the free volume of polymer films was considered to contribute to the slowdown of water intake. Another cause for the slowdown of water intake is later discussed. With the increase in exposure dose, the water intake in the PHS films with TPS-nf became fast. For the films with exposure doses higher than 20 mJ cm^{-2}, the frequency increased after the initial decrease in the frequency.

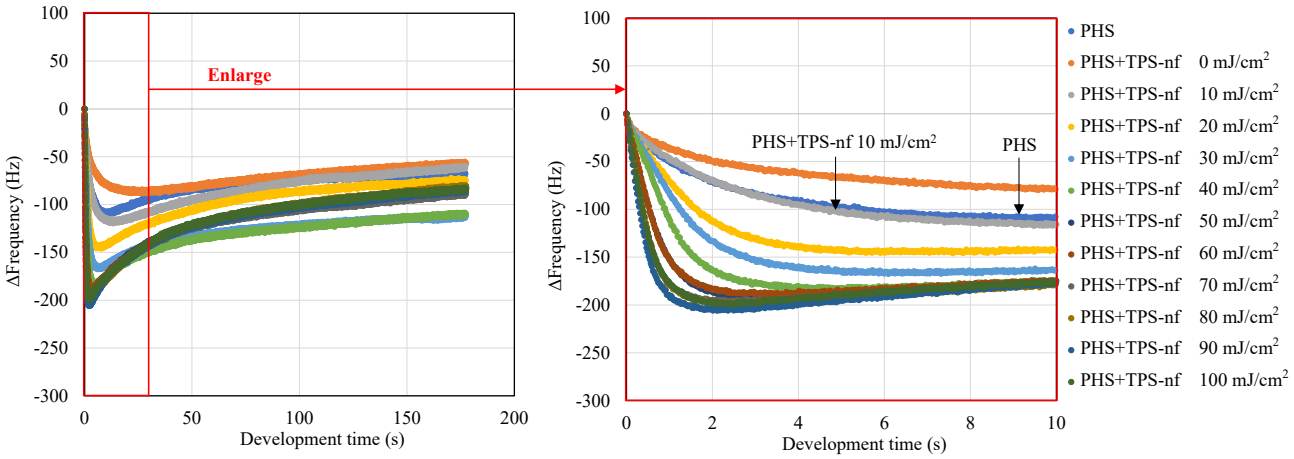

Fig. 1-5. QCM charts of PHS films of 300 nm thickness obtained in water. The exposure doses were changed from 0 to 100 mJ cm^{-2} in steps of 10 mJ cm^{-2}.

After the QCM experiment, the films were dried and the film thickness was measured, as shown in **Table 1-4**. No significant film loss was observed. Therefore, these decreases in the frequency indicate not the dissolution of PHS films but the relaxation of the polymer matrix, which means the softening of the films. The rate of decrease in frequency immediately after dropping QCM substrates into water was evaluated by fitting an exponential function to the QCM charts, as shown in **Fig. 1-6**.

$$\Delta f = \Delta f_{\mathrm{low}}[1 - \exp(-kt)], \tag{1-17}$$

where Δf_{low}, k, and t are the lowest frequency change, a rate constant, and time, respectively. The observed rate constants are plotted in **Fig. 1-7**. The observed rate constant increased with increasing exposure dose.

Table 1-4. Film thicknesses in nm after QCM measurement. The initial film thickness was 309.5 nm. The exposure doses were changed from 0 to 100 mJ cm^{-2}.

Dose (mJ cm^{-2})	0	10	20	30	40	50	60	70	80	90	100
Thickness (nm)	309.0	306.3	304.3	308.8	307.8	314.6	310.7	310.1	310.5	317.7	315.3

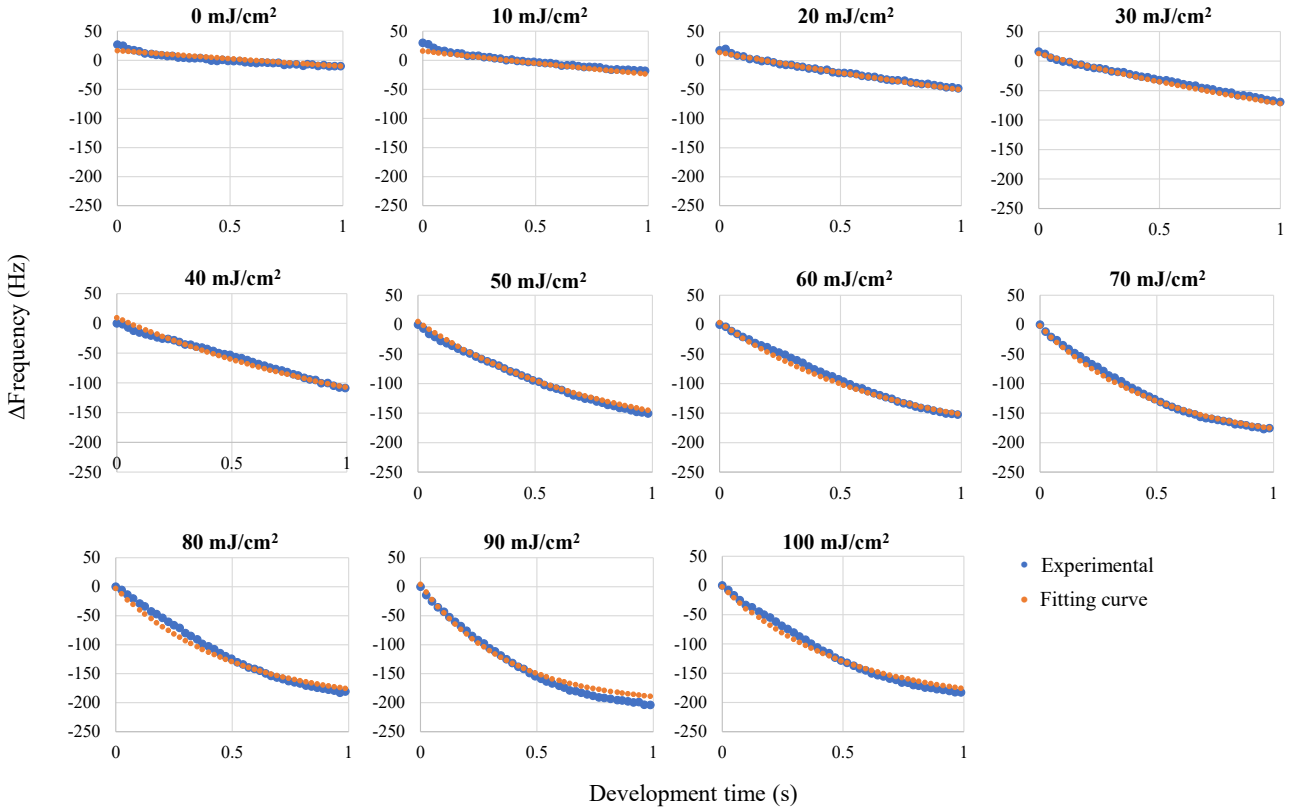

Fig. 1-6. Fitting of exponential function to QCM charts shown in **Fig. 1-5**.

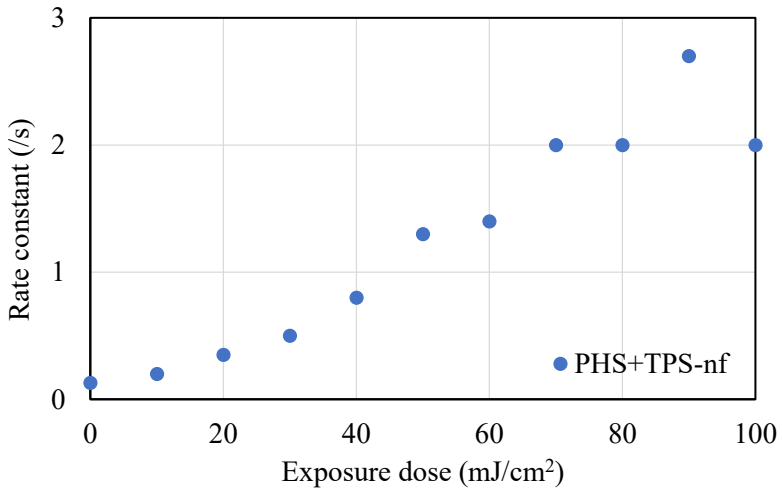

Fig. 1-7. The exposure dose dependence of observed rate constants estimated from QCM charts (**Fig. 1-5**).

The contact angles were measured to clarify the relationship between the surface free energy and the water intake. **Figure 1-8** shows the dependences of the contact angles of water, diiodomethane,

hexadecane, and ethylene glycol on the exposure dose of UV light. The contact angles were measured at 1, 6, 11, 16, and 21 s after the landing of probe liquid droplets on the PHS films. The contact angle of water decreased with increasing exposure dose. The contact angle of diiodomethane seems roughly constant independent of the exposure dose. The contact angle of hexadecane increased with increasing exposure dose. Although the contact angle of ethylene glycol was approximately constant independent of the exposure dose, it decreased with time after the landing of droplets.

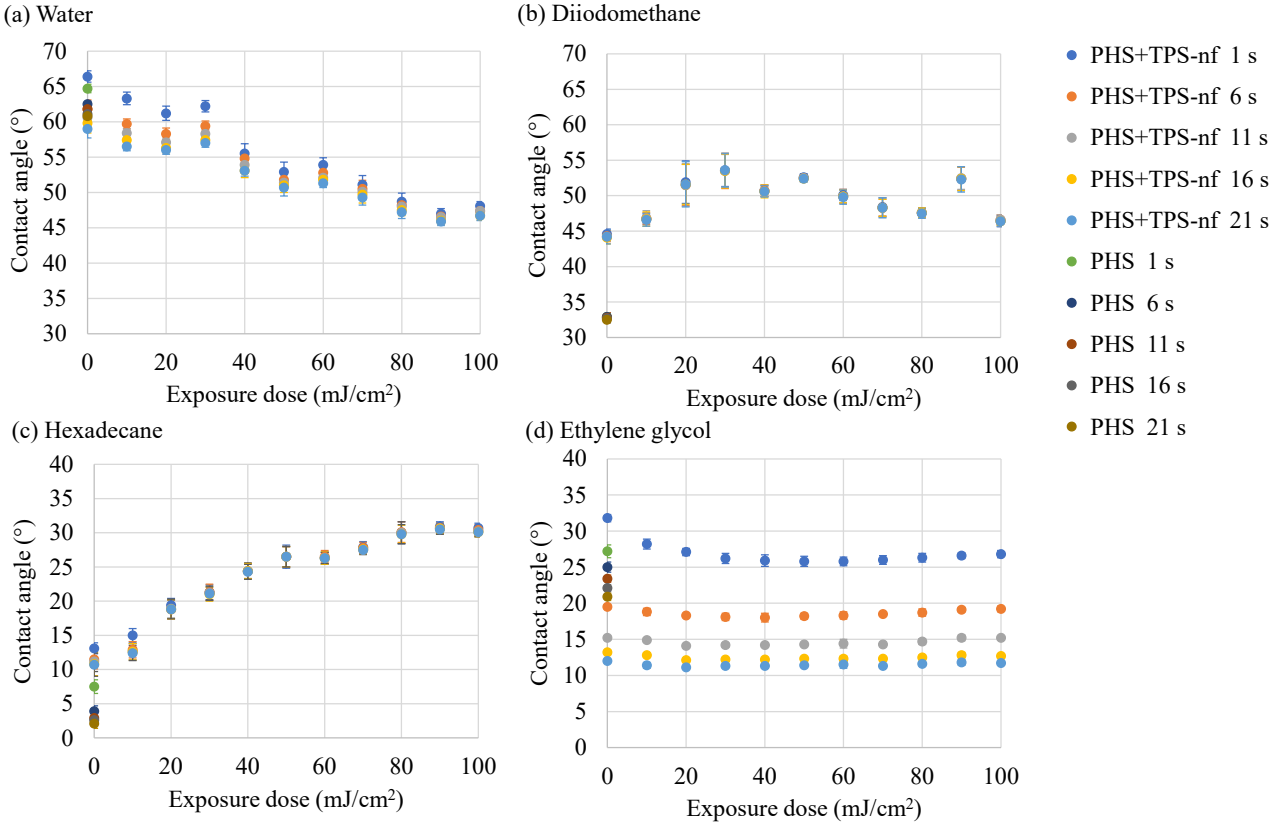

Fig. 1-8. Dependence of contact angles of (a) water, (b) diiodomethane, (c) hexadecane, and (d) ethylene glycol on exposure dose. The contact angles were measured at 1, 6, 11, 16, and 21 s after the landing of probe liquid droplets on PHS films.

The surface free energy was calculated by the OWRK method. **Figure 1-9(a)** shows the surface free energy calculated using water and diiodomethane as the probe liquids. With the increase in exposure dose, the surface free energy increased. A similar trend to that of the exposure dose dependence of water intake rate constants (**Fig. 1-7**) was observed. The dispersion component of

surface free energy is shown in **Fig. 1-9(b)**. The dispersion force is a temporary attractive force induced when the electrons in two adjacent atoms that make the atoms form temporary dipoles. Upon the addition of TPS-nf to polymer films, the dispersion component decreased. Upon exposure to UV light, TPS-nf molecules were decomposed.[25)]

$$(Ph_3S^+X^-)^* \rightarrow \text{Ph-}Ph_2S + H^+X^-, \qquad (1\text{-}18)$$

Here, $Ph_3S^+X^-$, Ph-Ph_2S, and H^+X^- are TPS-nf, benzenesubstituted diphenyl sulfide, and nonafluoro-1-butanesulfonic acid, respectively. The dispersion component slightly decreased with increasing exposure dose, namely, with the decomposition of TPS-nf. The polar component of surface free energy is shown in **Fig. 1-9(c)**. The polar component increased with increasing exposure dose, similarly to the surface free energy. The generation of acids is considered to have increased the polar component. Consequently, the surface free energy increased, as shown in **Fig. 1-9(a)**.

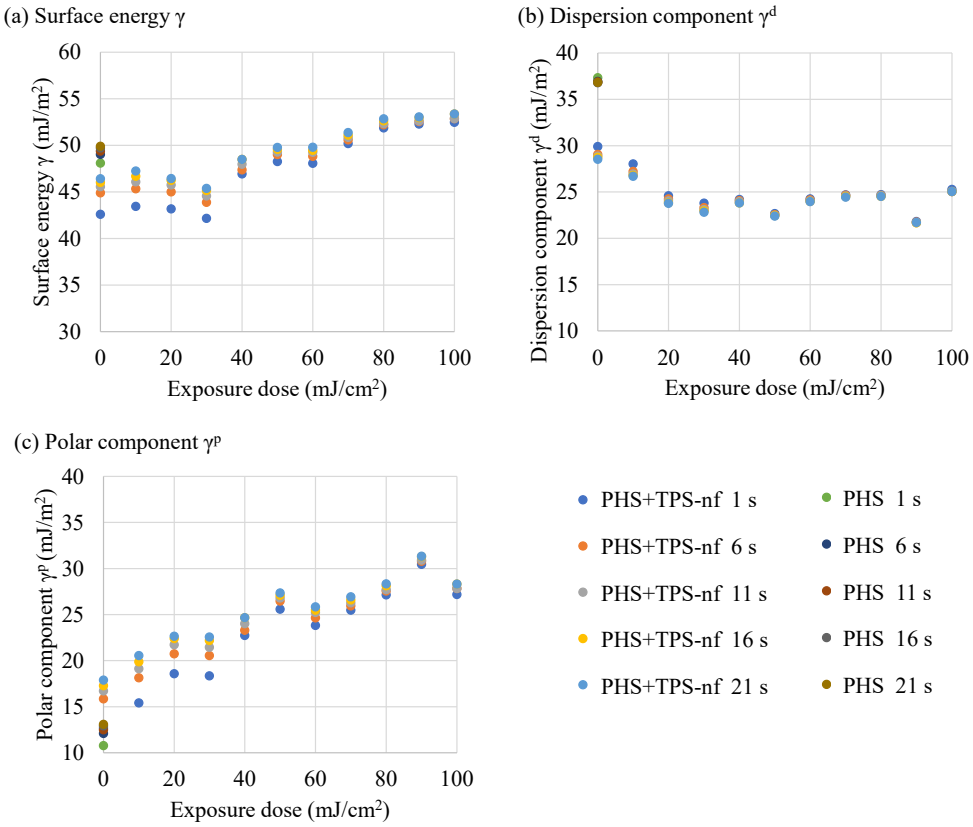

Fig. 1-9. (a) Surface free energy, (b) its dispersion component, and (c) its polar component, obtained by OWRK method. The probe liquids were water and diiodomethane.

The surface free energy and its components were calculated by the OWRK method using water and hexadecane. The calculation results are shown in **Fig. 1-10**. Similar trends to the exposure dose dependences obtained using water and diiodomethane (**Fig. 1-9**) were observed except for the PHS film without TPS-nf. In the combination of water and hexadecane, the estimation error of the dispersion component may have increased because the dispersion component of hexadecane is close to that of water, as shown in **Table 1-1**. On the other hand, no such difference was observed in the estimation of the polar component.

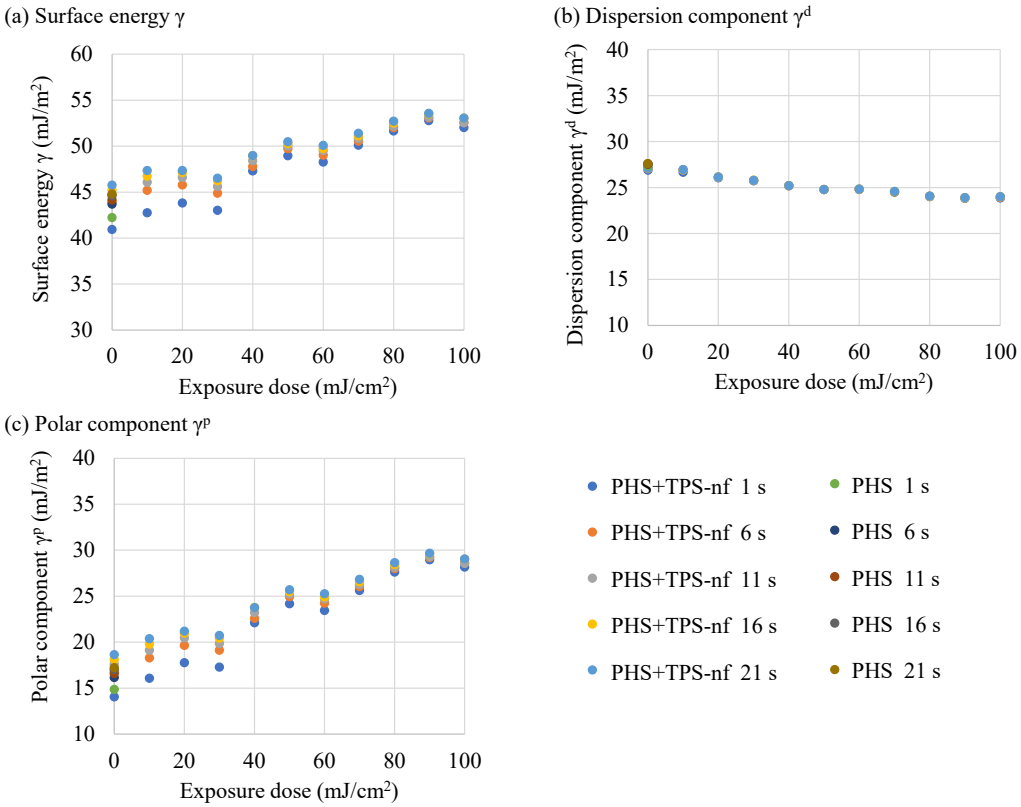

Fig. 1-10. (Color online) (a) Surface free energy and its (b) dispersion component and (c) polar component obtained by OWRK method. The probe liquids were water and hexadecane.

The calculation results obtained by the Kitazaki–Hata method are shown in **Fig. 1-11**. Water, diiodomethane, and hexadecane were used as probe liquids. The surface free energy increased with the exposure dose, as shown in **Fig. 1-11(a)**. Although the absolute values of surface free energies differed, a similar trend to that obtained by the OWRK method was observed. The dispersion component of

surface free energy [**Fig. 1-11(b)**] slightly decreased with increasing exposure dose, similarly to the OWRK method. The polar component of the PHS films without TPS-nf was 30 mJ m^{-2}, whereas that of PHS films with TPS-nf was 15 mJ m^{-2}. The polar component of surface free energy [**Fig. 1-11(c)**] seems to be roughly constant (10–20 mJ m^{-2}), independent of the exposure dose, or to slightly increase. The hydrogen bonding component of surface free energy [**Fig. 1-11(d)**] did not change upon the addition of TPS-nf. It has been reported that the ratio of free OH groups to hydrogen-bonded OH groups in PHS films did not change upon the addition of TPS-nf.[23] The hydrogen bonding component increased with the exposure dose. These results suggest that some counterparts of hydrogen bonding were TPS-nf before exposure. The hydrogen bonding component is considered to have increased by the decomposition of TPS-nf. In the OWRK method, the hydrogen bonding component is included in the polar component.

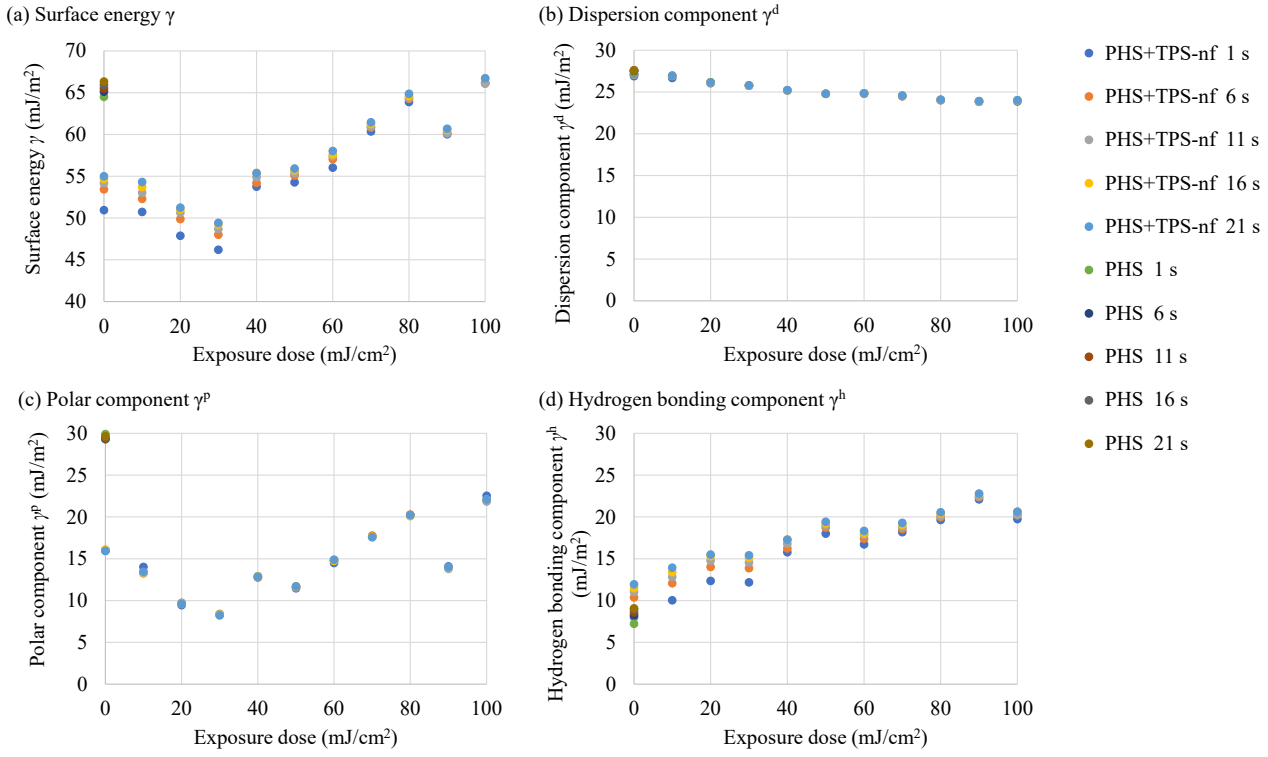

Fig. 1-11. (a) Surface free energy and its (b) dispersion component, (c) polar component, and (d) hydrogen bonding component obtained by the Kitazaki–Hata method. The probe liquids were water, diiodomethane, and hexadecane.

Finally, the acid–base method was used to analyze the surface free energy, as shown in **Fig. 1-12**. Water, hexadecane, and ethylene glycol were used as probe liquids. The surface free energy increased with the exposure dose, similarly to the results obtained using the other methods. The LW component of surface free energy means the same as the dispersion component in the other methods. The LW component slightly decreased with increasing exposure dose, as shown in **Fig. 1-12(b)**. **Figure 1-12(c)** shows the dependence of the acid (electron–acceptor) component of surface free energy on exposure dose. Upon exposure to UV light, the acid component was approximately constant (5 mJ m^2). On the other hand, the base (electron–donor) component increased with the exposure dose, as shown in **Fig. 1-12(d)**. Upon exposure to UV light, the acids were generated through the decomposition of TPS-nf. The increase in the base component indicates that the concentrations of anions and/or the electron-rich parts of molecules increased at the PHS film surface with the exposure dose. The acids at the surface dissociate upon coming in contact with water.[26] The concentrations of anions of dissociated acids are considered to have increased at the surface with the exposure dose.

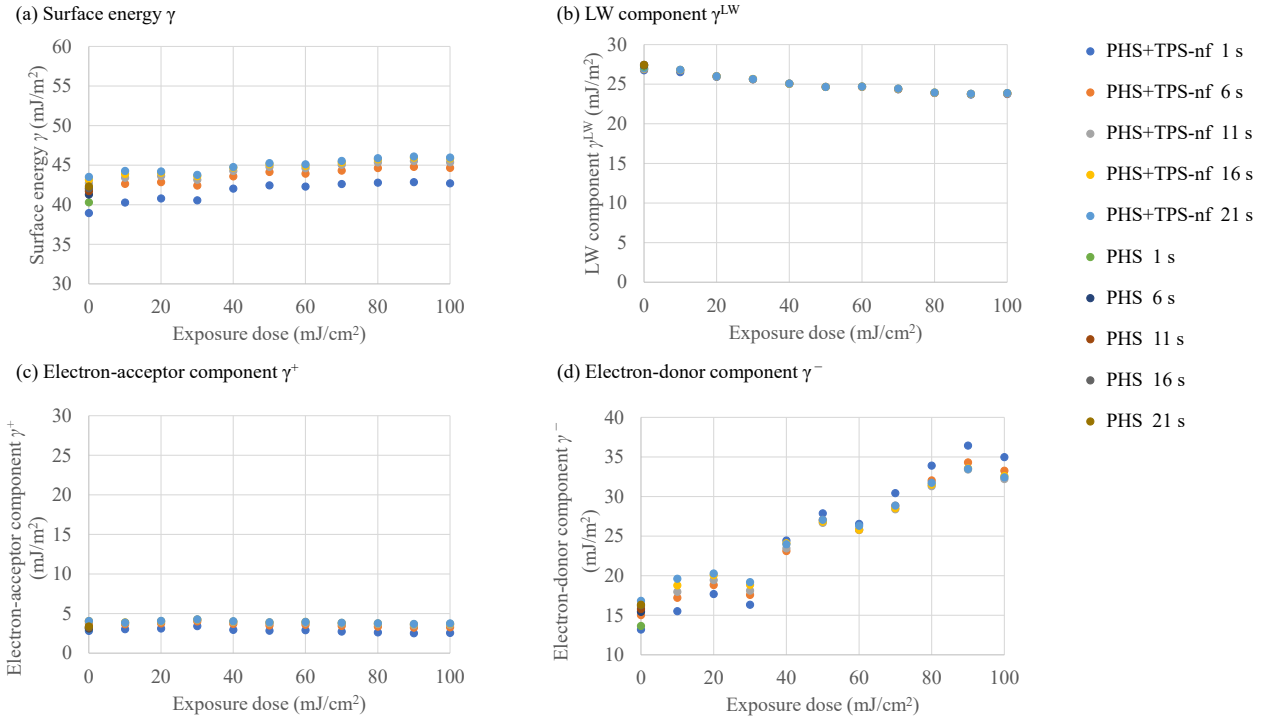

Fig. 1-12. (a) Surface free energy and its (b) LW component, (c) acid (electron–acceptor) component, and (d) base (electron–donor) component, obtained by the acid–base method. The probe liquids were water, hexadecane, and ethylene glycol.

Figure 1-13(a) shows the QCM charts obtained during the development of PHS films with 2.38 wt% TMAH developer. The exposure dose dependence of observed rate constants is shown in **Fig. 1-13(b)**. The rate constants were estimated from the QCM charts (**Fig. 1-14**). The initial film thickness was approximately 300 nm. All the films were completely dissolved within 4 s. The PHS film without TPS-nf was dissolved the fastest among all the PHS films. The speed of weight loss was significantly decreased upon the addition of TPS-nf. The speed of weight loss of PHS films with TPS-nf increased with the exposure dose. This increase in dissolution speed corresponded to the increase in water intake speed. However, the water intake kinetics of the PHS film without TPS-nf was approximately the same as that of PHS films with TPS-nf exposed to 10 mJ cm^{-2} UV light, as shown in **Fig. 1-5**. Therefore, the interaction of TPS-nf with OH groups, which was discussed previously, is also considered to have delayed the dissolution of PHS molecules.

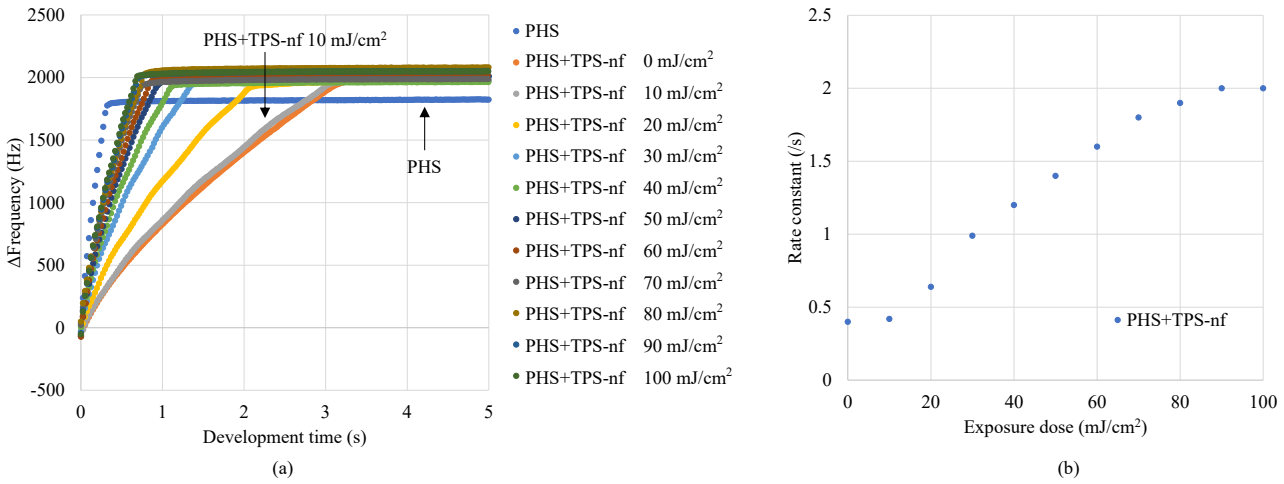

Fig. 1-13. (a) QCM charts of PHS films of 300 nm thickness and (b) the exposure dose dependence of observed rate constants estimated from QCM charts. The polymer films were developed using 2.38 wt% TMAH developer. The exposure doses were changed from 0 to 100 mJ cm^{-2} in steps of 10 mJ cm^{-2}.

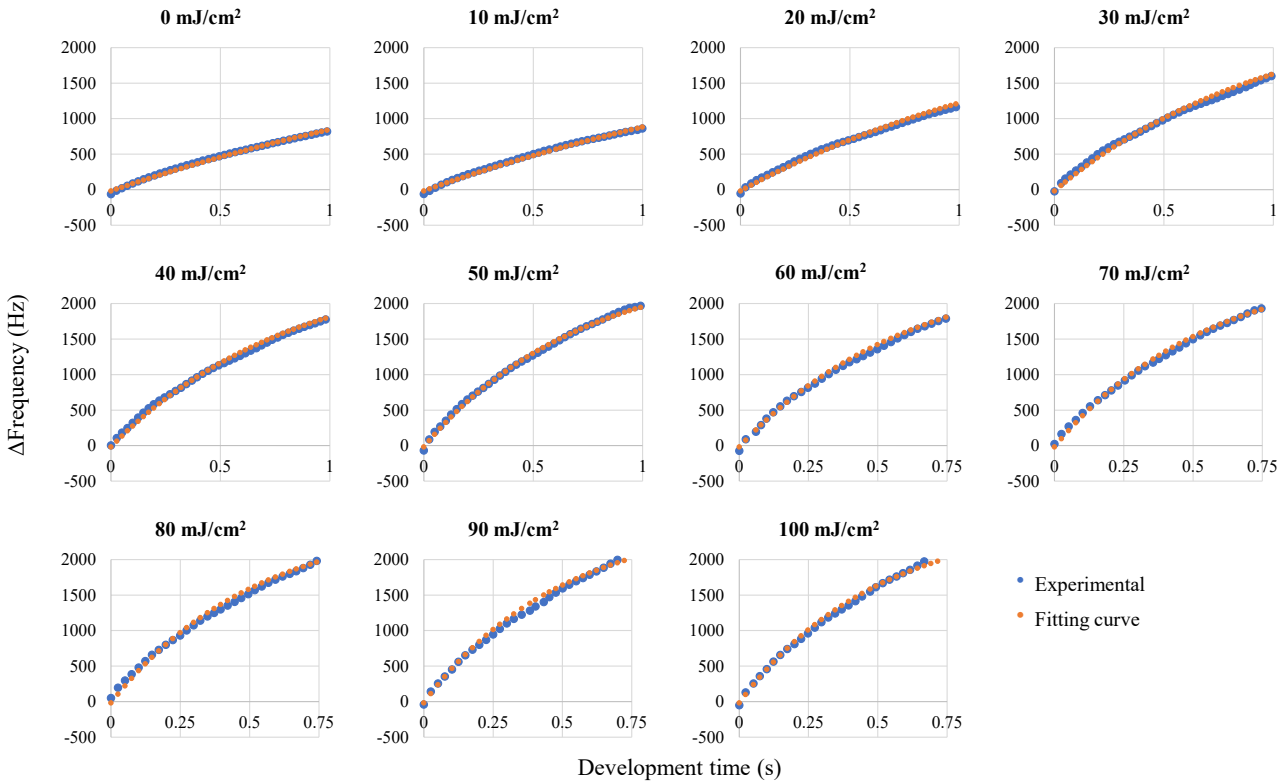

Fig. 1-14. Fitting of exponential function to QCM charts shown in **Fig. 1-13(a)**.

In this chapter, three different methods were used to analyze the surface free energies of PHS films with and without TPS-nf. The surface free energy of PHS films decreased upon the addition of TPS-nf in the OWRK and Kitazaki–Hata methods and did not change in the acid–base method. The dispersion component decreased in the OWRK method, whereas the polar component decreased in the Kitazaki–Hata method. Because the water intake became slow upon the addition of TPS-nf, the surface free energy is considered to be decreased by the addition of TPS-nf. However, its component, namely, its cause is inconclusive. For the PHS films with TPS-nf, the surface free energy and the rate constant of water intake increased with the exposure dose. The dispersion component decreased with the increase in exposure dose. The decrease in the dispersion component is considered to have facilitated the water penetration into the PHS films. The polar component increased with the exposure dose. According to the Kitazaki–Hata method, the increase in the polar component was due to the increase in the hydrogen bonding component. The results obtained by the acid–base method suggest that the

concentration of anions of dissociated acids increased at the surface. Therefore, the anions of dissociated acids are considered to have increased the hydrogen bonding component of surface energy. The increase in the hydrogen bonding component is considered to accelerate the water intake. The increase in the polar component (particularly the hydrogen bonding component) and the decrease in the dispersion component are the reasons why the swelling and dissolution rates of PHS films with TPS-nf increased with the exposure dose.

1-4. Conclusions

In section 1-3-1, the kinetics of viscosity and PHS concentration during development of PHS films in 2.38 wt% TMAH aqueous solution was clarified. The maximum PHS concentration achievable during development corresponded to approximately the TMAH concentration (0.26 M) independently of the film thickness. The schematic is shown in **Fig. 1-15**. The increase in viscosity caused by the dissolution of PHS polymer affected the dissolution kinetics even in the case of the dissolution of flat thin films without patterns. These results suggest that the stagnation of polymer molecules significantly affects the dissolution kinetics of resist films on which nanoscale features are printed.

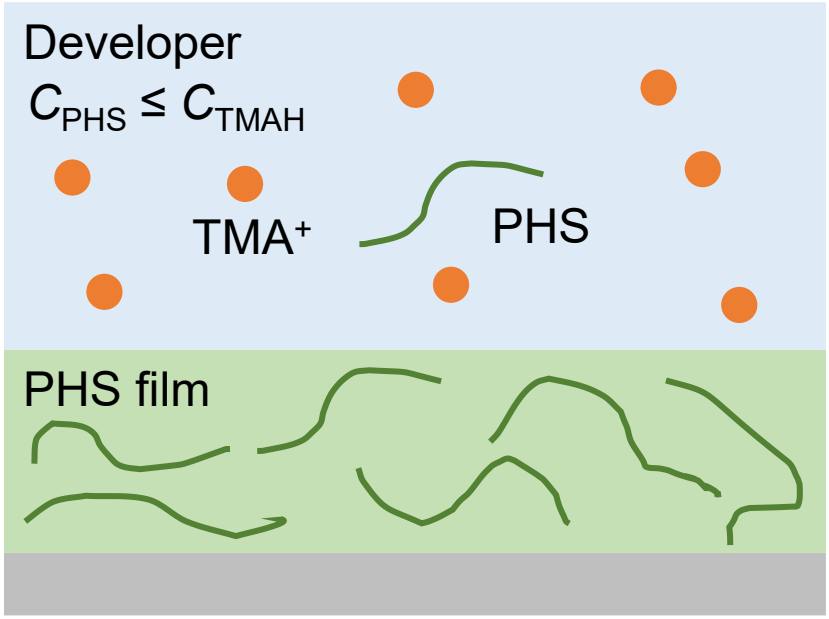

Fig. 1-15. Schematics of the relationship between C_{PHS} and TMAH concentration C_{TMAH} during development. TMA^+ denotes a tetramethylammonium cation. Note that C_{PHS} denotes the concentration of the monomer units of PHS in the developer.

In section 1-3-2, the relationship between surface free energy and swelling kinetics of PHS film in alkaline aqueous solution was investigated by the QCM method. Three different methods were used to analyze the surface free energies of PHS films with and without TPS-nf. The surface free energy is considered to be decreased by the addition of TPS-nf. However, its component, namely, its cause is inconclusive. For the PHS films with TPS-nf, the surface free energy and the rate constant of water intake increased with the exposure dose. The decrease in the dispersion component is considered to have facilitated the water penetration into the PHS films. The increase in the hydrogen bonding component is considered to accelerate the water intake. The increase in the polar component (particularly the hydrogen bonding component) and the decrease in the dispersion component are the reasons why the swelling and dissolution rates of PHS films with TPS-nf increased with the exposure dose.

References

1) H. Yamamoto, T. Kozawa, A. Nakano, K. Okamoto, Y. Yamamoto, T. Ando, M. Sato, H. Komano, and S. Tagawa, Jpn. J. Appl. Phys. **43**, L848 (2004).
2) A. Nakano, T. Kozawa, K. Okamoto, S. Tagawa, T. Kai, and T. Shimokawa, Jpn. J. Appl. Phys. **45**, 6866 (2006).
3) T. Kozawa and S. Tagawa, Jpn. J. Appl. Phys. **49**, 030001 (2010).
4) W. Hinsberg, F. A. Houle, S. W. Lee, H. Ito, and K. Kanazawa, Macromolecules **38**, 1882 (2005).
5) T. Itani and J. J. Santillan, Appl. Phys. Express **3**, 061601 (2010).
6) J. J. Santillan and T. Itani, Jpn. J. Appl. Phys. **52**, 06GC01 (2013).
7) L. Long, J. Chen, A. Neureuther, P. Naulleau, and P. Ashby, Proc. SPIE **12292**, 1229206 (2022).
8) A. Sekiguchi, J. Photopolym. Sci. Technol. 26, 479 (2013).
9) H. Tsubaki, W. Nihashi, T. Tsuchihashi, T. Fujimori, M. Momota, and T. Goto, J. Photopolym. Sci. Technol. **28**, 489 (2015).
10) A. Tsuneishi, S. Uchiyama, and T. Kozawa, Jpn. J. Appl. Phys. **57**, 046501 (2018).
11) A. Nakajima, K. Watanabe, K. Matsuoka, T. Kozawa, Y. Komuro, D. Kawana, and A. Yamazaki, Jpn. J. Appl. Phys. **59**, 036505 (2020).
12) N. Maeda, A. Konda, K. Okamoto, T. Kozawa, and T. Tamura, Jpn. J. Appl. Phys. **59**, 086501 (2020).

13) N. Tanaka, K. Watanabe, K. Matsuoka, K. Azumagawa, T. Kozawa, T. Ikeda, Y. Komuro, and D. Kawana, Jpn. J. Appl. Phys. **60**, 066503 (2021).
14) O. Loebich, Gold Bull. **5**, 2 (1972).
15) G. Sauerbrey, Z. Phys. **155**, 206 (1959).
16) M. A. Green, Sol. Energy Mater. Sol. Cells, **92**, 1305 (2008).
17) D. K. Owens and R. C. Wendt, J. Appl. Polym. Sci. **13**, 1741 (1969).
18) D. H. Kaelble, J. Adhes. **2**, 66 (1970).
19) Y. Kitazaki and T. Hata, Nippon Setchaku Kyoukaishi **8**, 131 (1972).
20) C. J. van Oss, Colloids Surf. A **78**, 1 (1993).
21) N. G. Tsierkezos and I. E. Molinou, J. Chem. Eng. Data **43**, 989 (1998).
22) T. Fukuyama, T. Kozawa, S. Tagawa, R. Takasu, H. Yukawa, M. Sato, J. Onodera, I. Hirosawa, T. Koganesawa, and K. Horie, Appl. Phys. Express **1**, 065004 (2008).
23) T. Fukuyama et al., Jpn. J. Appl. Phys. **48**, 06FC03 (2009).
24) T. Fukuyama et al., J. Photopolym. Sci. Technol. **22**, 105 (2009).
25) J. L. Dektar and N. P. Hacker, J. Am. Chem. Soc. **112**, 6004 (1990).
26) E. Virga, E. Spruijt, W. M. de Vos, and P. M. Biesheuvel, Langmuir **34**, 15174 (2018).

Chapter 2

Dissolution dynamics of PHS resists in alkaline developers different from TMAH

2-1. Swelling and dissolution kinetics of PHS in tetrabutylammonium hydroxide (TBAH) aqueous solutions −in comparison with TMAH aqueous solutions

2-1-1. Introduction

In EUV lithography, 0.55 NA tools have been developed[1–2] and optical resolution has reached 8 nm half-pitch.[3] With the sharpening of optical images, the capability of resist materials has become a serious concern in lithography. However, the resist materials responding to such a fine optical image are not yet available. The resolution-limiting factors of resist materials have been intensively investigated.[4–12] Development (the dissolution of resist materials in a developer) is key to achieving such ultrafine imaging. 2.38 wt% tetramethylammonium hydroxide (TMAH) aqueous solution is a standard developer for the lithography used in the high-volume production of semiconductor devices.

Recently, an alternative developer has attracted considerable attention, because the performance of chemically amplified resists (CARs) is approaching their limit for the 2.38 wt% TMAH developer. A tetrabutylammonium hydroxide (TBAH) aqueous solution is a typical alternative developer.[13–16] It was reported that the pattern collapse of the 2-methyl-2-adamantylmethacrylate-mevalonic-lactonemethacrylate resist was markedly reduced for thick films when using the TBAH developer. It was suggested that TBAH functioned as a surfactant and had good solubility for the exposed region of resist films.[13] A 20% LWR improvement due to the improvement of the dissolution contrast was also reported as an effect of using the TBAH developer for a copolymer resist of polyhydroxystyrene with a high-activation- energy blocking group.[14] The increased molecular weight of tetraalkylammonium hydroxide was proposed to be the cause of the improvement in dissolution contrast. The effects of the TBAH developer were examined for four different EUV resist materials.[15] The lithographic performance improvement was reported to vary depending on the type of resist used. Although the effects of the TBAH developer on the resist performance have been investigated, the difference between the dissolution kinetics in TMAH and TBAH developers is still unclear. In this section, the swelling and dissolution kinetics of PHS films in TMAH and TBAH aqueous solutions were studied

by the QCM method. The effect of the alkyl chain of tetraalkylammonium hydroxides is discussed.

2-1-2. Experimental methods

2-1-2-1. Materials

PHS (Mw = 11 000) and propylene glycol monomethyl ether acetate (PGMEA) were purchased from Sigma-Aldrich. The resist polymers were prepared by protecting the hydroxyl groups of PHS with t-butoxycarbonyl groups. The protection ratio was changed from 5% to 70%. The 2.38 wt% TMAH aqueous developer NMD-3 was purchased from Tokyo Ohka Kogyo. The diluted developers (1.57, 1.19, 0.60, and 0.24 wt% TMAH) were also prepared by diluting NMD-3 with distilled water. Hereafter, 2.38, 1.57, 1.19, 0.60, and 0.24 wt% TMAH aqueous developers are called 100%, 66%, 50%, 25%, and 10% TMAH developers, respectively, for convenience. TBAH aqueous solution (40 wt%) was purchased from Sigma-Aldrich. 6.78, 4.47, 3.39, 1.69, and 0.68 wt% TBAH aqueous solutions were also prepared by diluting the purchased liquid with distilled water. The normalities of 2.38 wt% TMAH and 6.78 wt% TBAH aqueous solutions were 0.26 N. Hereafter, 6.78, 4.47, 3.39, 1.69, and 0.68 wt% TBAH aqueous solutions are called 100%, 66%, 50%, 25%, and 10% TBAH developer, respectively, for convenience. The molecular structures of PHS, TMAH, and TBAH are shown in **Fig. 2-1**.

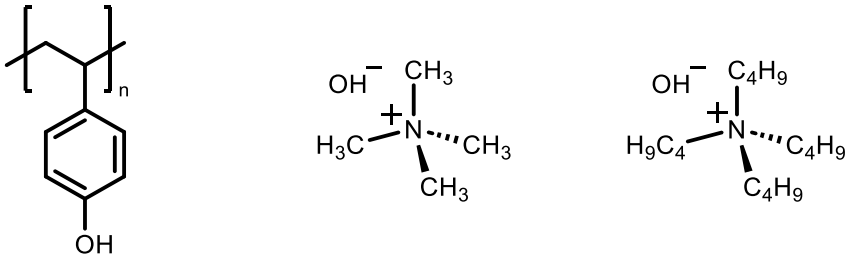

Poly(4-hydroxystyrene) (PHS) M_w=11000 Protection ratio:0-70%

Tetramethyammonium hydroxide (TMAH)

Tetrabutylammonium hydroxide (TBAH)

0.26, 0.17, 0.13, 0.065, 0.026, 0 mol/L (**100**, 66, 50, 25, 10, 0% developers)

Fig. 2-1. Molecular structures of samples used.

2-1-2-2. QCM measurement

The PHS powders were dissolved in PGMEA and the concentration was adjusted to prepare films with thicknesses of approximately 30, 60, 110, and 310 nm. The films spin-coated onto QCM substrates were prebaked at 90 °C for 90 s. The dissolution kinetics of PHS films was measured using a QCM-based development analyzer (Litho Tech Japan RDAQz3). The films were developed in the developers (or distilled water) at 23 °C and then rinsed in water. The film thicknesses before and after development were measured using an ellipsometer (Meiwafosis FS-1).

QCM measurement yields the weight change on Au electrodes sandwiching the quartz crystal by detecting the resonance frequency of the quartz crystal. The decrease and increase in weight should correspond to the swelling and dissolving of the polymer, respectively. The change in frequency obtained by measurement can be converted to the change in weight in accordance with Sauerbrey's equation:[17)]

$$\Delta f = -\frac{2{f_0}^2}{A\sqrt{\rho_q \mu_q}}\Delta m. \tag{2-1}$$

Here, Δf, f_0, Δm, A, ρ_q, and μ_q are the frequency change, the resonant frequency of the unloaded QCM substrate, the mass change of the material on the substrate, the piezoelectrically active crystal area, the density of quartz, and the shear modulus of the quartz used as the AT-cut crystal, respectively. Equation (2-1) assumes that the material observed on the substrate is rigid. However, the transient swelling layer is not rigid. We should take into account this fact in our consideration. The impedance change ΔZ corresponds to the viscosity or viscoelasticity of the surrounding. The impedances of the 100% TMAH and PHS-saturated 100% TMAH developers were measured using QCM substrates. The impedance change ΔZ caused by PHS saturation was obtained. Similarly, the impedance change ΔZ caused by PHS saturation was evaluated for the 100% TBAH developer.

2-1-3. Results and discussion

2-1-3-1. PHS dissolution kinetics in 100% TMAH and 100% TBAH aqueous solutions

PHS films without the protection of hydroxyl groups were developed using the 100% TMAH and 100% TBAH developers. **Figure 2-2** shows the obtained QCM charts. The vertical axes in **Figs. 2-2(a)** and **2(b)** represent the frequency change of QCM substrates. The frequency in atmosphere was set to 0 (base value). The horizontal axes represent the development time in seconds. At 0 s, the QCM substrates were immersed into the developers. The frequency immediately dropped by approximately 700–960 Hz because of the increase in the viscosity of the environment. The following dissolution dynamics significantly differed between TMAH and TBAH developers. In the 100% TMAH developer, the transient swelling layer was too thin to be clearly observed.[18] The frequency increased almost linearly and then became constant (complete dissolution). The linear increase in frequency indicates the linear weight loss of PHS films. Because the transient swelling layer was thin, the film thickness is likely to decrease linearly with the development time. The rate of frequency change did not depend on the film thickness. This also suggests that the transient swelling layer was thin. In the 100% TBAH developer, a slight decrease in frequency was observed after the initial drop of frequency. Then, the frequency was approximately constant for some time, depending on the initial film thickness. After the plateau, the frequency again decreased for the initial film thicknesses of 30, 59, and 308 nm. Subsequently, the frequency rapidly increased and became constant. For the initial film thickness of 115 nm, the second decrease was not observed. The rate of rapid increase before complete dissolution was lower than that observed in the 100% TMAH developer.

Figures 2-2(c) and **2-2(d)** show the impedance change of QCM substrates during development. The decay of impedance Z was fitted by[19]

$$Z = -\frac{Z_0}{(t - t_0)^a} + b, \tag{2-2}$$

where Z_0, t, t_0, a, and b are a constant, the time in seconds, the time reference in seconds, the attenuation rate (a dimensionless parameter), and the baseline, respectively. The fitting results are shown in **Fig.**

2-3. Using b as a baseline, the impedance change ΔZ ($= Z - b$) is plotted in **Figs. 2-2(c)** and **2-2(d)**. Using Eq. (2-2), the rate of impedance change was calculated as

$$-\frac{dZ}{dt} = -\frac{d\Delta Z}{dt} = \frac{aZ_0}{(t-t_0)^{a+1}}. \tag{2-3}$$

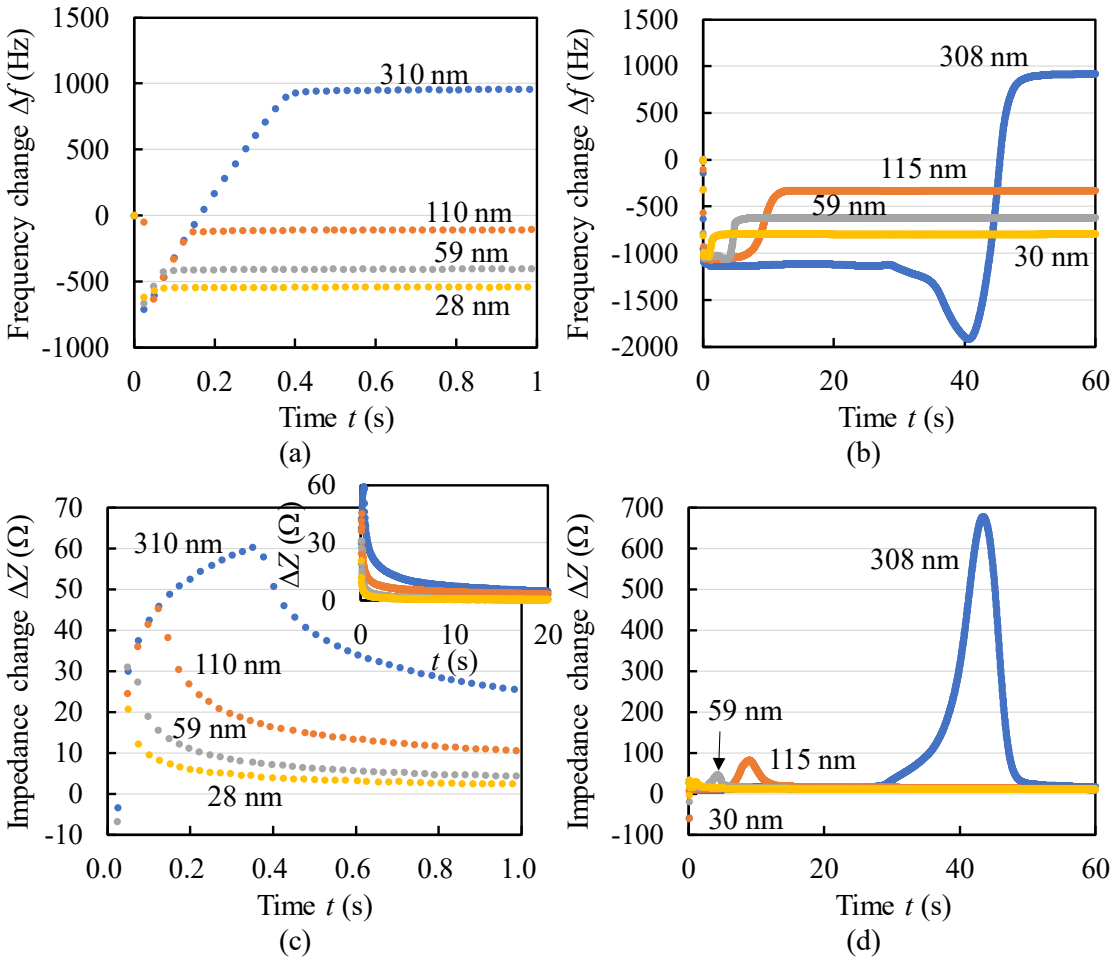

Fig. 2-2. QCM charts of PHS films during development in (a), (c) 100% TMAH and (b), (d) 100% TBAH developers. The numerical values in nm in the graphs are the initial thicknesses of PHS films.

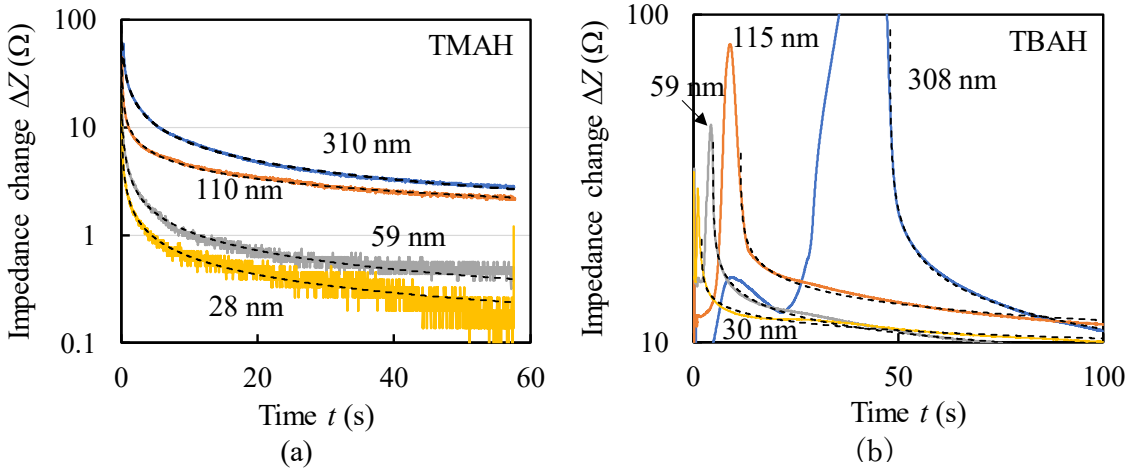

Fig. 2-3. Results of fitting to the experimental data shown in (a) **Fig. 2-2(c)** and (b) **Fig. 2-2(d)**. The dashed lines represent the fitted curves.

The relationship between ΔZ and $-dZ/dt$ is shown in **Fig. 2-4**. The impedance changes of saturated PHS solutions from pure developers without PHS molecules were measured by dropping the saturated solution on QCM substrates. The impedances of 0.26 mol l^{-1} TMAH and TBAH aqueous solutions saturated with PHS were approximately 50 and 30 Ω, respectively. The dissolution of PHS films in the 100% TMAH developer progressed at a lower or slightly higher impedance than that under the PHS-saturated condition. The rate of increase in impedance did not depend on the film thickness, similarly to the frequency change. On the other hand, the rate of impedance decay depended on the film thickness when it was compared at the same impedance change, as shown in **Fig. 2-4**. The impedance change is considered to mainly reflect the viscosity change caused by a change in PHS concentration in the 100% TMAH developer, because the transient swelling layer was thin and the impedance change was, at most, slightly higher than that under the PHS-saturated condition. These experimental results indicate that the transport rate of PHS molecules from a resist film to a developer did not depend on the film thickness when the initial film thickness was less than 300nm. The rate of impedance decay indicates the diffusion of polymer molecules near the resist surface to the bulk solution. When the rates of impedance decay were compared at the same impedance for the same developer, the low rate indicates a low gradient of PHS concentration in the direction perpendicular to the resist surface.

Therefore, **Fig. 2-4** suggests that the gradient of PHS concentration in the developer (a driving force of diffusion) decreased with an increase in initial film thickness. Note that the boundary between the transient swelling layer and the developer containing PHS molecules is obscure.

In the 100% TBAH developer, the maximum impedance change was approximately the same as the impedance change under a PHS-saturated condition (approximately 30 Ω) even at the initial film thickness of 30 nm. The impedance change significantly exceeded that under the PHS-saturated condition for the initial film thickness greater than 60 nm. An impedance change larger than the PHS-saturated impedance change mainly reflects the viscosity (or viscoelasticity) of not the developer but the resist film. For the PHS films with the initial thicknesses of 30, 59, and 308 nm, the frequency decreased after the plateau (for example, after the development time of approximately 30 s for the 308 nm thick PHS film), as shown in **Fig. 2-2(b)**. The impedance change shown in **Fig. 2-2(d)** indicates that an increase in the viscosity of the PHS film decreased the frequency. With a large increase in impedance, the frequency rapidly increased. For the frequency change, the increase due to weight loss and the decrease due to an increase in viscosity are considered to progress concurrently. This is considered to be one reason why the frequency drop immediately before the dissolution was not observed for the 115 nm thick PHS film unlike the other cases. The rates of impedance decay were significantly lower than those observed in the 100% TMAH developer when they were compared at the same impedance change. This suggests that the diffusion of PHS molecules in the 100% TBAH developer was slower than that in the 100% TMAH developer. The dependence of the decay rate on the initial film thickness showed a trend similar to that in the case of the 100% TMAH developer.

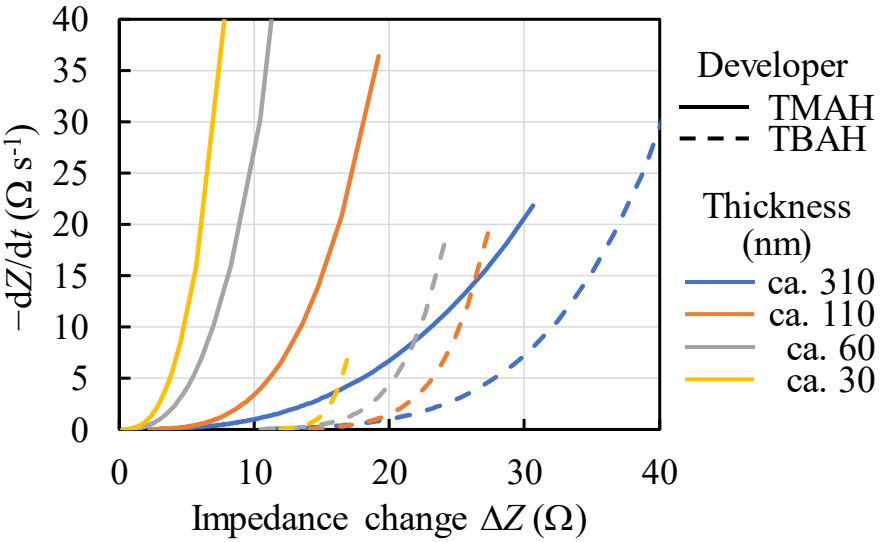

Fig. 2-4. Effects of film thickness and type of developer used on the relationship between ΔZ and $-dZ/dt$ ($=-d\Delta Z/dt$). The developers were 100% TMAH and 100% TBAH. The protection ratio of PHS was 0%.

2-1-3-2. PHS dissolution kinetics dependency on TMAH and TBAH concentrations

The dependence of dissolution kinetics on the concentration of tetraalkylammonium hydroxide was investigated. **Figure 2-5** shows the QCM charts of PHS films during development in the TMAH and TBAH developers. The initial film thickness was approximately 300 nm. The alkaline concentration was decreased from 100% to 0% (pure water). In TMAH developers, the dissolution rate decreased with the dilution of the developer, as shown in **Fig. 2-5(a)**. At a 25% concentration, the PHS film slightly dissolved (27 nm) within the development time of 180 s after slow swelling. At a 10% concentration, the PHS film did not dissolve. In pure water, the PHS film did not dissolve either. The PHS film swelled in water and the 10% TMAH developer. The swelling was greater in 10% developer than in water. The slight dissociation of the hydroxyl groups in the diluted developer is considered to have weakened the intra- and intermolecular interactions of the PHS polymer, consequently promoting water intake. In TBAH developers, the PHS film did not dissolve at a 66% concentration within the development time of 180 s, as shown in **Fig. 2-5(b)**. The QCM charts obtained in the 10%, 25%, 50%, and 66% developers were almost identical to each other. The swelling in the 10% TBAH developer was less than that in the 10% TMAH developer. These results indicate that the penetration speed of

TBA cations is significantly lower than that of TMA cations because of the long alkyl chain.

Figures 2-5(c) and **2-5(d)** show the impedance change during development. The maximum impedance change in the TMAH developer decreased on decreasing the TMAH concentration. This probably reflected the decrease in the solubility of PHS. The rate of increase in impedance decreased with the TMAH concentration. On the other hand, the impedance was almost constant during development in the 10%, 25%, 50%, and 66% TBAH developers. **Figure 2-6** shows (a) results of fitting to the experimental data shown in **Fig. 2-5(c)** and (b) the effect of TMAH concentration on the relationship between ΔZ and $-dZ/dt$. The protection ratio of PHS was 0%. The rate of impedance decay was independent of TMAH concentration within the concentration range of 1.19–2.38 wt%. The diffusion of PHS molecules to the bulk solution did not depend on the TMAH concentration when it was compared at the same viscosity (approximately the same PHS concentration) and at the same initial film thickness.

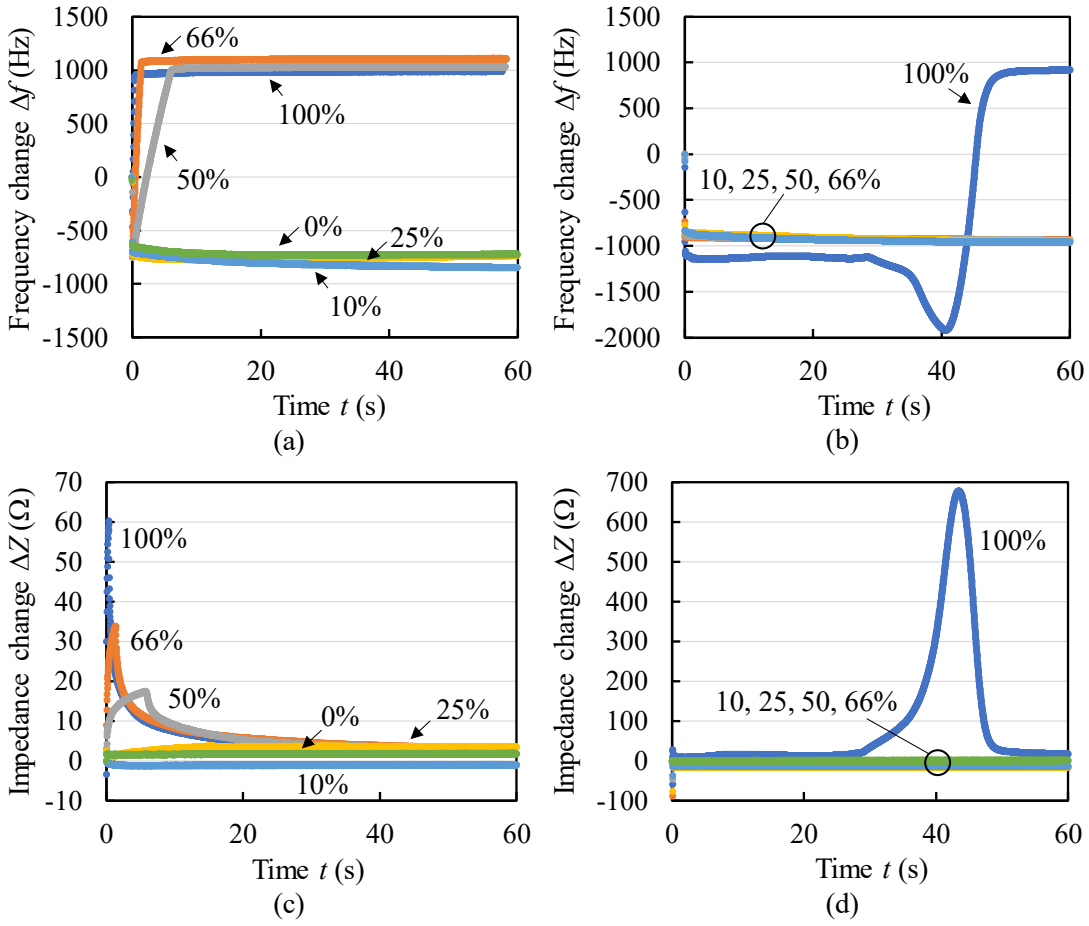

Fig. 2-5. QCM charts of PHS films during development in (a), (c) TMAH and (b), (d) TBAH developers. The numerical values in % in the graphs are the relative concentrations of tetraalkylammonium hydroxide. The initial thickness of PHS films was approximately 300 nm.

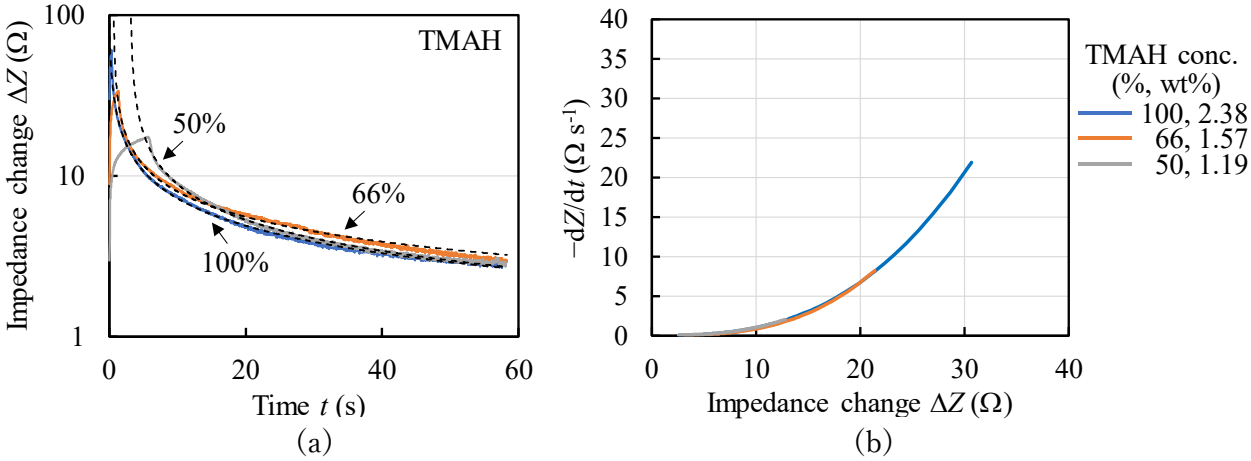

Fig. 2-6. (a) Results of fitting to the experimental data shown in **Fig. 2-5(c)**. The dashed lines represent the fitted curves. (b) Effect of TMAH concentration on relationship between ΔZ and $-dZ/dt$ (= $-d\Delta Z/dt$). The protection ratio of PHS was 0%.

2-1-3-3. Dissolution kinetics dependency on the protection ratio of hydroxyl groups of PHS

The dependence of dissolution kinetics on the protection ratio of the hydroxyl groups of PHS was investigated. **Figure 2-7** shows the QCM charts of PHS films during development in the TMAH and TBAH developers. In the TMAH developer, the dissolution rate decreased monotonically with an increase in protection ratio up to 30%, as shown in **Fig. 2-7(a)**. The mode of dissolution was not changed by increasing the protection ratio up to 30%. At a 50% protection ratio, the PHS film did not dissolve and no swelling was observed. The dissolution kinetics of the 70% protected PHS film was approximately the same as that of the 50% protected PHS film. In the TBAH developer [**Fig. 2-7(b)**], the dissolution kinetics of the 5% protected PHS film was similar to that of the 0% protected PHS film with an initial thickness of 115 nm. The 5% protected PHS film dissolved without a negative peak immediately before complete dissolution. At 10% protection, the mode of dissolution changed. After the plateau and increase, the frequency slightly decreased again and then rapidly increased. In the protection ratio range of 15%–50%, only swelling was observed. The rate of swelling decreased with an increase in protection ratio. At a 70% protection ratio, swelling was not observed.

Figures 2-7(c) and **2-7(d)** show the effects of protection ratio on the impedance change during development. In the 100% TMAH developer, the maximum impedance change decreased with an increase in protection ratio, as shown in **Fig. 2-7(c)**. This is considered to be due to the decrease in solubility in the developer with an increase in protection ratio, similarly to the case of the dilution of the TMAH developer. The rate of increase in impedance decreased with an increase in protection ratio. In the 100% TBAH developer, the maximum impedance change was significantly decreased by protecting the hydroxyl groups of PHS. However, the maximum impedance change of the 10% protected PHS film was larger than that of the 5% protected PHS film. The effect of protection in the case of the 100% TBAH developer was complex, unlike the case of the 100% TMAH developer. This is considered to be because the impedance changes for the 100% TMAH and 100% TBAH developers mainly reflect the polymer concentration in the developer and the viscosity of the polymer film,

respectively. **Figure 2-8** shows (a) results of fitting to the experimental data shown in **Fig. 2-7(c)** and (b) the effect of the protection ratio of PHS on the relationship between ΔZ and $-dZ/dt$ in the 100% TMAH developer. The rate of impedance decay was independent of the protection ratio within the protection ratio range of 0%–30%. The diffusion of PHS molecules to the bulk solution did not depend on the protection ratio when it was compared at the same viscosity.

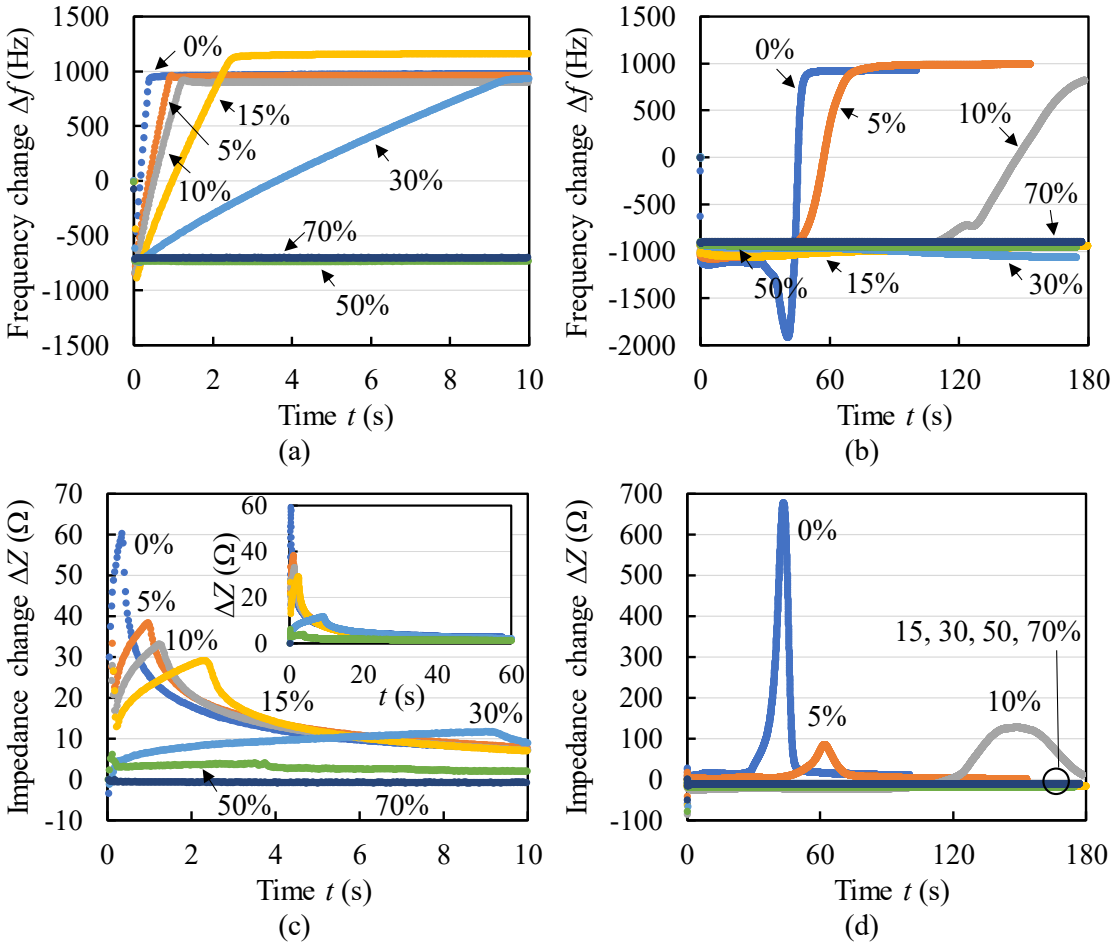

Fig. 2-7. QCM charts of PHS films during development in (a), (c) TMAH and (b), (d) TBAH developers. The numerical values in % in the graphs are the protection ratios of PHS hydroxyl groups. The initial thickness of PHS films was approximately 300 nm.

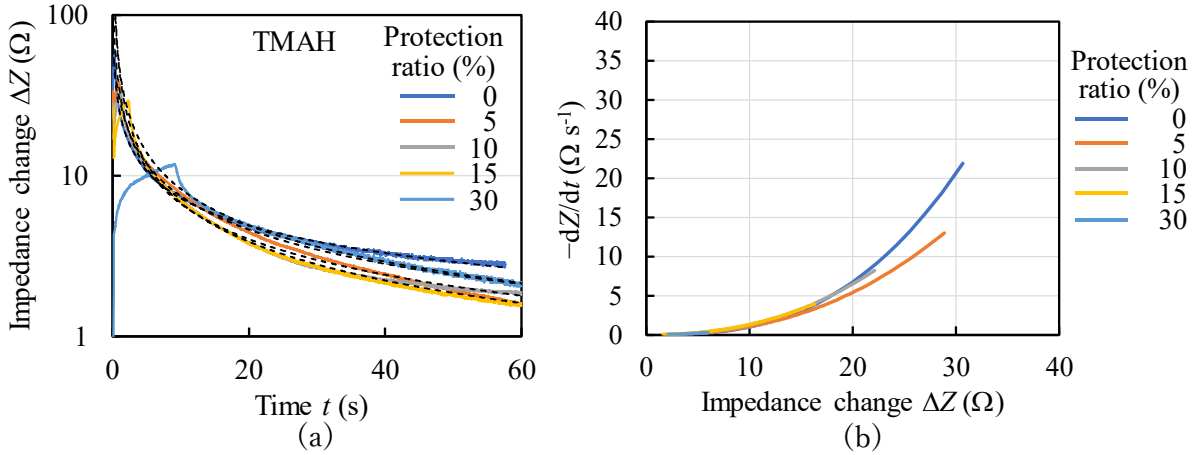

Fig. 2-8. (a) Results of fitting to the experimental data shown in **Fig. 2-7(c)**. The dashed lines represent the fitted curves. (b) Effect of protection ratio of PHS on relationship between ΔZ and $-dZ/dt$ ($=-d\Delta Z/dt$). The developer was 100% TMAH.

2-1-4. Conclusion

In TMAH and TBAH developers, the effects of the alkaline concentration and protection ratio on the swelling and dissolution of the resist polymer were investigated. Not only the dissolution rate but also the mode of dissolution depended on the molecular structure of tetraalkylammonium hydroxide. The impedance changes for the 100% TMAH and 100% TBAH developers are considered to mainly reflect the polymer concentration in the developer and the viscosity of the polymer film, respectively. For polymer matrices with strong hydrogen bond networks such as PHS, the penetration of tetrabutylammonium cations is considered to be strongly suppressed by their long alkyl chains. The dissolution and swelling trends are summarized in **Table 2-1**.

Table 2-1. Summary of dissolution and swelling trends of PHS films.

Developer	Variable		Dissolution	Swelling
TMAH	Thickness		Linear	Thin
	Conc.	>50%	Linear	Thin
		<10%	Insoluble	Swelling
	Protection ratio	<30%	Linear	Swelling
		>50%	Insoluble	No swelling
TBAH	Thickness		Nonlinear	Thick
	Conc.	100%	Nonlinear	Thick
		<66%	Insoluble	Slight swelling
	Protection ratio *p*	<10%	Nonlinear	Thick
		>15%	Insoluble	Swelling rate decreased to p = 50% No swelling p >70%

2-2. Dissolution dynamics of poly(4-hydroxystyrene) in potassium hydroxide (KOH) and sodium hydroxide (NaOH) aqueous solutions investigated by quartz crystal microbalance (QCM) method

2-2-1. Introduction

Tetrabutylammonium hydroxide (TBAH) is a typical organic alkali for the alternative alkaline developer. [13-16,20] The fundamentals of the dissolution dynamics in tetraalkylammonium hydroxide (TAAH) aqueous solution have been investigated in terms of the TAAH concentration,[20-22] the protection ratio of the hydroxyl groups of PHS,[20-22] the decomposition of acid generators dispersed in PHS films,[23,24] the molecular weight of PHS,[18] the polydispersity of PHS,[25] the electrostatic interaction of ionized PHS,[26] and the interaction of PHS with the underlayer.[19] Among them, the molecular size of the tetraalkylammonium cation was reported to significantly affect the dissolution dynamics of PHS films. With the increase in molecular size of the tetraalkylammonium cation, the transient swelling layer became thick.[21] However, the details of the size effect are still unclear.

In this section, the dissolution dynamics of PHS in sodium hydroxide (NaOH) and potassium hydroxide (KOH) aqueous solutions were investigated by a quartz crystal microbalance (QCM) method to clarify the effects of alkaline cations smaller than tetramethylammonium cations on the dissolution dynamics. Generally, we cannot expect a significant improvement in resist performance by simply applying the alternative developers to the current CARs because the current resists have been optimized to the standard TMAH developer. However, it is important to clarify the fundamentals of dissolution dynamics in alternative alkaline developers for the improvement of resist materials and processes.

2-2-2. Experimental methods

2-2-2-1. Materials

PHS (Mw = 11000), propylene glycol monomethyl ether acetate (PGMEA), NaOH, and KOH were

purchased from Sigma-Aldrich. The resist polymers were prepared by protecting the hydroxyl groups of PHS with *t*-butoxycarbonyl (tBOC) groups. The protection ratio was changed from 5 to 40 mol%. Hereafter, the partially protected PHS is also called PHS for convenience, unless otherwise specified. The alkaline concentrations in aqueous solution were adjusted to be 0.26, 0.17, 0.13, 0.065, and 0.026 mol l^{-1}.

2-2-2-2. QCM measurement

The dissolution dynamics (the temporal changes of frequency and impedance) of PHS films in the developers were measured using a QCM-based dissolution analyzer (Lithotech Japan RDA-Qz3).[27] QCM measurement yields the weight and viscosity changes on Au electrodes sandwiching the quartz crystal by detecting the resonance frequency of the quartz crystal and the impedance of the QCM device circuit, respectively.[20,28] **Figure 2-9** shows the schematic charts of frequency and impedance changes, obtained by the QCM method. Upon the immersion of the QCM substrate into the developer, the frequency immediately drops due to the increase in the viscosity of the environment. The following decrease and increase in frequency basically correspond to the swelling and dissolving of the polymer, respectively. The impedance change indicates the viscosity changes of the polymer film and/or developer. In the experiments of dissolution dynamics, the PHS powders were dissolved in PGMEA and the concentration was adjusted to prepare films with thicknesses of approximately 30, 60, 110, and 300 nm. The films spin-coated onto QCM substrates were prebaked at 90 °C for 90 s. The films were developed in the developers at 23 °C and then rinsed in water.

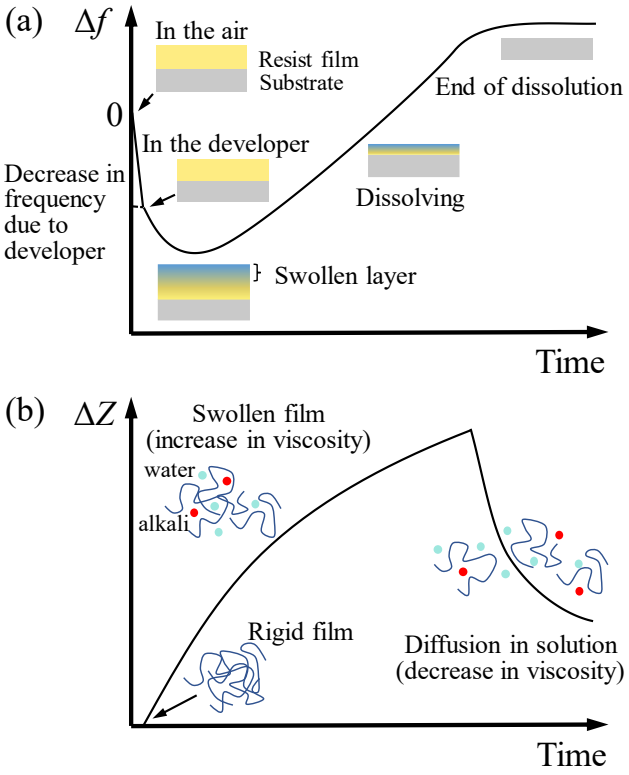

Fig. 2-9. The schematic charts of (a) frequency change and (b) impedance change, obtained by the QCM method.

2-2-2-3. Impedance measurement

The impedance of developers saturated with PHS was measured using a QCM digital controller (Stanford research systems QCM200). In the experiments to determine the impedance of the saturated developer, the PHS powders were dissolved in the developer by applying ultrasonic agitation. The KOH aqueous solutions were left to stand for 1 day. The NaOH aqueous solutions with PHS were prepared without ultrasonic agitation and applied to the impedance measurement just after the sample preparation because the deprotection of PHS in NaOH aqueous solutions was suspected.[29] This decomposition is considered not to affect the measurement of kinetics because the time scale of decomposition is on the order of hours.[29] If the dissolution residue was observed before the impedance measurement, the solution was regarded as "saturated." The dissolution residue in the saturated solution was removed using a polytetrafluoroethylene (PTFE) filter with 0.45 μm pore size. The QCM substrate was set in the cup-shaped folder. The alkaline aqueous solutions saturated with PHS were

dropped onto the QCM substrate using a Pasteur pipette until the QCM output became constant. The impedance was measured at 23 °C using the QCM digital controller.

2-2-3. Results and discussion

2-2-3-1. The impedance of alkaline aqueous solutions with PHS

The impedance of alkaline aqueous solutions with PHS was measured. The impedance changes caused by the PHS saturation $\Delta Z_{saturation}$ are listed in **Table 2-2**. PR0, PR5, PR10, PR15, and PR25 represent 0, 5, 10, 15, 25 mol% tBOC-protected PHS. $\Delta Z_{saturation}$ of 0.26 mol l−1 TMAH aqueous solution with PHS (PR0) was 55.8 Ω.[28] The solubilities of PHS in 0.26 mol l^{-1} KOH and NaOH aqueous solutions are considered not to much differ from that in 0.26 mol l^{-1} TMAH aqueous solution (a standard developer).

Table 2-2. The impedance changes of 0.26 mol l^{-1} alkaline aqueous solutions saturated with PHS. The base line was the impedance of pure developer.

Alkaline	$\Delta Z_{saturation}$ (Ω)				
	PR0	PR5	PR10	PR15	PR25
KOH	50	42	45	29	14
NaOH	62	45	52	43	23

2-2-3-2. PHS dissolution kinetics in 0.26 mol l^{-1} KOH and NaOH aqueous solutions

The dissolution dynamics of PHS (PR0) films in 0.26 mol l^{-1} KOH and NaOH aqueous solutions were measured by the QCM method. The QCM charts are shown in **Fig. 2-10**. The baseline of frequency change Δf was set at the frequency of QCM substrate with PHS film in the atmosphere. The baseline of impedance change ΔZ was set at the impedance of the QCM substrate in neat KOH and NaOH aqueous solutions. The QCM charts obtained for the film thickness of 300 nm are first discussed. Δf dropped immediately after immersing the QCM substrates into KOH and NaOH aqueous solutions, then increased linearly, and finally became constant or nearly constant. The initial drop of Δf indicates

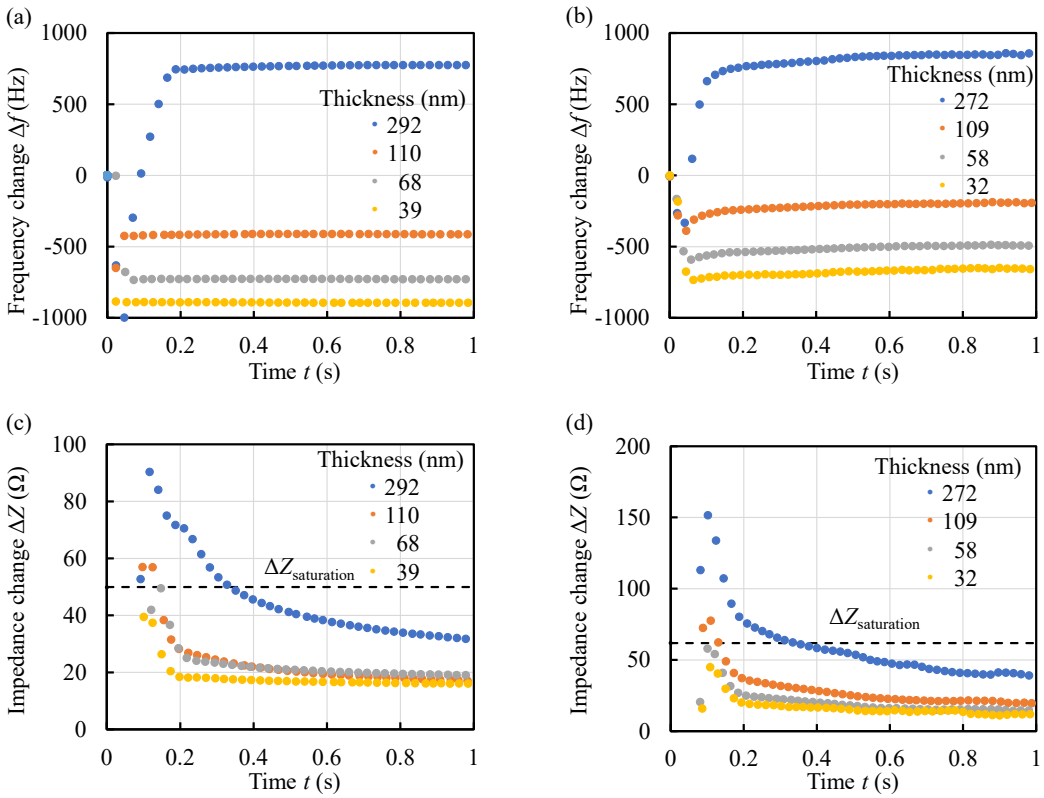

Fig. 2-10. QCM charts of PHS (PR0) films during development in (a), (c) 0.26 mol l^{-1} KOH and (b), (d) 0.26 mol l^{-1} NaOH aqueous solutions.

the increase of viscosity around the QCM substrate caused by the change of its surroundings from gas to liquid. Δf increased with the weight loss of PHS (PR0) film caused by the dissolution. If the PHS (PR0) films are completely dissolved, Δf became constant, as observed in 0.26 mol l^{-1} KOH aqueous solution [**Fig. 2-10(a)**]. In the case of 0.26 mol l^{-1} TMAH aqueous solution, Δf was reported to become constant, similar to 0.26 mol l^{-1} KOH aqueous solution.[20] However, Δf slowly increased after the rapid increase in 0.26 mol l^{-1} NaOH aqueous solution. The PHS (PR0) film with 300 nm thickness was reported to require approximately 0.4 s for the complete dissolution in 0.26 mol l^{-1} TMAH aqueous solution.[20] The dissolution times were approximately 0.2 and 0.1 s in 0.26 mol l^{-1} KOH and NaOH aqueous solutions, respectively, if the slow increase of Δf observed in NaOH aqueous solution is neglected. The ionic radius of potassium cation is larger than that of sodium cation. The basicity of KOH is higher than that of NaOH.[30-32] Therefore, the size of the cation rather than basicity is considered to have affected the dissolution rate. When a polymer film swells, Δf decreases lower than

Δf due to the viscosity of the developer (roughly −800 Hz), by gaining weight by absorbing developer molecules. Hereafter, $\Delta f_{\text{developer}}$ denotes the initial decrease of Δf due to the viscosity of the developer. Δf of PHS (PR0) film reached −1000 Hz in 0.26 mol l^{-1} KOH aqueous solution, although it was close to the time resolution of the QCM apparatus. Such a decrease in Δf suggests the formation of a transient swelling layer. In spite of slower dissolution than in KOH aqueous solution, the decrease in Δf immediately after the immersion into 0.26 mol l^{-1} TMAH aqueous solution was smaller than that in 0.26 mol l^{-1} KOH aqueous solution. (Δf immediately after the immersion almost agreed with $\Delta f_{\text{developer}}$ in 0.26 mol l^{-1} TMAH aqueous solution).[20] Considering these facts, Δf immediately after the immersion into 0.26 mol l^{-1} NaOH aqueous solution probably exceeded $\Delta f_{\text{developer}}$, although it was not observed owing to the insufficient time resolution. Hereafter, ΔZ of PHS (PR0) film with a thickness of 300 nm is discussed. ΔZ indicates the viscosity of the developer when the polymer film is sufficiently rigid. When the polymer film is softened by swelling, ΔZ mainly indicates the viscosity of the polymer film, because the viscosity of polymer film is generally larger than that of the developer.[20] In either case, the increase of ΔZ indicates the increase of viscosity. The dashed lines in **Figs. 2-10(c)** and **2-10(d)** indicate the corresponding $\Delta Z_{\text{saturation}}$. Although ΔZ reachable during development approximately agreed with $\Delta Z_{\text{saturation}}$ in 0.26 mol l^{-1} TMAH aqueous solution,[20] ΔZ significantly exceeded $\Delta Z_{\text{saturation}}$ in 0.26 mol l^{-1} KOH and NaOH aqueous solutions. In 0.26 mol l^{-1} TMAH aqueous solution, the speed of the dissolution (the complete or nearly complete separation of molecular interaction between polymer molecules) of PHS molecules is almost equal to the speed of the diffusion of PHS molecules because the swelling was hardly observed.[20] However, the speed of the dissolution in 0.26 mol l^{-1} KOH and NaOH aqueous solutions is considered to be faster than the diffusion of PHS molecules because the diffusion of potassium and sodium cations into PHS films is faster than TMA cations owing to their small sizes. Thereby, the oversaturated condition was temporarily created near the surface of PHS films. The increase of ΔZ was more prominent for sodium cations than potassium cations. For the decay of ΔZ kinetics in 0.26 mol l^{-1} KOH aqueous solution, a shoulder was observed,

as shown in **Fig. 2-10(c)**. This shoulder is considered to be a short version of similar kinetics observed during the development of poly(4-hydroxystyreneco-methacrylic acid) (PHSMA) film.[33] It was clearly observed that the thickness of the transient swelling layer was kept constant for a while during the development of PHSMA in diluted TMAH developer. This is typical for the dissolution with Case II diffusion.[34-37] The shoulder observed in **Fig. 2-10(c)** suggests that the thickness of the transient swelling layer (oversaturated region) was temporarily constant. Such a shoulder was not observed in 0.26 mol l^{-1} NaOH aqueous solution. This is because the time resolution was insufficient or because the transient swelling layer was too thick to be observed. Either way, this was caused by the smallness of sodium cations. The dissolution of PHS (PR0) films with thicknesses of 110, 60, and 30 nm is considered to proceed similarly to that with a thickness of 300 nm.

2-2-3-3. PHS dissolution kinetics dependency on KOH and NaOH concentrations

The effects of alkaline concentration on the dissolution kinetics were investigated, by diluting 0.26 mol l^{-1} alkaline aqueous solutions. The QCM charts obtained for PHS (PR0) films with a thickness of 300 nm are shown in **Fig. 2-11**. The dissolution rate was decreased with the dilution. For KOH aqueous solutions, the PHS (PR0) films dissolved with similar kinetics within the KOH concentration range of 0.13–0.26 mol l^{-1}. The shoulder observed in **Fig. 2-10(c)** became evident by the dilution, as shown in the inset of **Fig. 2-11(c)**. The flat part of the shoulder slightly increased with development time, which suggests that the thickness of the transient swelling layer slightly increased with the progress of development. When the KOH concentration decreased to 0.065 mol l^{-1}, the dissolution kinetics was significantly changed. Δf slowly decreased until 4 s after immersion, then slowly increased until 6 s, and rapidly increased to be completely dissolved. ΔZ slowly increased until 5 s after immersion, then rapidly increased, reached the maximum value at 7 s earlier than the dissolution time (the time when Δf became constant) (8 s), and finally decreased. The rapid dissolution started after the rapid swelling of the PHS (PR0) film. The difference between the peak time of ΔZ and the dissolution time is caused

probably because there still remained a swollen film on the QCM substrate after reaching the fully swollen condition. At 0.026 mol l^{-1}, a slow swelling was observed.

The kinetics in the 0.17 mol l^{-1} NaOH aqueous solution was similar to that in the 0.26 mol l^{-1} solution. At 0.13 and 0.065 mol l^{-1}, a shoulder was observed in the decay of ΔZ, as shown in **Fig. 2-11(d)**. At 0.026 mol l^{-1}, the dissolution kinetics were significantly changed, similar to the case of 0.065 mol l^{-1} KOH aqueous solution. Δf rapidly decreased until 10 s after immersion, then rapidly increased, and reached a constant value approximately at 25 s. ΔZ reached the maximum approximately at 15 s. The peak time of ΔZ did not agree with the dissolution time, similar to the case of the KOH solution. The swelling in 0.026 mol l^{-1} NaOH aqueous solution was larger than that in 0.065 mol l^{-1} KOH aqueous solution.

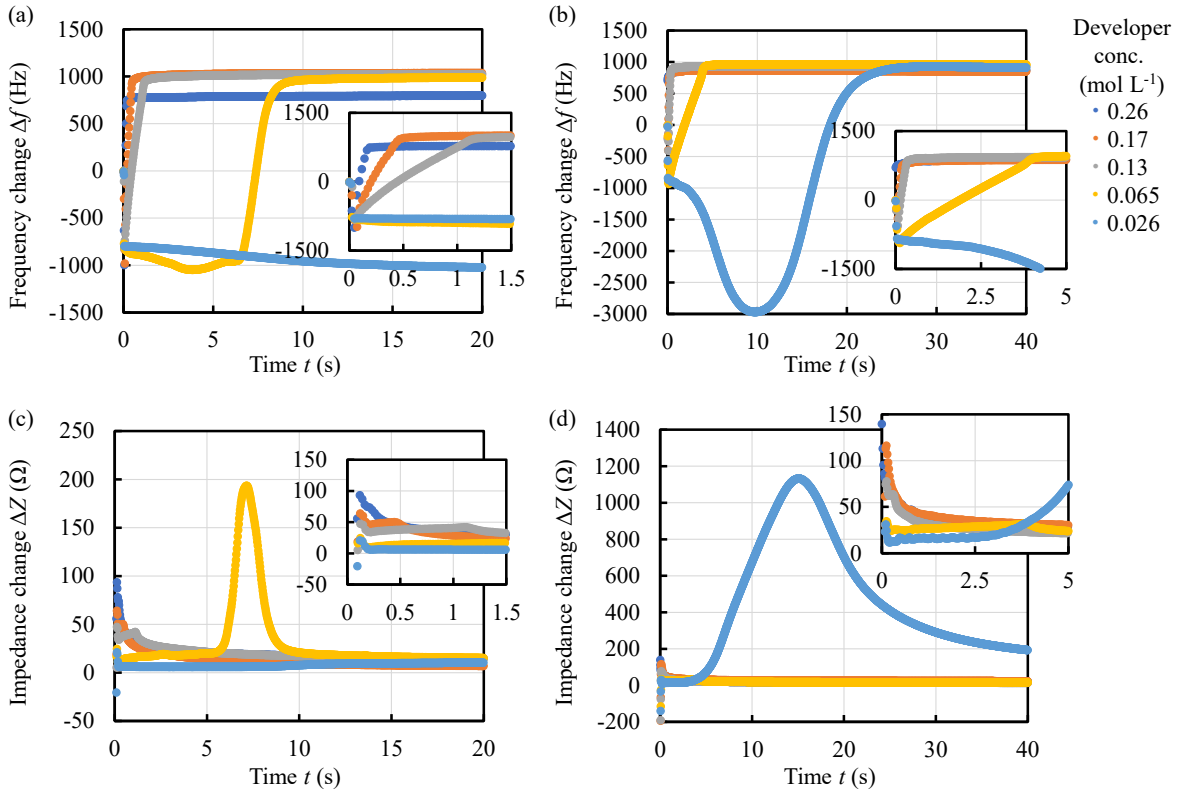

Fig. 2-11. QCM charts of PHS (PR0) films during development in (a), (c) KOH and (b), (d) NaOH aqueous solutions. The alkaline concentrations were 0.26, 0.17, 0.13, 0.065, and 0.026 mol l^{-1}. The initial thickness of PHS films was approximately 300 nm. The insets are enlarged graphs. The vertical axes of insets represent (a), (b) frequency change in Hz and (c), (d) impedance change in Ω. The horizontal axes represent the development time in s.

2-2-3-4. Dissolution kinetics dependency on the protection ratio of hydroxyl groups of PHS

The effects of the polarity of the polymer on the dissolution kinetics were investigated by partially protecting the hydroxyl groups of PHS molecules with tBOC. **Figure 2-12** shows the QCM charts obtained by changing the protection ratio of PHS. The dissolution rate decreased with the protection ratio, namely, the nonpolar component of PHS films. In both 0.26 mol l^{-1} KOH and NaOH aqueous solutions, the PHS films dissolved within the protection ratio range of 0–25 mol%, while they did not dissolve without showing a change in Δf and ΔZ at the protection ratio higher than 35%. For 0.26 mol l^{-1} KOH aqueous solution, PHS (PR0-PR15) dissolved with similar kinetics. The duration of the "flat" part of the shoulder in the decay of ΔZ extended with the increase of protection ratio. The "flat" part was not actually flat and increased linearly with the development time, which suggests that the transient swelling layer became thick with development time. This trend was more evident upon the increase of the nonpolar component of PHS films [**Fig. 2-12(c)**] than upon the decrease of alkaline concentration [**Fig. 2-11(c)**]. The kinetics of ΔZ for PHS (PR25) film resembled those for PHS (PR0) films in 0.065 mol l^{-1} KOH and 0.026 mol l^{-1} NaOH aqueous solutions. This suggests that the nonpolar interaction between polymer molecules had a significant impact on the dissolution dynamics at the protection ratio of 25 mol%. For 0.26 mol l^{-1} NaOH aqueous solution, the shoulder in the decay of ΔZ started to be observed when the protection ratio increased to 5 mol% and showed a similar trend observed in KOH aqueous solution. When the protection ratio increased, a large increase of ΔZ (>100 Ω) was not observed during the development in both 0.26 mol l^{-1} KOH and NaOH aqueous solutions, unlike the case when the alkaline concentration was decreased. This is probably because the capacity of containing water decreased with the protection of hydroxyl groups.

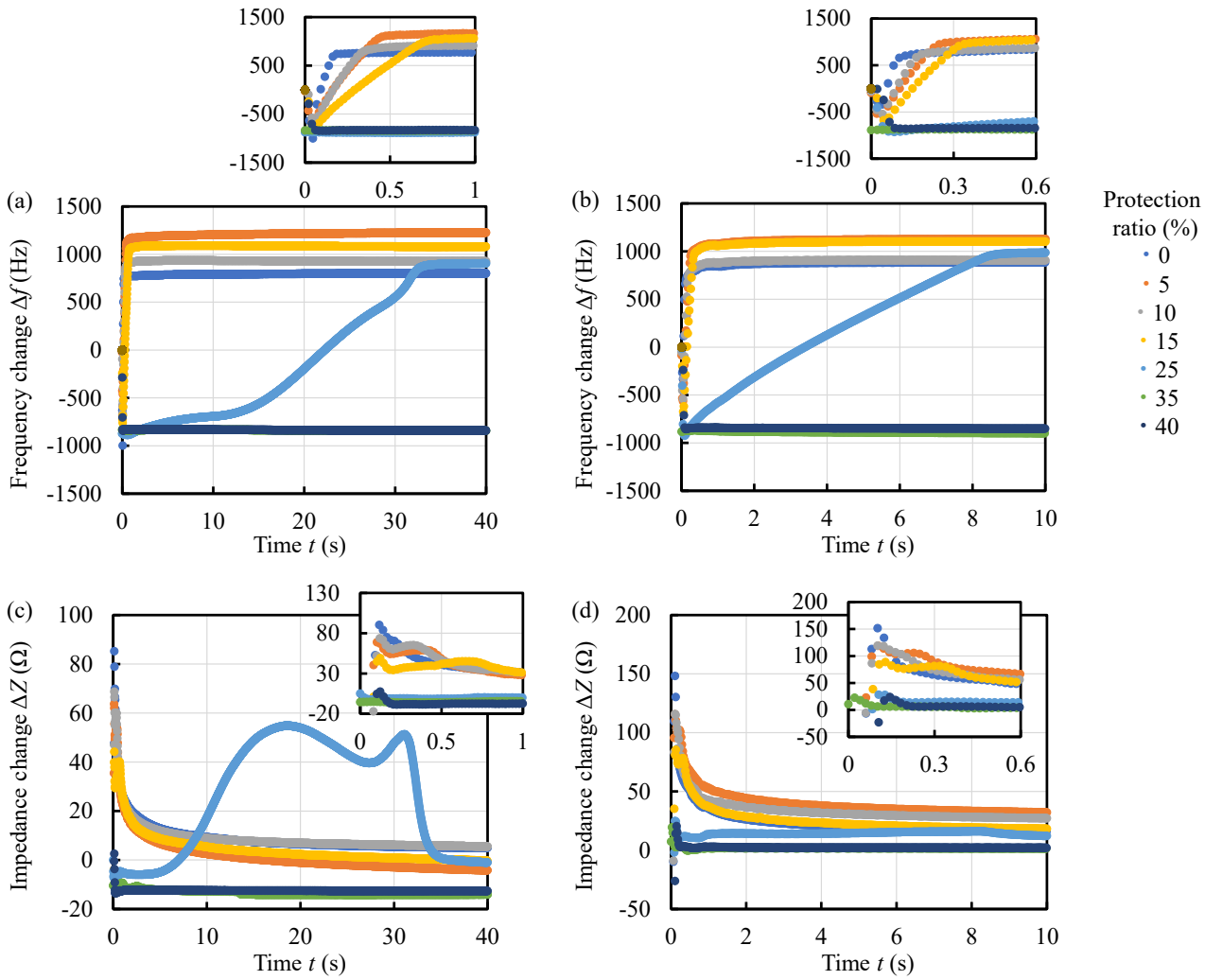

Fig. 2-12. QCM charts of PHS films during development in (a), (c) KOH aqueous solution and (b), (d) NaOH aqueous solution. The alkaline concentration was 0.26 mol l−1. The initial thickness of PHS films was approximately 300 nm. The insets are enlarged graphs. The vertical axes of insets represent (a), (b) frequency change in Hz and (c), (d) impedance change in Ω. The horizontal axes represent the development time in s.

2-2-4. Conclusion

The dissolution dynamics of PHS in KOH and NaOH aqueous solutions were investigated to clarify the effects of small alkaline cations on the dissolution dynamics of typical backbone polymer for CARs by the QCM method. Because of the smallness of alkaline cations, the partially protected PHS films showed characteristic dissolution dynamics, which are different from those observed in TMAH aqueous solutions. The maximum impedance reachable during development significantly exceeded that of the developer saturated with PHS, unlike the case of tetramethylammonium cation. The speed

of the dissolution in 0.26 mol l^{-1} KOH and NaOH aqueous solutions is considered to be faster than the diffusion of PHS molecules because of the fast diffusion of potassium and sodium cations into PHS films. Thereby, the oversaturated condition was temporarily created near the surface of PHS films. It was found that the transient swelling layer became thick by either increasing or decreasing the size of alkaline cations from tetramethylammonium and tetraethylammonium cations.

References

1) A. B. Kelleher, presented at SPIE Advanced Lithography + Patterning (San Jose, CA, 2024).
2) J. G. Garcia-Santaclara, R. Peeters, R. Ballegoij, S. Lok, J. Schoot, Paul Gräupner, P. Kuerz, J. Mallmann, G. Storms, and P. Vanoppen, presented at SPIE Advanced Lithography + Patterning (San Jose, CA, Protectionnn2024).
3) J. Schoot, E. Setten, K. Troost, S. Lok, R. Peeters, J. Stoeldraijer, J. Benschop, J. Zimmermann, P. Graeupner, P. Kuerz, and W. Kaiser, Proc. SPIE **11323**, 1132307 (2020).
4) D. F. Kyser, J. Vac. Sci. Technol. B **1**, 1391 (1983).
5) D. R. S. Cumming, S. Thoms, S. P. Beaumont, and J. M. R. Weaver, Appl. Phys. Lett. **68**, 322 (1996).
6) S. Yasin, D. G. Hasko, and H. Ahmed, Appl. Phys. Lett. **78**, 2760 (2001).
7) E. A. Dobisz, S. L. Brandow, R. Bass, and J. Mitterender, J. Vac. Sci. Technol. B **18**, 107 (2000).
8) W. Chen and H. Ahmed, Appl. Phys. Lett. **62**, 1499 (1993).
9) W. Chen and H. Ahmed, J. Vac. Sci. Technol. B **11**, 2519 (1993).
10) S. Yasin, D. G. Hasko, and H. Ahmed, Appl. Phys. Lett. **78**, 2760 (2001).
11) M. Khoury and D. K. Ferry, J. Vac. Sci. Technol. B **14**, 75 (1996).
12) A. N. Broers, A. C. F. Hoole, and J. M. Ryan, Microelectron. Eng. **32**, 131 (1996).
13) S. Takechi, A. Kotachi, M. Takahashi, and I. Hanyu, Proc. SPIE **3049**, 519 (1997).
14) T. Itani and J. J. Santillan, J. Vac. Sci. Technol. B **27**, 2986 (2009).
15) K. Matsunaga, H. Oizumi, K. Kaneyama, G. Shiraishi, K. Matsumaro, J. J. Santillan, and T. Itani, J. Photopolym. Sci. Technol. **23**, 613 (2010).
16) T. Itani and J. J. Santillan, Appl. Phys. Express **3**, 096501 (2010).
17) G. Sauerbrey, Z. Phys. **155**, 206 (1959).
18) A. Nakajima, K. Watanabe, K. Matsuoka, T. Kozawa, Y. Komuro, D. Kawana, and A. Yamazaki, Jpn. J. Appl. Phys. **59**, 036505 (2020).
19) T. Otsuka, Y. Jin, N. Tanaka, and T. Kozawa, Jpn. J. Appl. Phys. **61**, 056503 (2022).
20) Y. T. Ito, H. Betsumiya, T. Kozawa, K. Sakamoto, and M. Muramatsu, Jpn. J. Appl. Phys. **61**, 066506 (2022).
21) H. Betsumiya, Y. T. Ito, T. Kozawa, K. Sakamoto, and M. Muramatsu, Jpn. J. Appl. Phys. **62**,

036503 (2023).
22) H. Betsumiya, Y. Jin, Y. T. Ito, T. Kozawa, K. Sakamoto, and M. Muramatsu, Jpn. J. Appl. Phys. **62**, 066501 (2023).
23) Y. Iwashige, Y. T. Ito, T. Kozawa, K. Sakamoto, and M. Muramatsu, Jpn. J. Appl. Phys. **62**, 036502 (2023).
24) Y. T. Ito and T. Kozawa, Jpn. J. Appl. Phys. **61**, 016502 (2022).
25) N. Tanaka, K. Watanabe, K. Matsuoka, K. Azumagawa, T. Kozawa, T. Ikeda, Y. Komuro, and D. Kawana, Jpn. J. Appl. Phys. **60**, 066503 (2021).
26) N. Tanaka, T. Kozawa, T. Ikeda, Y. Komuro, and D. Kawana, Jpn. J. Appl. Phys. **61**, 086509 (2022).
27) A. Sekiguchi, J. Photopolymer Sci. Technol. **26**, 479 (2013).
28) Y. T. Ito, K. Watanabe, Y. Jin, T. Kozawa, K. Sakamoto, and M. Muramatsu, Jpn. J. Appl. Phys. **63**, 018002 (2024).
29) K. Nakamura, T. Nakajima, H. Kayahara, E. Nomura, and H. Taniguchi, Tetrahedron Lett. **45**, 495 (2004).
30) R. H. Stokes, J. Am. Chem. Soc. **67**, 1689 (1945).
31) S. Licht, Anal. Chem. **57**, 514 (1985).
32) G. Wilczek-Vera, E. Rodil, and J. H. Vera, AIChE J. **50**, 445 (2004).
33) Y. Iwashige, K. Watanabe, Y. T. Ito, T. Kozawa, K. Sakamoto, and M. Muramatsu, Jpn. J. Appl. Phys. **63**, 026504 (2024).
34) C. Y. Hui and K. C. Wu, J. Appl. Phys. **61**, 5129 (1987).
35) N. L. Thomas and A. H. Windle, Polymer **23**, 529 (1982).
36) C. Y. Hui, K. C. Wu, R. C. Lasky, and E. J. Kramer, J. Appl. Phys. **61**, 5137 (1987).
37) A. Tsuneishi, S. Uchiyama, and T. Kozawa, Jpn. J. Appl. Phys. **57**, 046501 (2018).

Chapter 3

Dissolution dynamics of PHS in organic developers

3-1. Introduction

Currently, highly sensitive resists, called chemically amplified resists (CARs),[1] have been used in the high-volume production lines of semiconductor devices. The dissolution dynamics of resist films in an industrial standard developer, 2.38 wt% (0.26 N) tetramethylammonium hydroxide (TMAH) aqueous solution has intensively been investigated,[2–8] because the resist materials should be optimized to the standard developer.

The pattern formation of CARs utilizes the dissolution of acidic polymer in an alkaline aqueous solution. In an alkaline aqueous developer, the acidic polymer films dissolved through the dissociation of hydroxyl (OH) groups. The typical acidic polymers for chemically amplified EUV resists are poly(4-hydroxystyrene) (PHS) and poly(4-hydroxystyrene-co-methacrylic acid) (PHSMA). PHS has OH groups with pK_a 9.87[9] and is dissolved in the standard developer, the pH of which is approximately 13. On the other hand, PHS is insoluble in pure water (pH 7). During development, pH near the PHS film surface is decreased by neutralization. Therefore, the maximum PHS concentration reachable during development approximately corresponds to the TMAH concentration.[10] The dissolution rate is limited by the neutralization.[10] **Figure 1-4** shows the dissolution kinetics of PHS films in 2.38 wt% TMAH aqueous developer. PHSMA has OH groups with pK_as of 9.87 (phenolic OH groups) and 4.76 (carboxylic acids).[9] The OH groups with pK_a 4.76 are preferentially dissociated in the standard developer, while the OH groups with pK_a 9.87 still maintain the hydrogen bonding.[11] This leads to the formation of a swelling layer thicker than in the case of PHS films.[11] Thus, in PHSMA, which is the most favorite base polymer for chemically amplified EUV resists, the OH groups that are not dissociated in the 2.38 wt% TMAH aqueous developer play an important role in the formation of the thick swelling layer. The control of the swelling layer caused by the phenolic OH groups is important for the suppression of resist pattern defects.

The alternative alkalis such as tetrabutylammonium hydroxide have been examined for improving the performance of CARs.[12–19] The organic developers have also been used for the negative tone

development of CARs although their range of application is limited.[1,20,21] The metal oxide resists (MORs)[22,23] and main-chain-scission-type resists[24,25] with organic developers have recently attracted much attention. Although the dissolution kinetics in organic developers has been investigated, the details are still unclear.[26–31] Fundamental understanding of dissolution dynamics is important because the development process is key to the formation of ultrafine resist patterns. In this study, we investigated the dissolution dynamics of partially protected PHS in organic developers by a quartz crystal microbalance (QCM) method to deepen the fundamental understanding of the dissolution dynamics of CARs. The PHS molecules in solid films are connected to each other through polar and nonpolar molecular interaction and hydrogen bonds. Although the dissociation of phenolic OH groups is considered to play a major role in the dissolution of PHS films, it is important to clarify the effects of the other interactions. We discuss the dissolution dynamics of PHS films observed in the solvents, in which the phenolic OH groups are hardly dissociated. Note that this study does not aim at developing the organic developers for the negative tone development of CARs. We aimed to obtain the fundamental knowledge of how the dissolution kinetics shown in **Fig. 1-4** changes when the phenolic OH groups are not dissociated, by using the organic developers. In this study, we used not PHSMA but PHS to eliminate the effect of hydrogen bonding due to the OH groups of carboxylic acids, because the methacrylic acid dissociates in water.

3-2. Experimental methods

3-2-1. Materials

Methanol, ethanol, 1-propanol, 2-propanol, 1-butanol, ethyl acetate, butyl acetate, and hexyl acetate were used as developers. Propylene glycol monomethyl ether acetate (PGMEA) was used as a casting solvent for PHS (Mw 11000). The polydispersity of PHS was 2.41. All the solvents and PHS were purchased from Sigma-Aldrich. The partially protected PHS were prepared by protecting the hydroxyl groups of PHS with t-butoxycarbonyl groups. The protection ratios were 25, 50, and 70 mol%.

Hereafter, PHS molecules with the protection ratios of 0, 25, 50, and 70 mol% are expressed as PR0, PR25, PR50, and PR70, respectively, for convenience. The partially protected PHS film is also hereafter simply called a PHS film unless otherwise specified.

3-2-2. Impedance and QCM measurement

The relationship between the impedance change ΔZ and PHS concentration is expressed as[14)]

$$\Delta Z = Z - Z_S = \alpha_Z C_{PHS}. \quad (3\text{-}1)$$

Here, Z_s and α_Z are an impedance of pure developer and a proportionality constant. α_Z indicates the effect of polymer concentration on the developer viscosity. The impedance of PHS solutions was measured to determine α_Z. PHS powders were dissolved in the developer by applying ultrasonic agitation. The concentrations of PHS monomer units were adjusted within a 0–0.5M range. Hereafter, the concentration of PHS monomer units is simply called PHS concentration for convenience. The solutions were left to stand for 1 d. The QCM substrate was set in the cup-shaped folder. The PHS solutions were dropped onto the QCM substrate using a Pasteur pipette until the QCM output became constant. The impedance was measured at 23 °C using the QCM digital controller (Stanford Research Systems QCM200).

For the measurement of dissolution kinetics, PHS powders were dissolved in PGMEA and the concentration was adjusted to prepare films with thicknesses of approximately 300 nm. The films spin-coated onto QCM substrates were prebaked at 90 °C for 90 s. The dissolution kinetics of PHS films was measured using a QCM-based development analyzer (Litho Tech Japan RDAQz3).[32)] QCM measurement yields the weight and viscosity changes on Au electrodes sandwiching the quartz crystal by detecting the resonance frequency of the quartz crystal and the impedance of the QCM device circuit, respectively. The decrease and increase in weight should correspond to the swelling and dissolution of the polymer, respectively. The change in frequency obtained by measurement is related to the change in weight in accordance with Sauerbrey's equation.[33)] The films were developed in the

developers at 23 °C and then rinsed in water. The film thicknesses before and after development were measured using an ellipsometer (Meiwafosis FS-1).

3-3. Results and discussion

3-3-1. Physical properties of materials

The relative dielectric constants, self-ionization constants, viscosity, and impedance of developers are listed in **Table 3-1**.[9,34–38] The relative dielectric constants of water and PHS are 80.2 and 5, respectively. The relative dielectric constant of the developer was changed between those of water and PHS (PR0). The self-ionization constants of pure water, 50% mixture with methanol, and 50% mixture with ethanol are 13.997, 14.097, and 14.88, respectively, at 25 °C.[9] The self-ionization constants of organic solvents used are higher than that of water. The acid dissociation constants pK_a of phenol in water and methanol are 9.87 and 14.2, respectively, at 25 °C.[9] As PHS is hardly dissociated in water, it is hardly dissociated in developers used in this study. The impedance ΔZ_{sol} in Table I is the impedance change induced when the QCM substrate was immersed into the pure developer. The baseline is the impedance in the atmosphere. Figure 2 shows the relationship between the measured ΔZ_{sol} and the viscosity of the developer. As previously reported,[10,39] the ΔZ_{sol} was well correlated with the viscosity. The viscosities of 50 vol% methanol, 50 vol% ethanol, 50 vol% 1-propanol, and 50 vol% 2-propanol aqueous developers were calculated using the fitting curve shown in **Fig. 3-1** and are listed in **Table 3-1**.

Table 3-1. Relative dielectric constant ε_r, self-ionization constant pK_{ap}, viscosity η, and impedance change ΔZ_{sol} of developers and PHS.

	ε_r at 20 °C	pK_{ap} [9]	η (mPa s) at 25 °C [35]	ΔZ_{sol} (Ω) at 23 °C
Water	80.2[9]	14.167	0.890[35]	255
Methanol	33.0[9]	16.71	0.544[35]	195
Ethanol	25.3[9]	18.9	1.074[35]	276
1-Propanol	20.8[9]	19.43	1.945[35]	378
2-Propanol	20.2[9]	20.3	2.04[35]	386
1-Butanol	17.8[9]	21.56	2.54[35]	451
50 vol% Methanol	-	-	1.60[a]	343
50 vol% Ethanol	-	-	2.29 [a]	427
50 vol% 1-Propanol	-	-	2.59 [a]	463
50 vol% 2-Propanol	-	-	2.92 [a]	503
Ethyl acetate	6.1[9]	22.83	0.423[35]	192
Butyl acetate	5.0 (23 °C)[34]	-	0.685[35]	233
Amyl acetate	4.8[9])	-	0.8618[37]	268
Hexyl acetate	4.4[35]	-	1.036[38]	292
PHS (PR0)	5[36]	-	-	-

a) These values were obtained by interpolating or extrapolating the reported viscosities using ΔZsol.

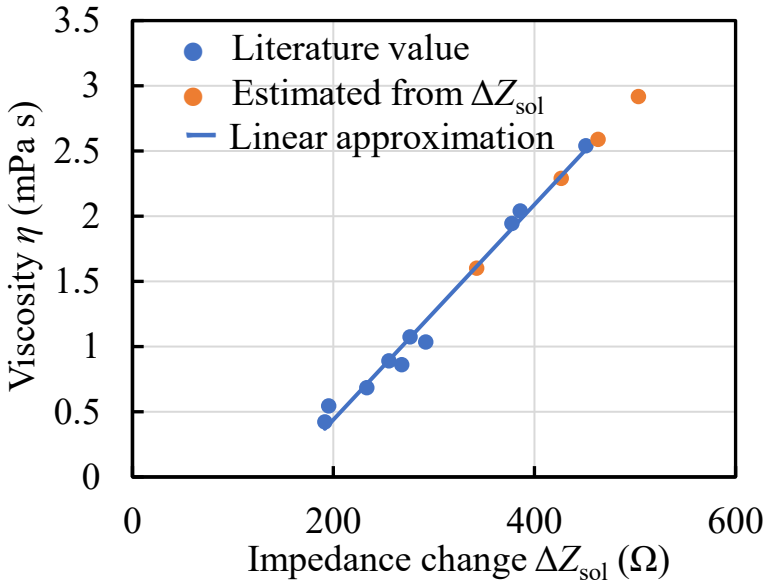

Fig. 3-1. Relationship between measured impedance change ΔZsol and viscosity. Blue dots indicate literature values for viscosity. Orange dots indicate viscosities estimated from ΔZsol. The solid line is a fitting curve (a linear approximation) to methanol, ethanol, 1-propanol, 2-propanol, 1- butanol, ethyl acetate, butyl acetate, amyl acetate, and hexyl acetate.

The solubility parameters of developers and PHS are listed in **Table 3-2**.[40] The solubility parameter δT of developers used ranges from 47.8 (water) to 17.4 $MPa^{1/2}$ (butyl acetate) and even smaller (amyl and hexyl acetates). The dispersion components of solubility parameters do not much differ. The polar components of solubility parameters ranged from 16.0 (water) to 3.7 $MPa^{1/2}$ (butyl acetate). The hydrogen bonding components of solubility parameters ranged from 42.3 (water) to 6.3 $MPa^{1/2}$ (butyl acetate). The surface free energy and its components of partially protected PHS films were calculated by the Kitazaki–Hata method[4] and are shown in **Fig. 3-2**. The surface free energy decreases with the increase of protection ratio. The polar and hydrogen bonding components of surface free energy decrease with the increase of protection ratio. The dispersion component of surface free energy slightly increases with the protection ratio.

Table 3-2. Solubility parameters of developers and PHS. δD, δP, and δH are the energies from dispersion forces between molecules, dipolar intermolecular forces between molecules, and hydrogen bonds between molecules, respectively. $\delta T=(\delta D^2+\delta P^2+\delta H^2)^{1/2}$.

	Solubility Parameters ($MPa^{1/2}$) at 25 °C[44]			
	δD	δP	δH	δT
Water	15.6	16.0	42.3	47.8
Methanol	15.1	12.3	22.3	29.6
Ethanol	15.8	8.8	19.4	26.5
1-Propanol	16.0	6.8	17.4	24.6
2-Propanol	15.8	6.1	16.4	23.6
1-Butanol	16.0	5.7	15.8	23.2
50 vol% Methanol	15.4	14.2	32.3	38.5
50 vol% Ethanol	15.7	12.4	30.9	36.8
50 vol% 1-Propanol	15.8	11.4	29.9	35.6
50 vol% 2-Propanol	15.7	11.1	29.4	35.1
Ethyl acetate	15.8	5.3	7.2	18.1
Butyl acetate	15.8	3.7	6.3	17.4
Amyl acetate	-	-	-	-
Hexyl acetate	-	-	-	-
PHS (PR0)[a]	17.6	10.0	13.7	24.4

*The solubility parameters of mixed solvents were obtained by the following equation:$[\delta D_m, \delta P_m, \delta H_m] = [(a \times \delta D_1 + b \times \delta D_2), (a \times \delta P_1 + b \times \delta P_2), (a \times \delta H_1 + b \times \delta H_2)]/(a + b)$,where a and b are the volumes of developers 1 and 2, respectively. a) These reported values were listed as a reference. For the polymers used in this study, see the surface free energies shown in **Fig. 3-2**.

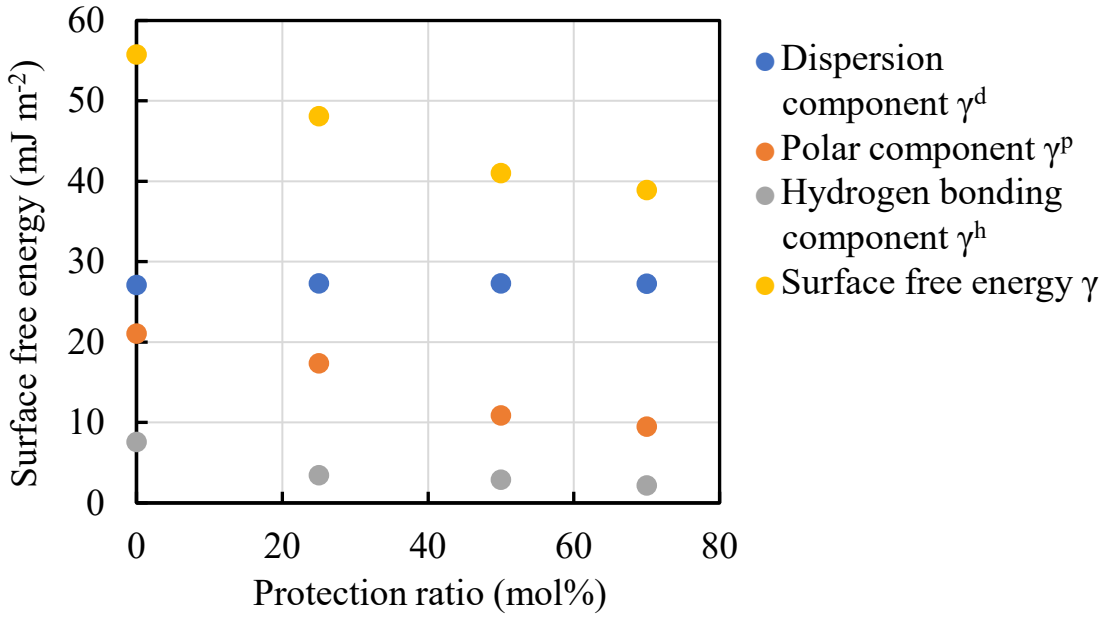

Fig. 3-2. Surface free energy γ of PHS films and its components calculated by Kitazaki–Hata method. The contact angles were measured 1 s after the landing of probe liquid droplets on PHS films. The probe liquids were water, diiodomethane, and hexadecane. Contact angles were taken from reference 19. γ^d, γ^p, and γ^h represent the dispersion, polar, and hydrogen bonding components of surface free energy, respectively.

3-3-2. Alcohol aqueous developer

The polarity of alcohols is relatively high among organic solvents. Using alcohols, the dissolution dynamics of PHS films was investigated. Methanol, ethanol, 1-propanol, 2-propanol, 1-butanol, and their mixture solution with 50 vol% water were used as developers. The relationship between ΔZ and C_{PHS}, namely, α_Z, was measured for each pure alcohol, as shown in **Table 3-3**. α_Z tended to increase with the decrease of alcohol polarity. The relative dielectric constant of PHS is lower than those of alcohols as shown in **Table 3-1**. α_Z is considered to have increased because the polarity of alcohol approaches that of PHS by increasing the alkyl chain length of alcohol. The dependence of α_Z on the protection ratio was unclear.

Table 3-3. Proportionality constant α_Z of alcohol.

Alcohol	Conc. (vol%)	α_Z (Ω nm^3)			
		PR0	PR25	PR50	PR70
Methanol	100	199	159	154	101
	50	144	-	-	-
Ethanol	100	195	221	227	-
	50	205	265	-	-
1-Propanol	100	279	352	403	282
	50	307	397	-	-
1-Butanol	100	361	381	312	-

The QCM charts obtained in 50 vol% alcohol aqueous developers are shown in **Fig. 3-3**. The left column in **Fig. 3-3** shows the temporal change of Δf during development. The baseline of Δf was set to the frequency of the QCM substrate with a polymer film in the air. The right column in **Fig. 3-3** shows the temporal change of ΔZ during development. The baseline of ΔZ was set to the impedance of the QCM substrate without a polymer film in a developer. Upon the immersion of the QCM substrate into the developer, Δf dropped due to the viscosity of the developer for all the samples. The decreases of Δf due to the viscosity of developer Δf_{vis} were 964, 1341, 1373, and 1422 Hz for 50 vol% methanol, ethanol, 1-propanol, and 2-propanol aqueous developers, respectively. The impedance of 50 vol% methanol, 50 vol% ethanol, 50 vol% 1-propanol, and 50 vol% 2-propanol aqueous developers were 343, 427, 463, and 503 Ω, respectively. The impedance charts were converted to the temporal dependence of polymer concentration in monomer unit C_{PHS} using the proportionality constant α_Z in **Table 3-3**, as shown in **Figs. 3-4(a)**, **3-4(c)**, **3-4(e)**, and **3-4(g)**. The values in the concentration range higher than 0.4 M were obtained by extrapolation. Therefore, the accuracy in the concentration range higher than 0.4 M is low. However, it is clear that the PHS concentration near the dissolution front is significantly higher than that observed during the development of PHS films in the 2.38 wt% TMAH aqueous developer (**Fig. 1-4**). Similarly, the impedance chart was converted to the viscosity chart, using the relationship between impedance and viscosity shown in **Fig. 3-1**, as shown in **Figs. 3-4(b)**,

3-4(d), **3-4(f)**, and **3-4(h)**. For the impedance range higher than 500 Ω, the previously reported calibration curve, which was calibrated in the impedance range from 300 to 1500 Ω,[10] was applied for the conversion. Because the maximum impedance change measured in this study was smaller than 1500 Ω, the viscosity charts shown in this study are reliable.

For the same developer, the dissolution rate decreased with the increase of protection ratio, because the polarities of 50 vol% alcohol aqueous solutions are significantly higher than that of PHS. For the same protection ratio, the dissolution rate increased with the increase of the alkyl chain length of normal alcohol. The initial swelling kinetics in the 50 vol% alcohol aqueous developer was different from that in the 2.38 wt% TMAH aqueous developer. The initial decrease of Δf (the decrease from $-\Delta f_{vis}$) in the 50 vol% alcohol aqueous developer was larger than that in the 2.38 wt% TMAH aqueous solution (approximately 0).[16] The increase of impedance during development from the impedance of pure developer was also larger in the 50 vol% alcohol aqueous developers than in the 2.38 wt% TMAH aqueous developer (less than 60 Ω).[16] In PHS films, phenolic OH groups form hydrogen bond networks with other phenolic OH groups and make the films rigid.[42–44] In TMAH aqueous developer, the developer molecules penetrate the PHS film through the polar interaction, assisted by the dissociation of phenolic OH groups, which breaks the hydrogen bond networks in PHS film. Owing to the destruction of the hydrogen bond network, the transient swelling layer is considered to be hardly formed. However, in a 50 vol% alcohol aqueous solution, the nonpolar interaction of the alkyl groups of alcohol with polystyrene backbone plays an important role in the dissolution of polymer films in addition to the polar interaction, as can be seen from the increase of dissolution rate with the alkyl chain length of alcohol. The nonpolar interaction of the alkyl groups of alcohol with polystyrene backbone means the interaction of the alkyl chains of alcohol with the alkyl chains and benzene rings of poly(4-hydxosystyrene) through the London dispersion force. The dissolution rate in 1-propanol aqueous developer was higher than that in 2-propanol aqueous developer.

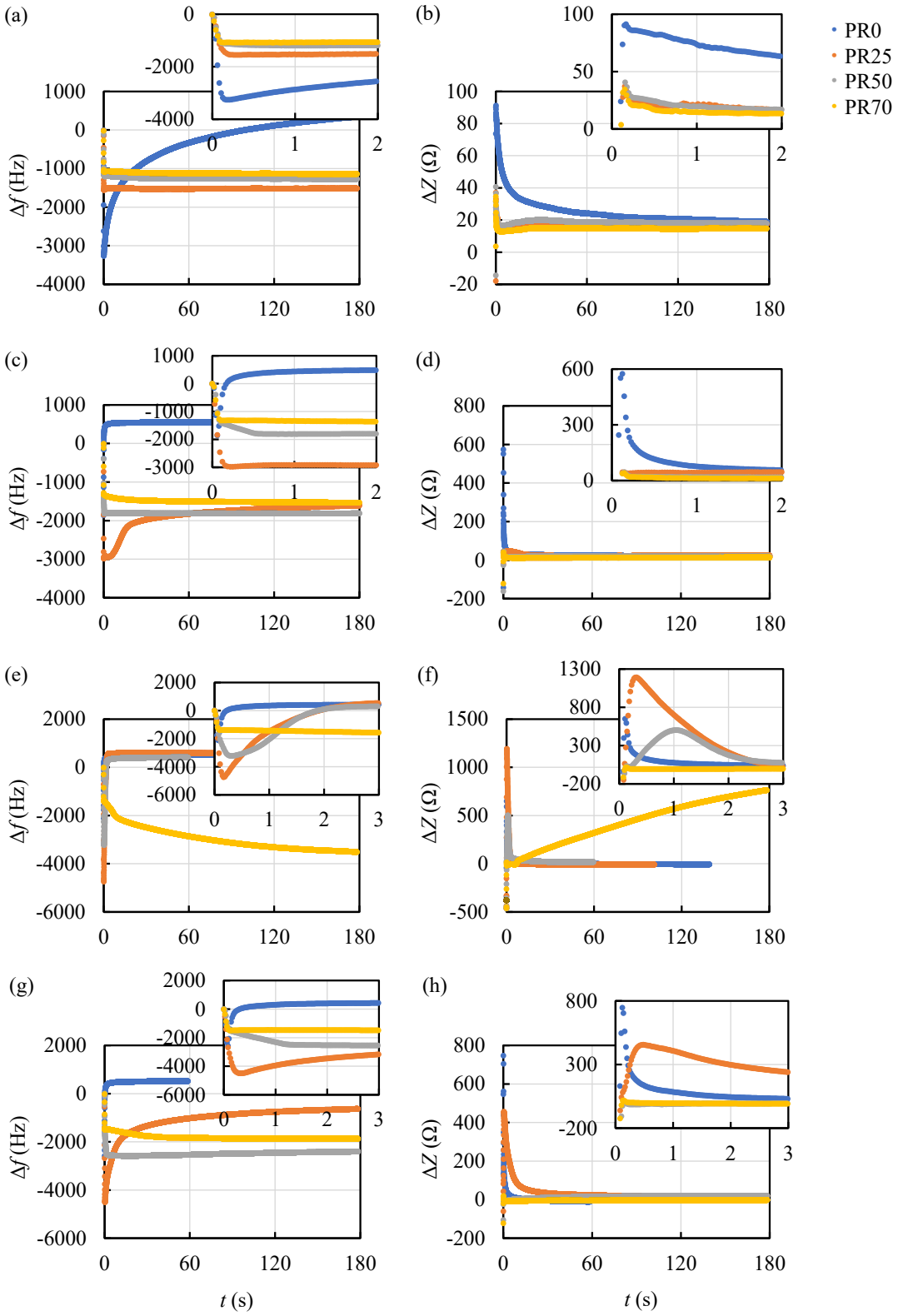

Fig. 3-3. QCM charts of PHS films developed in (a), (b) 50 vol% methanol, (c), (d) 50 vol% ethanol, (e), (f) 50 vol% 1-propanol and (g), (h) 50 vol% 2- propanol. The vertical axes in (a), (c), (e), and (g) represent the frequency change. The vertical axes in (b), (d), (f), and (h) represent the impedance change. The protection ratio was varied from 0 to 25, 50, and 70 mol%.

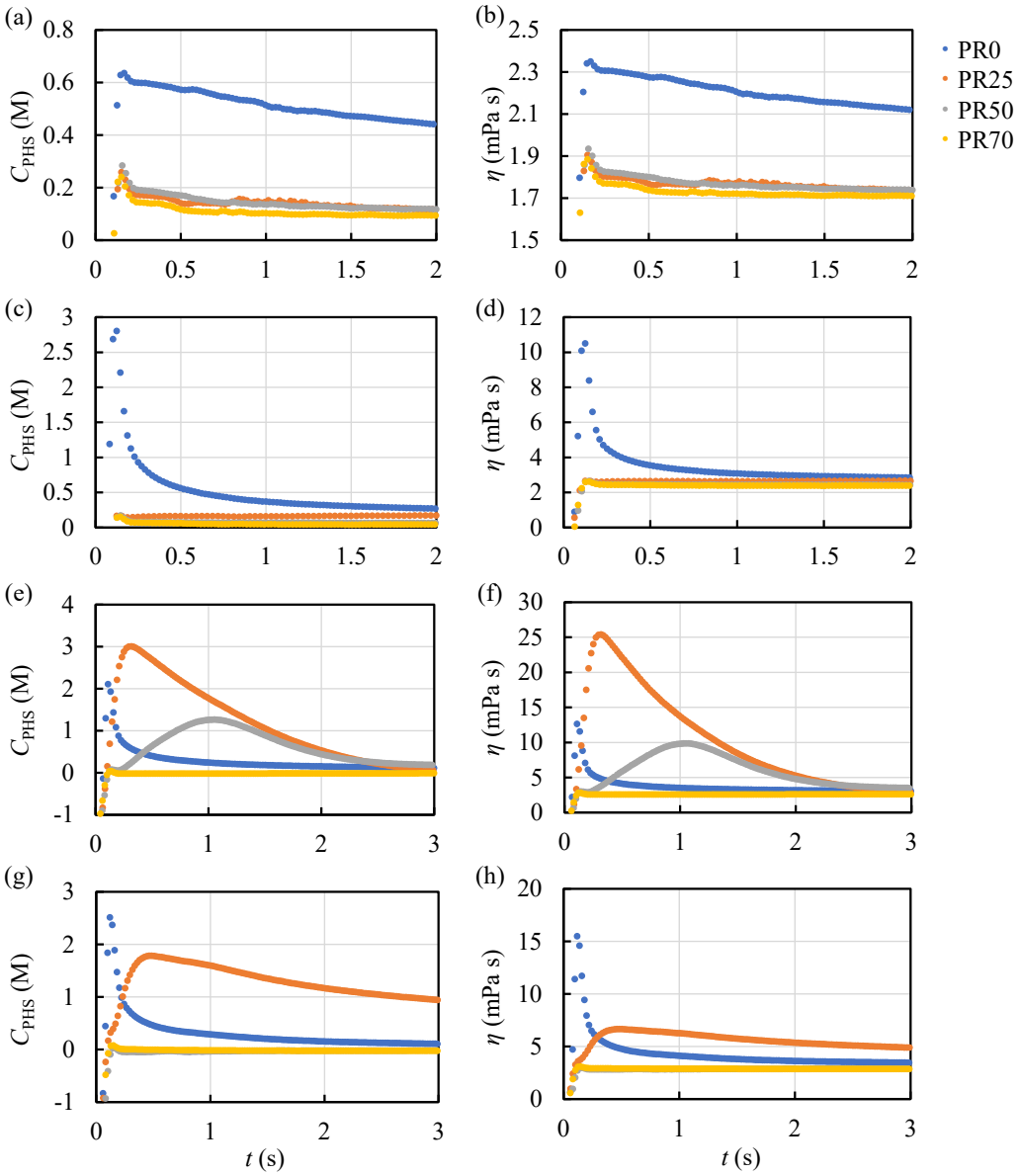

Fig. 3-4. Dissolution kinetics of PHS films in (a), (b) 50 vol% methanol, (c), (d) 50 vol% ethanol, (e), (f) 50 vol% 1-propanol and (g), (h) 50 vol% 2-propanol developers: (a), (c), (e), (g) PHS concentration chart near dissolution front C_{PHS} and (b), (d), (f), (h) viscosity chart. The protection ratio was varied from 0 to 25, 50, and 70 mol%.

This indicates that the normal alkyl chain is superior to the branched alkyl chain in separating PHS molecules. Unlike the dissolution in the TMAH aqueous developer, the hydrogen bond network is considered to play an important role in the formation of the transient swelling layer in the 50 vol% alcohol aqueous developer, because the phenolic OH groups are not dissociated.

In the samples that were neither dissolved nor swelled in developers [PR25 in **Figs. 3-3(a)** and **3-**

3(b) and PR50 in **Figs. 3-3(c)** and **3-3(d)**], the decrease of Δf from $-\Delta f_{vis}$ was observed immediately after the immersion. In such a case, both Δf and ΔZ were approximately constant in TMAH aqueous developer.[16] Although the alcohol molecules penetrated the free volumes of PHS films through the nonpolar interaction, the rigidity of PHS films was not changed probably due to the intact hydrogen bond networks. For the dissolution kinetics, PHS films were dissolved with Case II diffusion in a 2.38 wt% TMAH aqueous developer.[18] The characteristics of the dissolution kinetics with Case II diffusion are the formation of a transient swelling layer (dissolution front) and steady-state front motion (linear weight loss).[8,45–47] In 50 vol% alcohol aqueous developers, the steady-state front motion (a linear weight loss of PHS film) was not observed. In particular, the dissolution rate significantly decreased near the QCM substrate.

3-3-3. Alcohol developer

The QCM charts obtained in the development of PHS films in pure alcohols are shown in **Fig. 3-5**. Δf_{vis} was 545, 809, 1068, and 1291 Hz in methanol, ethanol, 1-propanol, and 1-butanol developers, respectively. The impedances of methanol, ethanol, 1-propanol, and 1-butanol developers were 195, 276, 378, and 451 Ω, respectively. QCM charts in **Fig. 3-5** were similarly converted to the concentration and viscosity charts, as shown in **Fig. 3-6**. For the same developer, PR0, PR25, and PR50 films were dissolved with approximately the same speed, and PR70 films were dissolved after being largely swelled. For all the alcohol developers used, the dissolution rate was largely changed at the protection ratio between 50 and 70 mol%. For the same protection ratio, the dissolution rate decreased with the increase of the alkyl chain length of alcohol except for the case of PR70 in methanol. In pure alcohol developers, the viscosity is considered to have affected the dissolution rate more than the polarity of alcohol, unlike the case of the 50 vol% alcohol aqueous developers. Except for PR0, PR25, and PR50 in methanol developers, the impedance change during development was significantly higher than that in the 2.38 wt% TMAH aqueous developer, similar to the case of 50 vol% alcohol aqueous

developers.

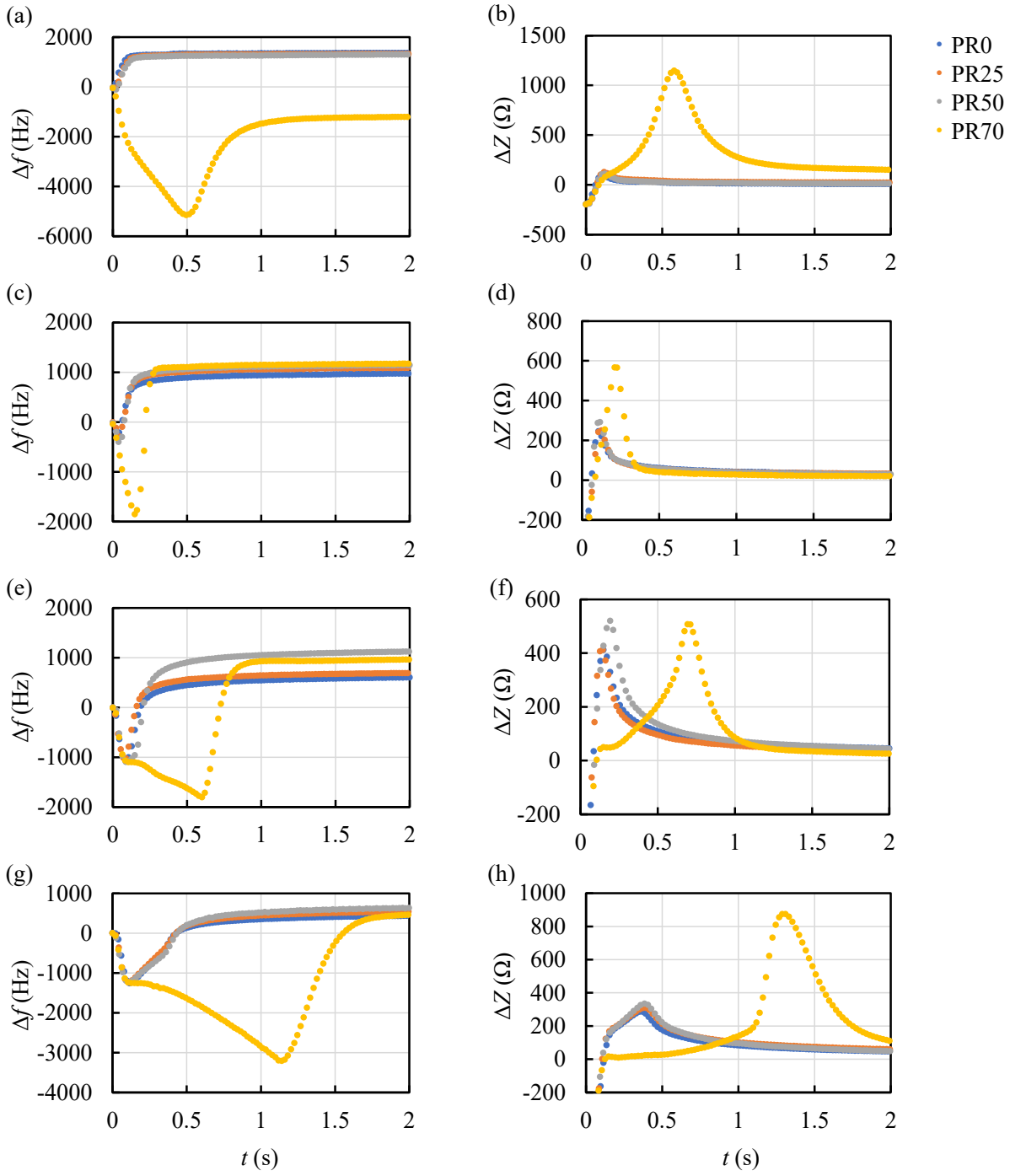

Fig. 3-5. QCM charts of PHS films developed in (a), (b) methanol, (c), (d) ethanol, (e), (f) 1-propanol, and (g), (h) 1-butanol. The vertical axes in (a), (c), (e), (g) represent the frequency change. The vertical axes in (b), (d), (f), (h) represent the impedance change. The protection ratio was varied from 0 to 25, 50, and 70 mol%.

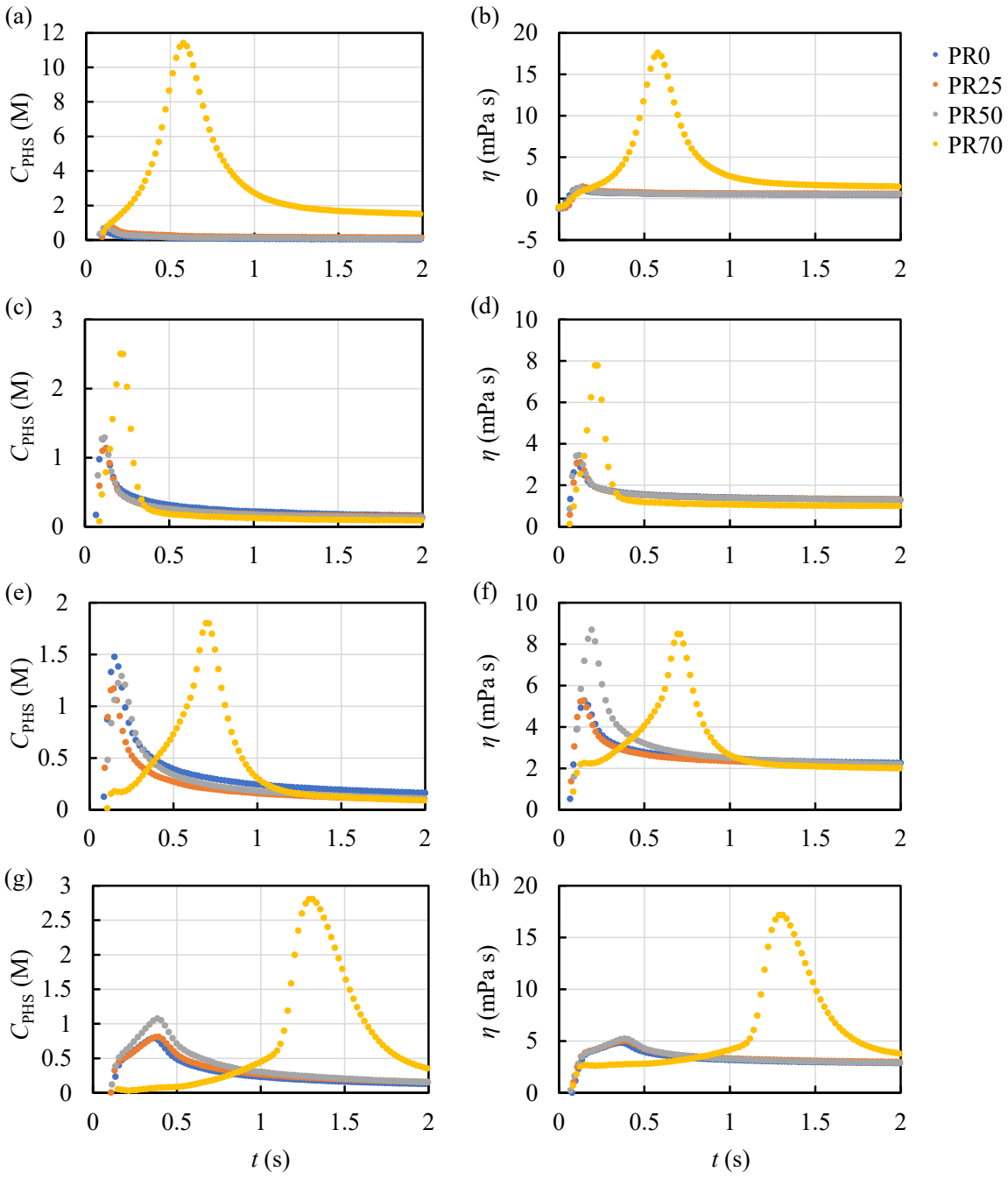

Fig. 3-6. Dissolution kinetics of PHS films in (a), (b) methanol, (c), (d) ethanol, (e), (f) 1-propanol and (g), (h) 2-propanol developers: (a), (c), (e), (g) PHS concentration chart near dissolution front and (b), (d), (f), (h) viscosity chart. The protection ratio was varied from 0 to 25, 50, and 70 mol%.

The large value of impedance change indicates the formation of a thick swelling layer. For PR0, PR25, and PR50, the maximum impedance change during development increased with increasing the alkyl chain length to three (propyl) and then decreased at the alkyl chain length of 4 (butyl). In 1-butanol

developer, the linear increases in Δf and ΔZ were observed at the development time of 0.1–0.4 s. Such a kinetics is characteristic of the dissolution with Case II diffusion. This kinetics is later discussed together with the results obtained using acetate developers. For PR0, PR25, and PR50 in methanol developer, the time resolution of the QCM apparatus may be inadequate.

3-3-4. Alkyl acetate developer

α_Z in alkyl acetates is listed in **Table 3-4**. α_Z increased with the decrease of polarity of alkyl acetates and with the increase of protection ratio. The dissolution dynamics was investigated using organic solvents with relatively low polarity: ethyl, butyl, and hexyl acetates, which are immiscible with water. The QCM charts obtained in the development of PHS films in alkyl acetate developers are shown in **Fig. 3-7**. Δf_{vis} was 514, 623, and 796 Hz in ethyl, butyl, and hexyl acetate developers, respectively. The impedances of ethyl, butyl, and hexyl acetate developers were 192, 233, and 292 Ω, respectively. QCM charts in **Fig. 3-7** were similarly converted to the concentration and viscosity charts, as shown in **Fig. 3-8**. For ethyl acetate developer, the dissolution kinetics of PHS films did not much depend on the protection ratio. The dissolution of PHS (PR0–70) films in ethyl acetate was close to the time resolution of the QCM apparatus. With the increase of alkyl chain length (the decrease of polarity), the dissolution rate decreased. This effect increased with the protection ratio. The dissolution rate in butyl and hexyl acetate developers increased with the protection ratio.

Table 3-4. Proportionality constant α_Z of alkyl acetate.

Developer	α_Z (Ω nm^3)			
	PR0	PR25	PR50	PR70
Ethyl acetate	132	157	161	180
Butyl acetate	173	212	206	234
Hexyl acetate	200	214	220	255

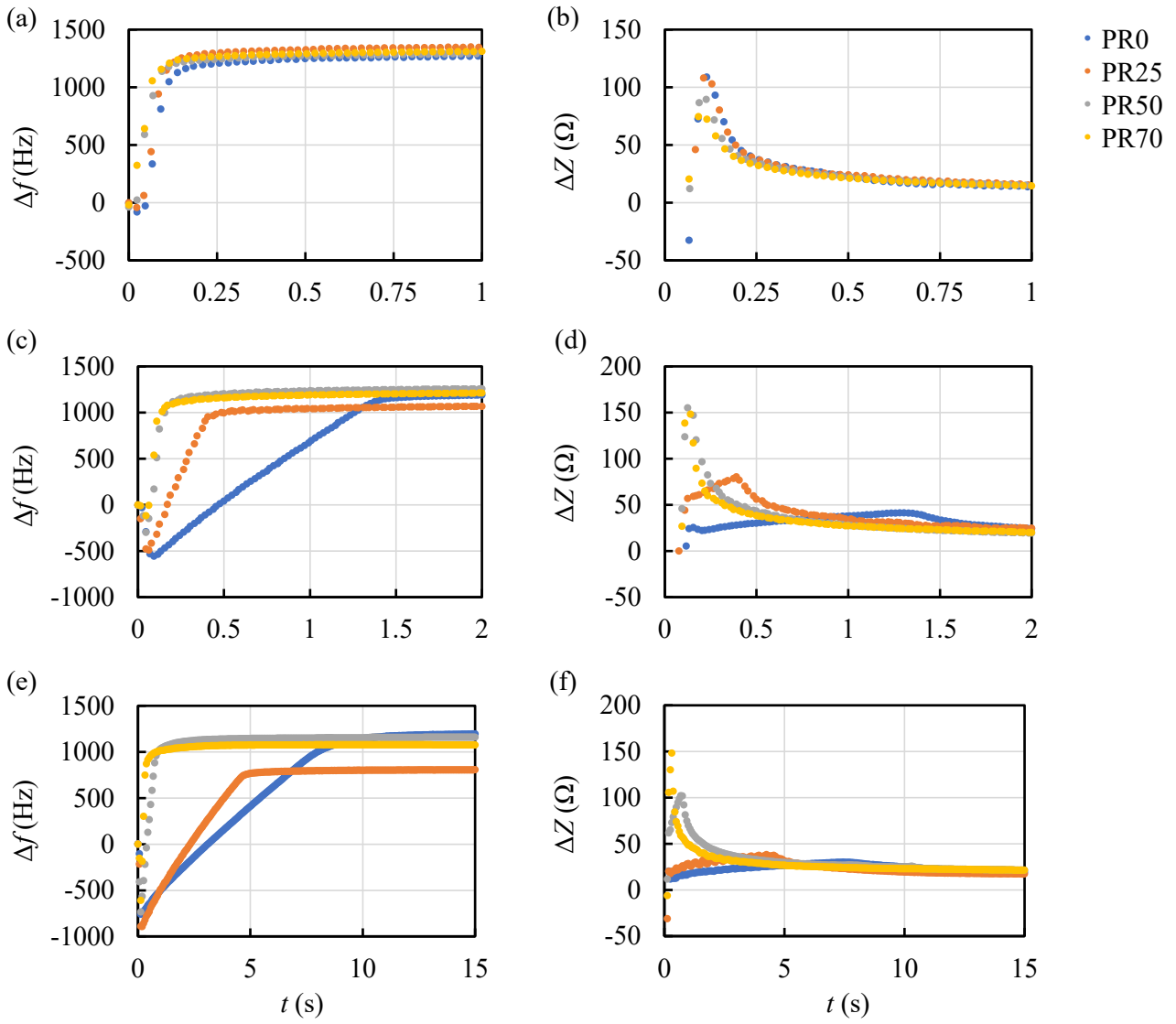

Fig. 3-7. QCM charts of PHS films developed in (a), (b) ethyl acetate, (c), (d) butyl acetate, and (e), (f) hexyl acetate. The vertical axes in (a), (c), and (e) represent the frequency change. The vertical axes in (b), (d), and (f) represent the impedance change. The protection ratio was varied from 0 to 25, 50, and 70 mol%.

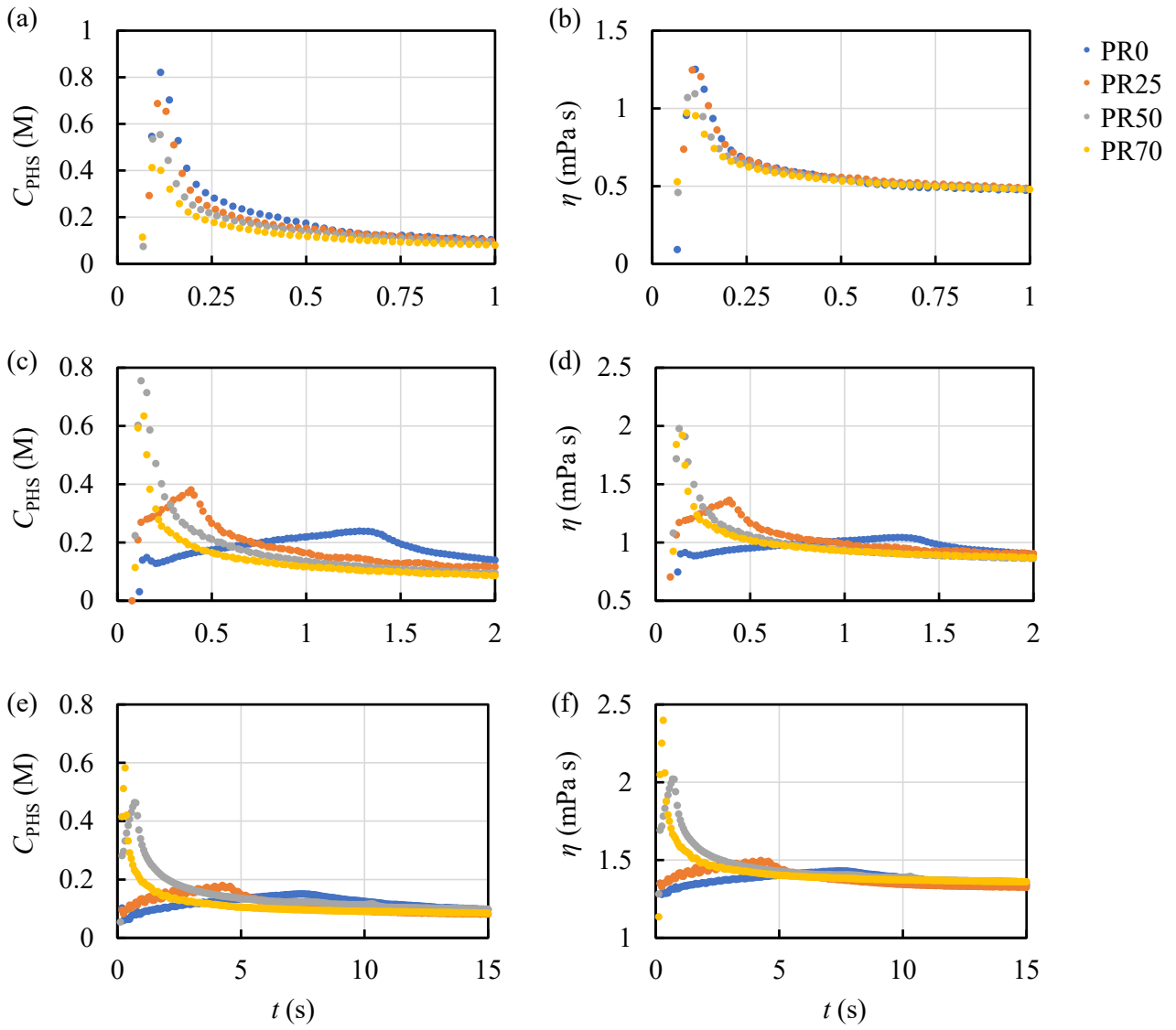

Fig. 3-8. Dissolution kinetics of PHS films in (a), (b) ethyl acetate, (c), (d) butyl acetate, and (e), (f) hexyl acetate developers: (a), (c), (e) PHS concentration chart near dissolution front and (b), (d), (f) viscosity chart. The protection ratio was varied from 0 to 25, 50, and 70 mol%.

The QCM charts of PHS (PR0 and PR25) films in butyl acetate and hexyl acetate developers and PHS (PR0, PR25, and PR50) in 1-butanol developer resembled those in the TMAH aqueous developers, namely, dissolution kinetics with case II diffusion.[16] In the TMAH aqueous developers, the time dependence of the dissolution rate of PHS films showed the saturation tendency due to the neutralization of TMAH with phenolic OH groups.[16] In the development of PHS (PR0 and PR25) films in butyl acetate developer and PHS (PR0, PR25, and PR50) films in 1-butanol developer, Δf increased linearly without showing the saturation tendency. The corresponding ΔZ also increased

linearly, which indicates that the PHS concentration near the film surface increased linearly during the dissolution of the film. In the development of PHS (PR0 and PR25) films in hexyl acetate developer, Δf increased linearly, while a slight saturation tendency was observed for ΔZ, similar to the development of PHS films in the 2.38 wt% TMAH aqueous developer. The reason for the saturation tendency in hexyl acetate developer is probably as follows. When the alkyl chain length increased from butyl acetate to hexyl acetate, the diffusion constant of PHS molecules in developers decreased owing to the increase in viscosity. The ratio of the diffusion constant in hexyl acetate to that in butyl acetate is approximately 0.66, which was estimated from the viscosities of hexyl and butyl acetates.[48] However, the speed of the transport of PHS molecules from the solid phase to the liquid phase became even slower, compared with the decrease in the diffusion constant. The initial rates of frequency changes in hexyl and butyl acetates are shown in **Table 3-5**. Consequently, the speed of the transport of PHS molecules from the solid phase to the liquid phase became relatively slower than the diffusion of PHS molecules in hexyl acetate developers. This mechanism is considered to have resulted in the appearance of saturation tendency, similarly observed during the development of PHS films in the 2.38 wt% TMAH aqueous developer. Note that the neutralization of alkalis by phenolic OH groups slows the dissolution rate in the TMAH aqueous developer, in which the dissociation of phenolic OH groups plays a major role in the dissolution of PHS. The clarification of details requires further investigation.

Table 3-5. The initial rates of frequency changes in butyl acetate $d\Delta f_b/dt$ and hexyl acetate $d\Delta f_h/dt$, calculated from the slope of frequency change shown in **Figs. 3-7(c)** and **3-7(d)**. The ratios of initial rates are also shown.

Polymer	PR0	PR25	PR50	PR70
$d\Delta f_b/dt$ (Hz s^{-1})	1450	4300	12000	14500
$d\Delta f_h/dt$ (Hz s^{-1})	280	420	2720	6850
$(d\Delta f_b/dt)/(d\Delta f_b/dt)$	0.19	0.098	0.23	0.47

3-4. Conclusion

The dissolution dynamics of partially protected PHS in organic developers was investigated by the

QCM method to deepen the fundamental understanding of the dissolution dynamics of CARs. The schematic of the dissolution processes is shown in **Fig. 3-9**. The dissolution dynamics in the solvents, in which the phenolic OH groups are hardly dissociated, was measured. In the 50 vol% alcohol aqueous developer, the nonpolar interaction of alcohols plays an important role in the separation of molecular interaction between polymer molecules in addition to the polar interaction. Upon the dissolution of PHS films, a large swelling was observed. The steady-state motion of the dissolution front was not observed. In pure alcohol developers, the dissolution kinetics was changed at the protection ratio between 50 and 70 mol%. By decreasing the polarity of the developer to hexyl acetate, the swelling tended to become small. In the hexyl acetate developer, the dissolution kinetics of PHS films became similar to that in TMAH aqueous developer although the dissociation of phenolic OH groups does not occur in the hexyl acetate developer.

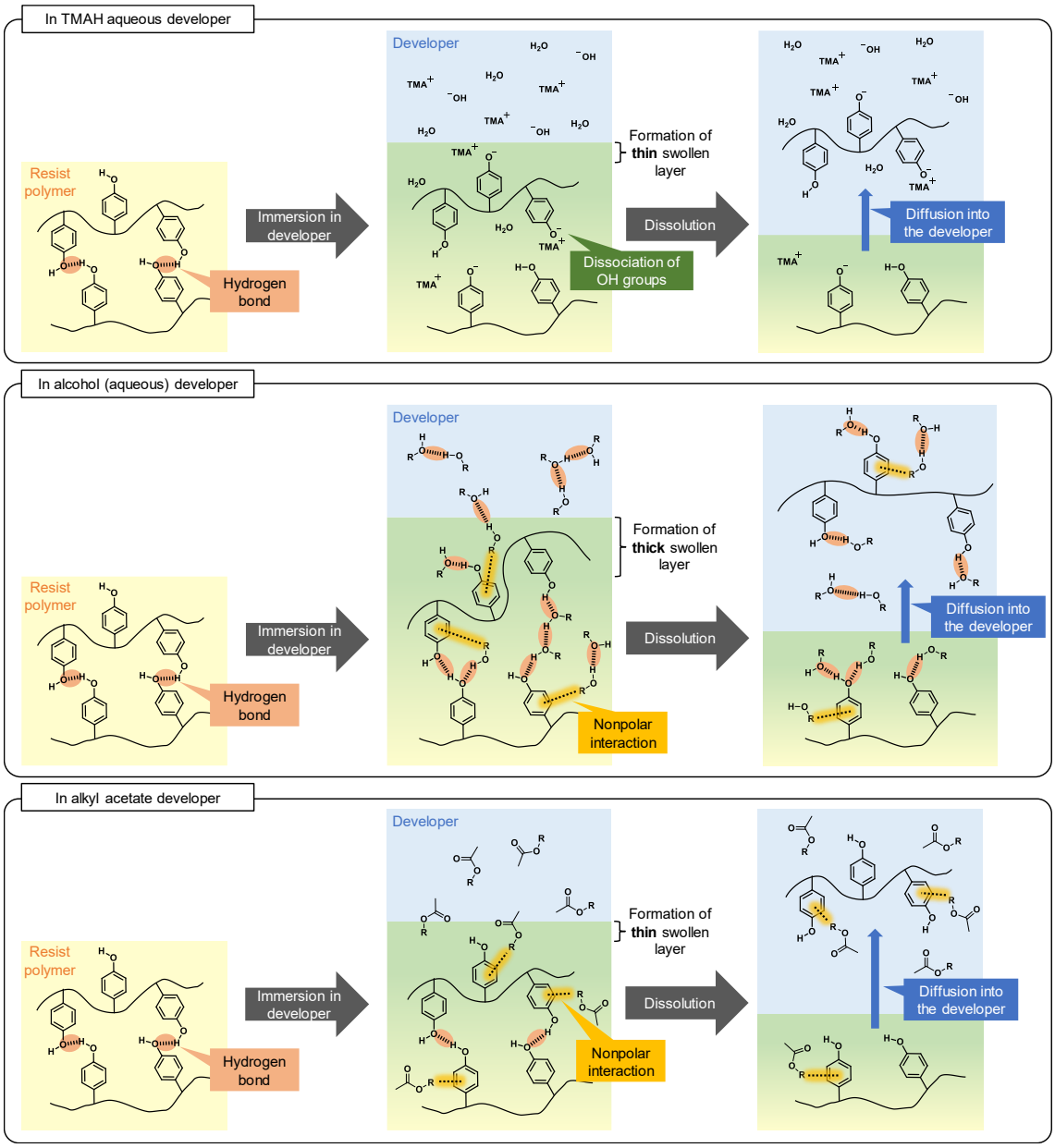

Fig. 3-9. Schematic of the dissolution processes.

References

1) H. Ito, *Microlithography/Molecular Imprinting Advances in Polymer Science Series* (Springer, Heidelberg, 2005) Vol. 172, p. 37.
2) J. Thackeray, T. H. Fedynyshyn, D. Kang, M. M. Rajaratnam, G. Wallraff, J. Opitz, and D. Hofer, J. Vac. Sci. Technol. B **14**, 4267 (1996).
3) M. T. Spuller, R. S. Perchuk, and D. W. Hess, J. Electrochem. Soc. **152**, G40 (2005).
4) W. Hinsberg, F. A. Houle, S. W. Lee, H. Ito, and K. Kanazawa, Macromolecules **38**, 1882 (2005).
5) M. Toriumi, T. Ohfuji, M. Endo, and H. Morimoto, J. Photopolym. Sci. Technol. **12**, 545 (1999).
6) H. Ito, IBM J. Res. Dev. **45**, 683 (2001).

7) T. Itani and J. J. Santillan, Appl. Phys. Express **3**, 061601 (2010).
8) A. Tsuneishi, S. Uchiyama, and T. Kozawa, Jpn. J. Appl. Phys. **57**, 046501 (2018).
9) Handbook of Chemistry: Pure Chemistry, The Chemical Society of Japan (Maruzen, Tokyo, 2021), Chap. 11 and 14, [in Japanese].
10) Y. T. Ito, K. Watanabe, Y. Jin, T. Kozawa, K. Sakamoto, and M. Muramatsu, Jpn. J. Appl. Phys. **63**, 018002 (2024).
11) Y. Iwashige, K. Watanabe, Y. T. Ito, T. Kozawa, K. Sakamoto, and M. Muramatsu, Jpn. J. Appl. Phys. **63**, 026504 (2024).
12) S. Takechi, A. Kotachi, M. Takahashi, and I. Hanyu, Proc. SPIE **3049**, 519 (1997).
13) T. Itani and J. J. Santillan, J. Vac. Sci. Technol. B **27**, 2986 (2009).
14) K. Matsunaga, H. Oizumi, K. Kaneyama, G. Shiraishi, K. Matsumaro, J. J. Santillan, and T. Itani, J. Photopolym. Sci. Technol. **23**, 613 (2010).
15) T. Itani and J. J. Santillan, Appl. Phys. Express **3**, 096501 (2010).
16) Y. T. Ito, H. Betsumiya, T. Kozawa, K. Sakamoto, and M. Muramatsu, Jpn. J. Appl. Phys. **61**, 066506 (2022).
17) Y. Iwashige, Y. T. Ito, T. Kozawa, K. Sakamoto, and M. Muramatsu, Jpn. J. Appl. Phys. **62**, 036502 (2023).
18) H. Betsumiya, Y. T. Ito, T. Kozawa, K. Sakamoto, and M. Muramatsu, Jpn. J. Appl. Phys. **62**, 036503 (2023).
19) H. Betsumiya, Y. Jin, Y. T. Ito, T. Kozawa, K. Sakamoto, and M. Muramatsu, Jpn. J. Appl. Phys. **62**, 066501 (2023).
20) S. Tarutani, H. Tsubaki, and S. Kanna, Proc. SPIE **6923**, 69230F (2008).
21) S. Tarutani, W. Nihashi, S. Hirano, N. Yokokawa, and H. Takizawa, J. Photopolym. Sci. Technol. **26**, 599 (2013).
22) S. T. Meyers et al., Proc. SPIE **11609**, 116090K (2021).
23) C. Luo, C. Xu, L. Lv, H. Li, X. Huang, and W. Liu, RSC Adv. **10**, 8385 (2020).
24) A. Shirotori, M. Hoshino, M. Fujimura, S. F. Yeh, H. S. Suh, D. D. Simone, G. Vandenberghe, and H. Sanuki, Proc. SPIE **12498**, 1249807 (2023).
25) K. Morita, Y. Tanaka, Y. Tanaka, and M. Asai, Proc. SPIE **12498**, 1249815 (2023).
26) S. H. Lee, J. K. Park, T. Cardolaccia, J. Sun, C. Andes, K. O'Connell, and G. G. Barclay, Proc. SPIE **8325**, 83250Q (2012).
27) J. J. Santillan, M. Shichiri, and T. Itani, Proc. SPIE **9051**, 90510O (2014).
28) L. K. Sundberg, G. M. Wallraff, L. D. Bozano, H. D. Truong, M. I. Sanchez, D. L. Goldfarb, K. E. Petrillo, and W. D. Hinsberg, Proc. SPIE **9051**, 90510S (2014).
29) H. Tsubaki, W. Nihashi, T. Tsuchibashi, T. Fujimori, M. Momota, and T. Goto, J. Photopolym. Sci. Technol. **28**, 489 (2015).
30) A. Nakajima, K. Matsuo, and T. Kozawa, Appl. Phys. Express **14**, 026501 (2021).
31) K. Ou, N. Tango, and T. Fujimori, Proc. SPIE **12750**, 127500A (2023).

32) A. Sekiguchi, J. Photopolm. Sci. Technol. **26**, 479 (2013).
33) G. Sauerbrey, Z. Phys. **155**, 206 (1959).
34) Seidenki Anzen Shisin 2007, *Technical Recommendations of National Institute of Occupational Safety and Health, JNIOSH-TR-No.42* (National Institute of Occupational Safety and Health, Tokyho, 2007), in Japanese].
35) *CRC Handbook of Chemistry and Physics 97th*, W. M. Haynes (ed.) (CRC Press Inc, Boca Raton, FL, 2016-2017), p. 6–210.
36) S. Mandal and M. Katiyar, Bull. Mater. Sci. **36**, 653 (2013).
37) S. L. Oswal, P. Oswal, and R. P. Phalak, Int. J. Thermophsics **17**, 1255 (1996).
38) H. Djojoputro and S. Ismadji, J. Chem. Eng. Data **50**, 727 (2005).
39) Y. T. Ito, T. Kozawa, K. Sakamoto, and M. Muramatsu, Jpn. J. Appl. Phys. **63**, 046501 (2024).
40) *CRC Handbook of Solubility Parameters and Other Cohesion Parameters 2nd*, A. F.-M. Barton (ed.) (CRC Press Inc, Boca Raton, FL, 1991) p. 96 and 442.
41) Y. Kitazaki and T. Hata, J. Adhesion Soc. Japan (Nippon Setchaku Kyoukaishi) **8**, 131 (1972), [in Japanese].
42) S. W. Kuo and F. C. Chang, Macromolecules **34**, 5224 (2001).
43) J. Dong and Y. Ozaki, Macromolecules **30**, 286 (1997).
44) T. Fukuyama et al., Jpn. J. Appl. Phys. **48**, 06FC03 (2009).
45) C. Y. Hui and K. C. Wu, J. Appl. Phys. **61**, 5129 (1987).
46) N. L. Thomas and A. H. Windle, Polymer **23**, 529 (1982).
47) C. Y. Hui, K. C. Wu, R. C. Lasky, and E. J. Kramer, J. Appl. Phys. **61**, 5137 (1987).
48) *Structures and Physical Properties of Polymers*, Y. Matushita (ed.) (Koudansha, Tokyo, 2013).

Chapter 4

Dissolution dynamics of zirconia nanocluster resist

4-1. Introduction

After the successful application of EUV lithography with a numerical aperture (NA) of 0.33 to semiconductor industry in 2019,[1] the development of high NA tools started. The EUV exposure tools with 0.55 NA will soon be available.[2] The increase of NA to 0.75 has been planned to further improve the optical resolution.[3] The development of resist materials is also ongoing to meet the requirement for responding to the increasingly improved optical images.[4] Among the candidates for the next-generation resist materials, the metal oxide resists, typically called MORs, are promising materials. In particular, the tin-oxo cage resists[5–7] have showed the excellent lithographic performance. However, they have not been applied to the high volume production of semiconductor devices owing to some insufficient properties such as the defect generation probability.

The MORs consist of metal oxide core and organic ligands. Upon exposure to radiations, the MORs are insolubilized owing to the formation of bridging ligands. For example, the butyl ligands are detached from tin upon exposure to EUV and subsequently replaced with hydroxyl ligands in the case of tin-oxo cage resist. The oxygen bridges between tin-oxo cages are generated through dehydration.[4–8] For the zirconia nanocluster resists with methacrylate (methacrylic acid anion) (MAA) ligands, more details have been investigated using hard X-ray photoelectron spectroscopy,[9] near edge X-ray absorption fine structure spectroscopy,[9] X-ray diffraction,[9] time-of-flight secondary ion mass spectrometry with gas cluster ion beam,[10] a mid-IR free electron laser,[11] scanning transmission electron microscopy,[12] simulation,[13,14] electron pulse radiolysis,[15–17] and γ-radiolysis with gas chromatography[18] and high performance liquid chromatography.[19] Upon exposure to ionizing radiations, the radical cations of MAA are generated through the direct oxidation by ionizing radiations (ionization) and the oxidation by the oxidizing agents also generated by ionizing radiation (hole transfer). The radical anions of MAA are also generated through the reduction by the reducing agents such as the thermalized electrons generated upon exposure to the ionizing radiations (electron transfer and electron attachment). Both radical cations and radical anions of MAA are decomposed to generate

α- carbon radicals. The bridging ligands are generated through the radical addition of MAA radical to MAA and/or the radical recombination between MAA radicals.[19)]

The development process is essential to the resist pattern formation. The dissolution kinetics is expected for the MORs to be different from the conventional polymer-type resists. Although the dissolution dynamics of MORs have been reported,[20)] the details are still unclear. In this study, we investigated the dissolution dynamics of zirconia nanocluster resist with MAA ligand by a quartz crystal microbalance (QCM) method. The developers used were ethyl, butyl, amyl (pentyl), hexyl, 2-methylbutyl, and 3-methylbutyl acetates. The differences from the dissolution dynamics of polymer type resists are discussed. In this study, a UV light with the wavelength of 254 nm was used to induce the crosslinking between MAA ligands instead of EUV. It has been reported that MAA ligands are directly crosslinked by UV without photoinitiators such as azobis(isobutyronitrile) (AIBN).[21)] With focusing on the effects of the crosslinking between MAA ligands on the dissolution dynamics, the UV light was used because the reproducibility of experiments with UV light (LED) is significantly higher than that with EUV radiation (emission from a plasma source). The fundamental understanding of dissolution dynamics is important for the design of high performance resist materials and processes.

4-2. Experimental methods

4-2-1. Materials

Propylene glycol monomethyl ether acetate (PGMEA), ethyl acetate, butyl acetate, amyl (pentyl) acetate, hexyl acetate, 2- methylbutyl acetate, and 3-methylbutyl acetate were purchased from Sigma-Aldrich. Probe solutions for contact angle measurement, namely, diiodomethane, hexadecane, and ethylene glycol, were purchased from Tokyo Chemical Industry, Sigma-Aldrich, and Wako, respectively.

4-2-2. QCM measurement

The ZrO_2 nanocluster with MAA (ZrO_2-MAA) solution in PGMEA was spin-coated on QCM substrate to form a thin film. The films spin-coated onto QCM substrates were prebaked at 90 °C for 90 s. The film thickness was adjusted to be approximately 200 nm. The ZrO_2-MAA films were exposed to 254 nm wavelength light (AS ONE Handy UV Lamp SLUV6) in the exposure dose range of 0–2000 mJ cm^{-2}. The exposure dose was measured by a UV intensity meter (ORC UV-M03A). The absorption coefficient of the ZrO_2-MAA films was 0.69 μm^{-1}. The reflectance of gold is 0.28 at the wavelength of 254 nm.[22] Thus, the absorbed UV light dose at the surface was 1.21 mJ cm^{-2} against the UV light exposure dose of 1mJ cm^{-2}. The dissolution dynamics (the temporal changes of frequency and impedance) of ZrO_2-MAA films with and without post exosure baking (PEB) was measured in the acetate developers using RDA-Qz3 (Lithotech Japan).[23] PEB condition was 90 °C and 90 s. The films were developed in the developers at 23 °C and then rinsed in isopropyl alcohol.

4-2-3. Contact angle measurement

For the measurement of contact angles, the ZrO_2-MAA films were prepared on Si substrates, similarly to those on QCM substrates. The ZrO_2-MAA films were exposed to 254 nm wavelength light in the exposure dose range of 0–1500 mJ cm^{-2}. For example, the absorbed dose upon 500 mJ cm^{-2} UV exposure on QCM substrate corresponds to that upon approximately 400 (397) mJ cm^{-2} UV exposure on Si. The reflectance of Si substrates is 0.69 at the wavelength of 254 nm.[24] Thus, the absorbed dose at the surface was 1.53 mJ cm^{-2} against the exposure dose of 1mJ cm^{-2}. The contact angles were measured using a contact angle meter (Kyowa Interface Science DMe-211). Water, hexadecane, diiodomethane, and ethylene glycol were used as probe liquids. The volume of liquid droplets was 2 μl for water and hexadecane, 1 μl for diiodomethane and ethylene glycol. The sizes of the liquid needles were 22 G for water, hexadecane, and ethylene glycol, and 18 G for hexadecane. The static contact angles were measured during the period of 1–21 s at intervals of 1 s after droplet landing. The

static contact angle was evaluated by a θ/2 method. The measurement was repeated 10 times and the obtained values were averaged.

4-3. Results and discussion

4-3-1. Dissolution kinetics in normal alkyl acetates developers (without PEB)

The dissolution dynamics of ZrO_2-MAA films was measured in acetates with different alkyl chains. **Figure 4-1** shows the QCM charts obtained for the development of ZrO_2-MAA films without PEB in acetates with normal alkyl chains. The vertical axes in **Figs. 4-1(a)**, **4-1(c)**, **4-1(e)**, and **4-1(g)** represent the frequency change Δf. The baseline for Δf was set at the frequency of QCM substrate with a ZrO_2-MAA film in the atmosphere. The vertical axes in **Figs. 4-1(b)**, **4-1 (d)**, **4-1(f)**, and **4-1(h)** represent the impedance change ΔZ. The baseline for ΔZ was set at the impedance of QCM substrate in a neat developer. Upon the immersion of QCM substrates into the developers, Δf dropped owing to the viscosities of developers. The viscosities of ethyl, butyl, amyl, and hexyl acetates at 25 °C are 0.423,[25] 0.685,[25] 0.8618,[26] and 1.036 mPa s,[27] respectively. The initial drops of Δf were 514, 623, 718, and 796 Hz for ethyl, butyl, amyl, and hexyl acetates, respectively. The initial rises of ΔZ (baselines for ΔZ) were 193, 235, 272, and 303 Ω for ethyl, butyl, amyl, and hexyl acetates, respectively. In either sample, the time required for complete dissolution increased with the progress in the formation of bridging ligands upon exposure to UV. After the drop due to the viscosity, Δf slowly decreased with the development time until its sudden increase. The slope in the slow decrease region decreased with the increase of the alkyl chain length of acetate. For the hexyl acetate, Δf was nearly constant until its sudden increase. With the sudden increase of Δf, ZrO_2-MAA films dissolved in developers. The slope at the sudden increase of Δf also decreased with the UV exposure dose. Near the surface of QCM substrate (the end of sudden increase of Δf), the slowdown of Δf was observed. Namely, the dissolution rate decreased near the substrate. This indicates the strong nonpolar interaction between Au electrode and organic ligands. After the slowdown, Δf became constant. Δf after becoming constant decreased

with the increase of UV exposure dose. This indicates the formation of insoluble layer.

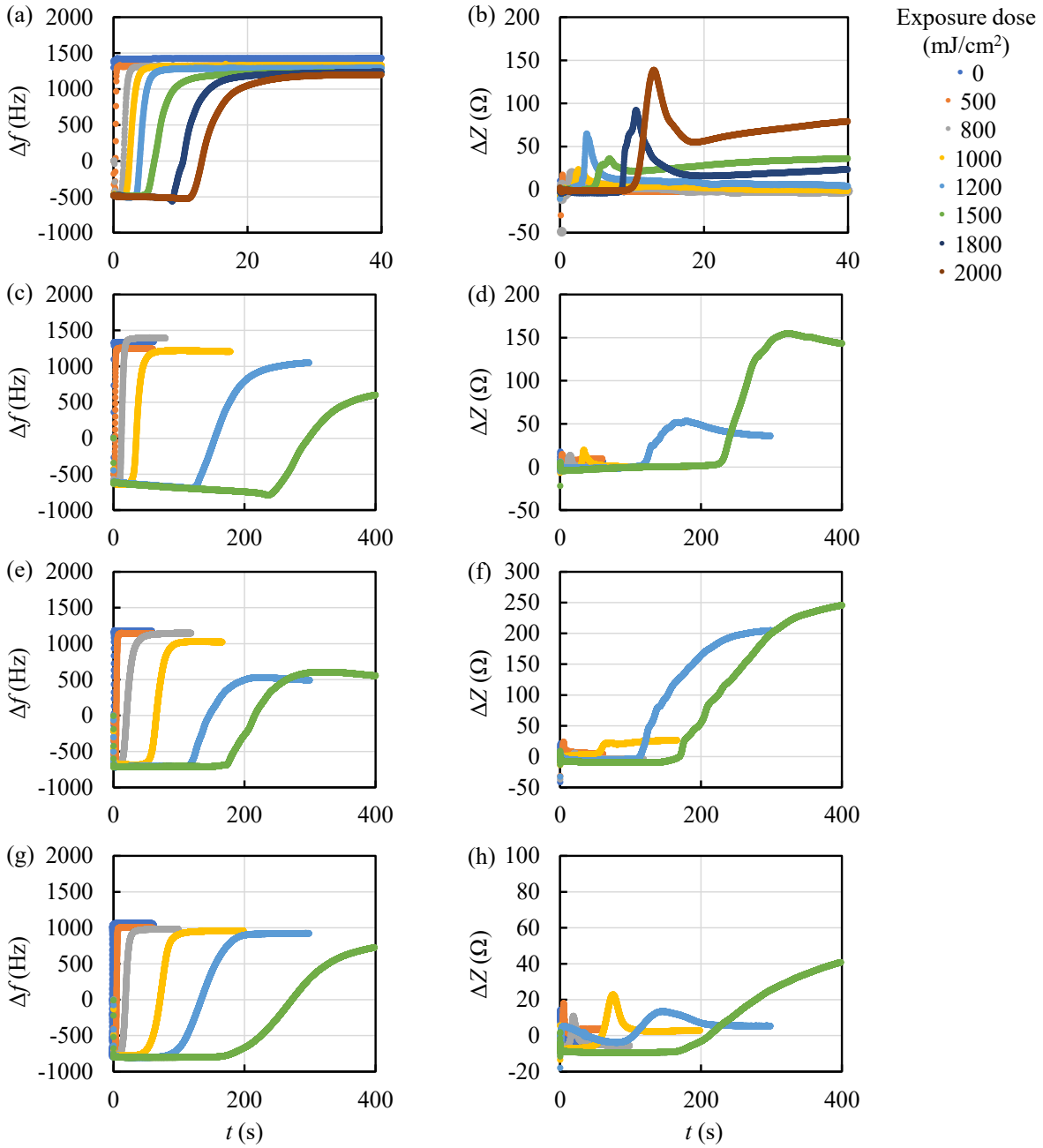

Fig. 4-1. QCM charts of ZrO_2-MAA films developed in (a), (b) ethyl acetate, (c), (d) butyl acetate, (e), (f) amyl acetate, and (g), (h) hexyl acetate. The vertical axes in (a), (c), (e), (g) represent the frequency change. The vertical axes in (b), (d), (f), (h) represent the impedance change. The samples were not subjected to PEB.

The maximum ΔZ during development was lower than 20 Ω for the UV exposure dose lower than 1000 mJ cm^{-2}, which suggests that ZrO_2-MAA films dissolved without significant swelling. At the UV

exposure dose higher than 1200 mJ cm^{-2}, the maximum ΔZ exceeded 50 Ω and increased with UV exposure dose in ethyl, butyl, and amyl acetates. In particular, ΔZ significantly increased at the UV exposure doses of 1200 and 1500 mJ cm^{-2}. The generation of bridging ligands is considered to have increased the capacity of containing solvent molecules and resulted in the formation of thick transient swelling layer. For hexyl acetate, the maximum ΔZ was lower than that for the other normal acetates. This is probably the effect of the molecular size of developer. The effect of polarity is discussed later with the experimental results. When ΔZ decreased to 0 after the increase, the films completely dissolved. When ΔZ did not decrease to 0, the swollen films remained on the QCM substrate. The time required for complete dissolution increased with the alkyl chain length of acetates. This is considered to be mainly caused by the increase in the viscosity of developer. However, there is a significant gap between the dissolution rates in ethyl and butyl acetates. This gap is probably owing to the size effect of developer molecules, similarly to the dissolution dynamics of poly(4- hydroxystyrene) (PHS) films in tetraalkylammonium hydroxide aqueous solutions, in which the gap between tetraethylammonium hydroxide and tetrapropylammonium hydroxide was observed.[28)]

In the dissolution of PHS films in 2.38 wt% tetramethylammonium hydroxide (TMAH) aqueous solution (the standard developer in semiconductor lithography), the peak time of ΔZ approximately corresponded to the end of the rise of Δf. This is because ΔZ in this case mainly indicates the viscosity of TMAH aqueous solution with PHS. However, in the dissolution of ZrO_2-MAA films in acetates, the peak time of ΔZ did not correspond to the end of the rise of Δf. When the peak time of ΔZ was earlier than the end of the rise of Δf, the explanation for the disagreement depends on whether the observed ΔZ indicates the over-saturated condition of the mixture of crosslinked ZrO_2-MAA and acetates or not. If it is not the over-saturated condition, the disagreement suggests that the supply rate of solutes from the film to the solution was not constant. Roughly speaking, the supply rate was higher than the diffusion of solute before the peak of ΔZ, and the supply rate was lower than the diffusion of solute after the peak. If it is over-saturated condition, the peak time indicates when the film viscosity was

maximized. Therefore, the disagreement simply indicates that the time when the film viscosity was maximized was different from when the film was mostly dissolved. This is natural consequence. We cannot currently conclude this problem, because it is not easy to determine ΔZ of acetate solutions with partially crosslinked ZrO_2-MAA. When the peak time of ΔZ was later than the end of the rise of Δf, ΔZ is considered to indicate the viscosity of ZrO_2-MAA film. For example, the slow increase of ΔZ after the peak in **Fig. 4-1(b)** is likely to indicate the increase in the viscosity of the swollen remaining ZrO_2-MAA film. ΔZ for UV exposure doses of 1200 and 1500 mJ cm^{-2} in **Fig. 4-1(f)** probably indicates the viscosity of ZrO_2-MAA films.

Thus, ZrO_2-MAA films showed characteristic dissolution dynamics, which is different from those of acidic polymers observed in alkaline aqueous solutions.

4-3-2. Dissolution kinetics in branched alkyl acetates developers (without PEB)

The effect of branched alkyl chain was investigated using 2-methylbutyl and 3-methylbutyl acetates as developers in comparison with amyl acetate. **Figure 4-2** shows the QCM charts of ZrO_2-MAA films without PEB developed in 2-methylbutyl and 3-methylbutyl acetates. The viscosity of 3-methylbutyl acetate is 0.827 mPa s at 25 °C.[27] The initial drops of Δf were 684 and 700 Hz for 2-methylbutyl and 3-methylbutyl acetates, respectively. The initial rises of ΔZ were 256 and 261 Ω for 2-methylbutyl and 3-methylbutyl acetates, respectively. The viscosity of 2-methylbutyl acetate is not available. However, it can be estimated to be 0.778 mPa s from the impedances of neat developers, as shown in **Fig. 4-3**. ZrO_2-MAA films became insoluble for 400 s at the UV exposure doses of 1000 and 1500 mJ cm^{-2} in 2-methylbutyl and 3-methylbutyl acetates, respectively. Compared with normal alkyl chain (amyl acetate), the time required for complete dissolution significantly increased in 2-methylbutyl acetate despite its low viscosity. The methyl branched at the 2nd position is considered to hinder the 2-methylbutyl acetate in infiltrating the ZrO_2-MAA film. However, the time required for complete dissolution decreased at the exposure dose lower than 1200 mJ cm^{-2} in 3-methylbutyl acetate. The

dissolution rate (the slope of Δf at the rapid increase) in 3-methylbutyl acetate was higher than that in amyl acetate owing to the decrease in viscosity, while the solubility is considered to be decreased at the exposure dose higher than 1500 mJ cm^{-2} owing to the increase in the polarity of developer.

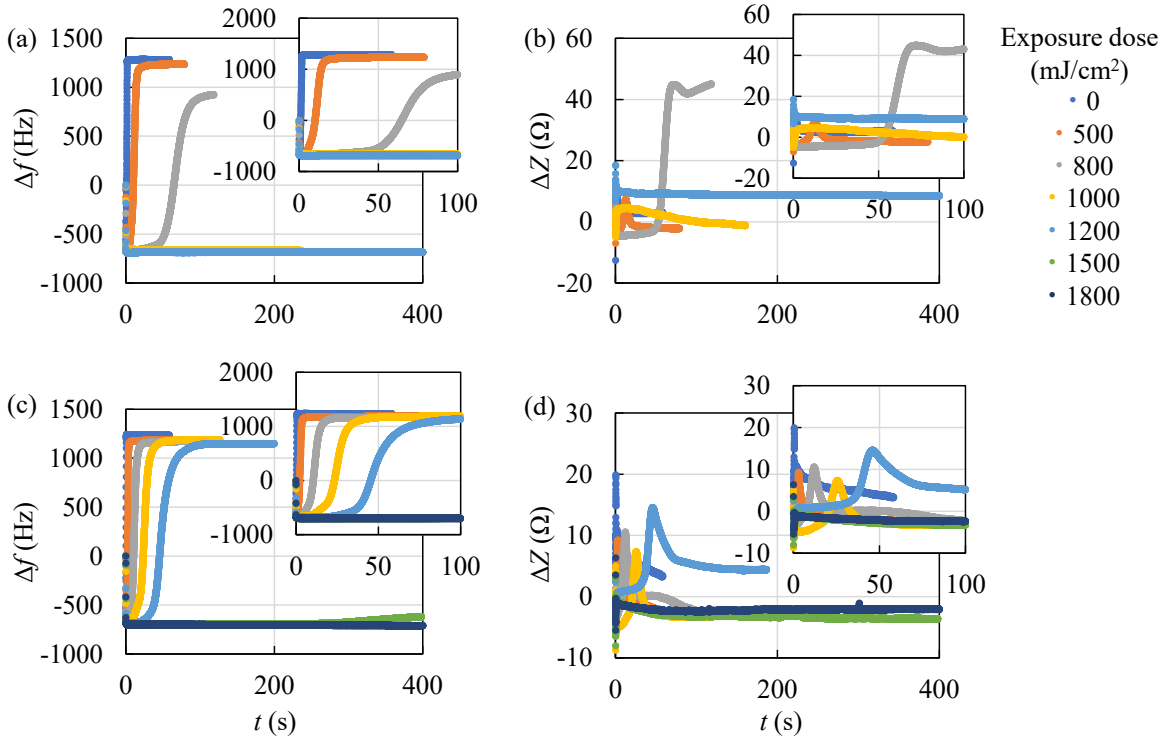

Fig. 4-2. QCM charts of ZrO_2-MAA films developed in (a), (b) 2-methylbutyl acetate and (c), (d) 3-methylbutyl acetate: (a), (c) frequency change and (b), (d) impedance change. The samples were not subjected to PEB.

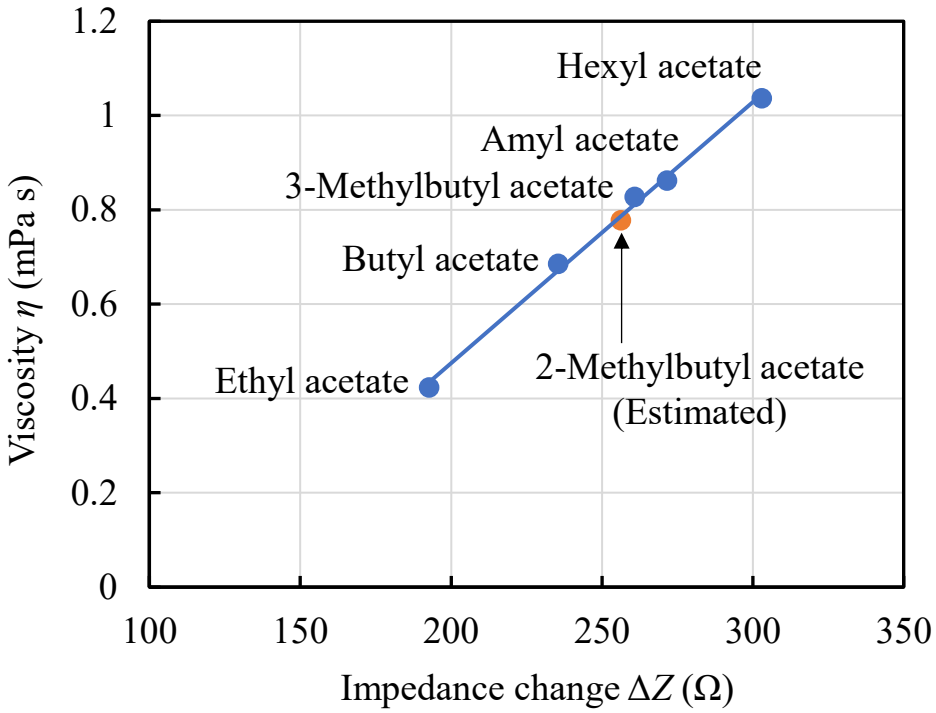

Fig. 4-3. Relationship between impedance change ΔZ and viscosity. Viscosities of ethyl,[25] butyl,[25] amyl,[26] hexyl,[27] 3-methylbutyl acetates[27] are literature values. The viscosity of 2-methylbutyl acetate was estimated from ΔZ. Here, the baseline of ΔZ is the impedance of QCM substrate with no film in the atmosphere. The solid line is a fitting curve (a linear approximation) to ethyl, butyl, 3-methlbutyl, amyl, and hexyl acetates.

4-3-3. Dissolution kinetics in normal alkyl acetates developers (with PEB)

The effects of PEB on the dissolution dynamics were investigated. **Figure 4-4** shows the QCM charts of ZrO_2-MAA films with PEB obtained in acetates with normal alkyl chain. In either developer, the time required for complete dissolution decreased by applying PEB. Unlike the case without PEB, a small negative peak in frequently kinetics was observed just before the rapid increase of Δf, as shown in **Figs. 4-4(a)** and **4-4(b)**. A large swelling was observed for the ZrO_2-MAA film with 2000 mJ cm^{-2} in butyl acetate and the ZrO_2-MAA film with 1800 mJ cm^{-2} in amyl acetate.

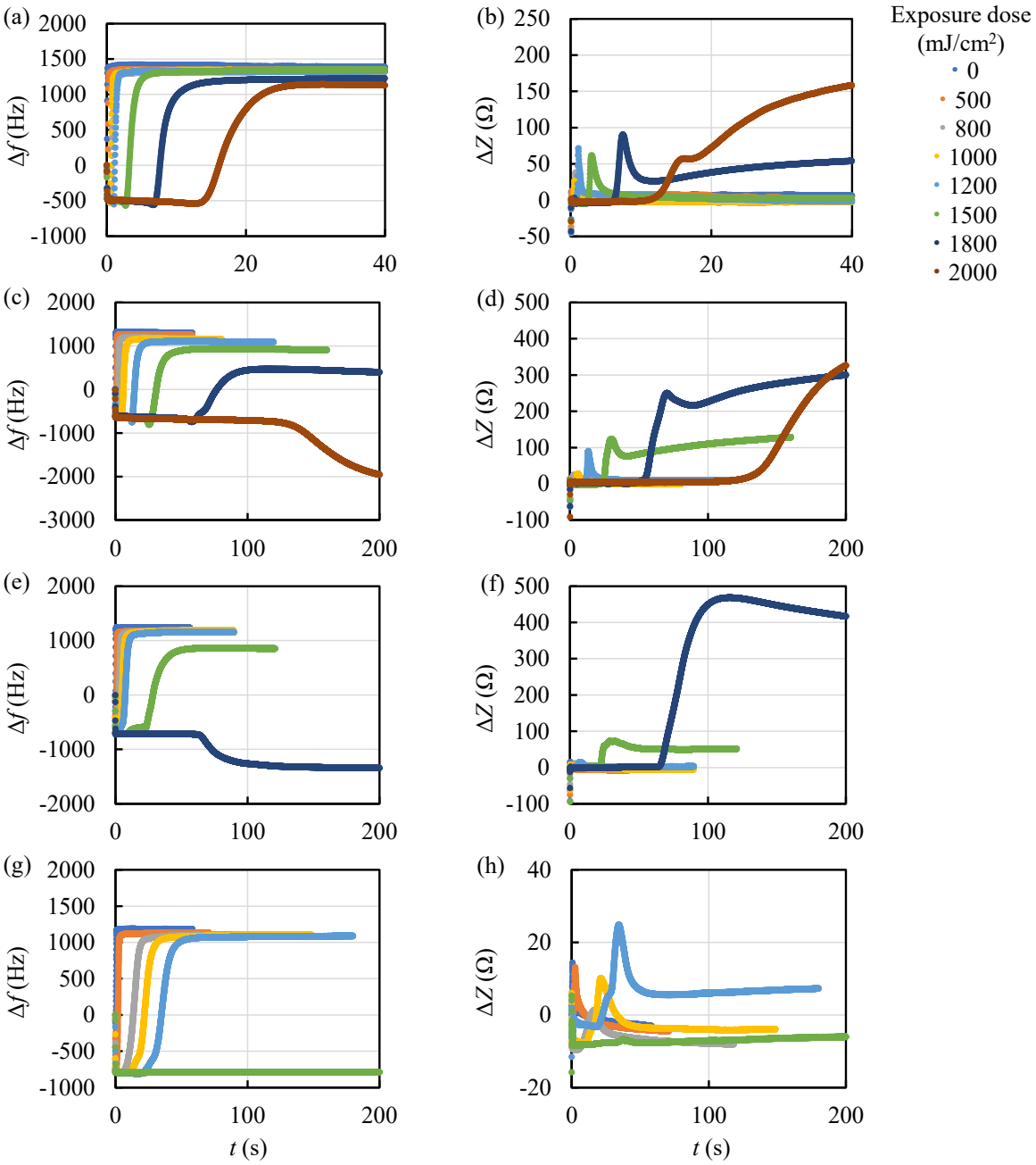

Fig. 4-4. QCM charts of ZrO_2-MAA films developed in (a), (b) ethyl acetate, (c), (d) butyl acetate, (e), (f) amyl acetate, and (g), (h) hexyl acetate: (a), (c), (e), (g) frequency change and (b), (d), (f), (g) impedance change. The samples were subjected to PEB.

4-3-4. Dissolution kinetics in branched alkyl acetates developers (with PEB)

Figure 4-5 shows the QCM charts of ZrO_2-MAA films with PEB obtained in acetates with branched alkyl chain. Similarly to the cases in the acetates with normal alkyl chain, the time required for complete dissolution decreased by applying PEB. Upon exposure to UV, the crosslinking between

MAA ligands[21] and the decarboxylation of MAA ligands[29] are induced. These reactions are considered to be promoted by applying PEB. The latter leads to the loss of coordination ability. We intended to promote the crosslinking by PEB. Despite our expectation, the UV exposure dose required for insolubilization increased. By applying PEB, the bridging ligands may be decomposed. The vacancy generated by the ligand decomposition may also have promoted the solvent absorption. For tin-oxo cage resists, it was reported that the butyl ligands are replaced with OH ligands after the detachment of butyl ligands in the presence of residual water molecules.[30] The polarity change is also a possible reason. However, the further investigation is required to elucidate the mechanism of PEB effects.

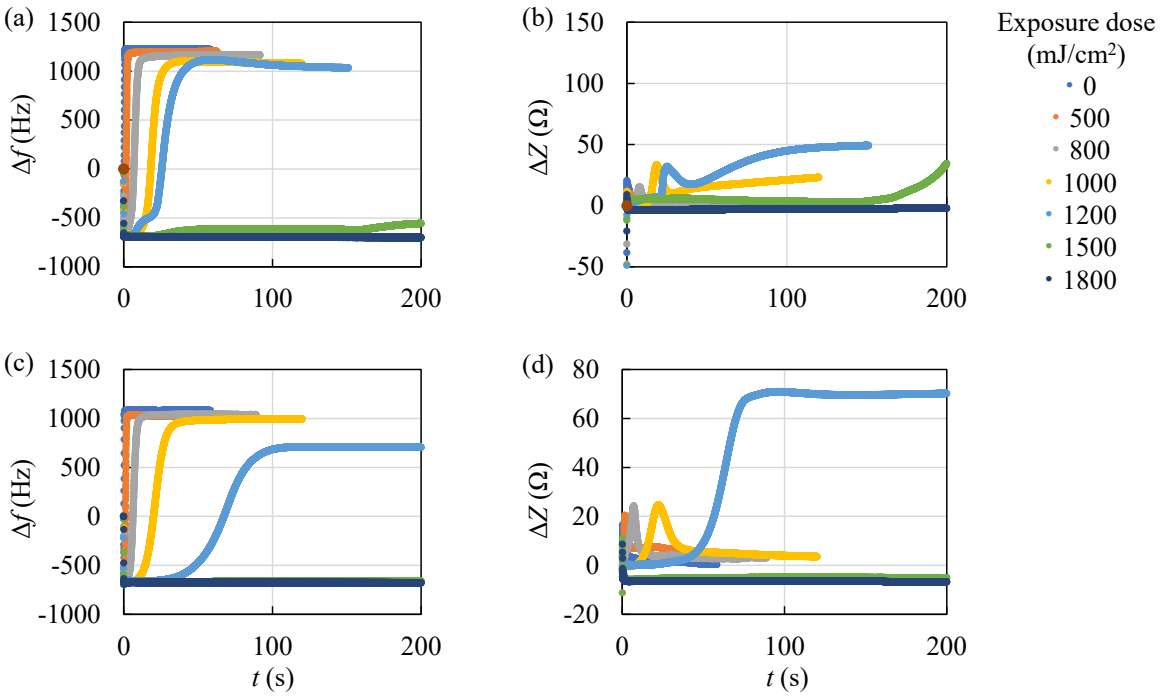

Fig. 4-5. QCM charts of ZrO_2-MAA films developed in (a), (b) 2-methylbutyl acetate, (c), (d) 3-methylbutyl acetate: (a), (c) frequency change and (b), (d) impedance change. The samples were subjected to PEB.

4-3-5. Surface free energy

The contact angles of water, diiodomethane, hexadecane, and ethylene glycol were measured for the ZrO_2-MAA films after the exposure to 0–1500 mJ cm^{-2} UV. The PEB effects on the contact angles

were also examined. Using the measured contact angles, the surface free energies and their components were calculated by Owens, Wendt, Rabel, and Kaelble (OWRK),[31,32] Kitazaki-Hata,[33] and acid–base methods.[34] **Figure 4-6** shows the dependence of surface free energy and its components on UV exposure dose for ZrO_2-MAA films. Although the surface free energy slightly increased with UV exposure, the change was little. The effect of PEB on the surface free energy was also little. These results suggest that the crosslinking between MAA ligands has major effect on the solubility change of ZrO_2-MAA films

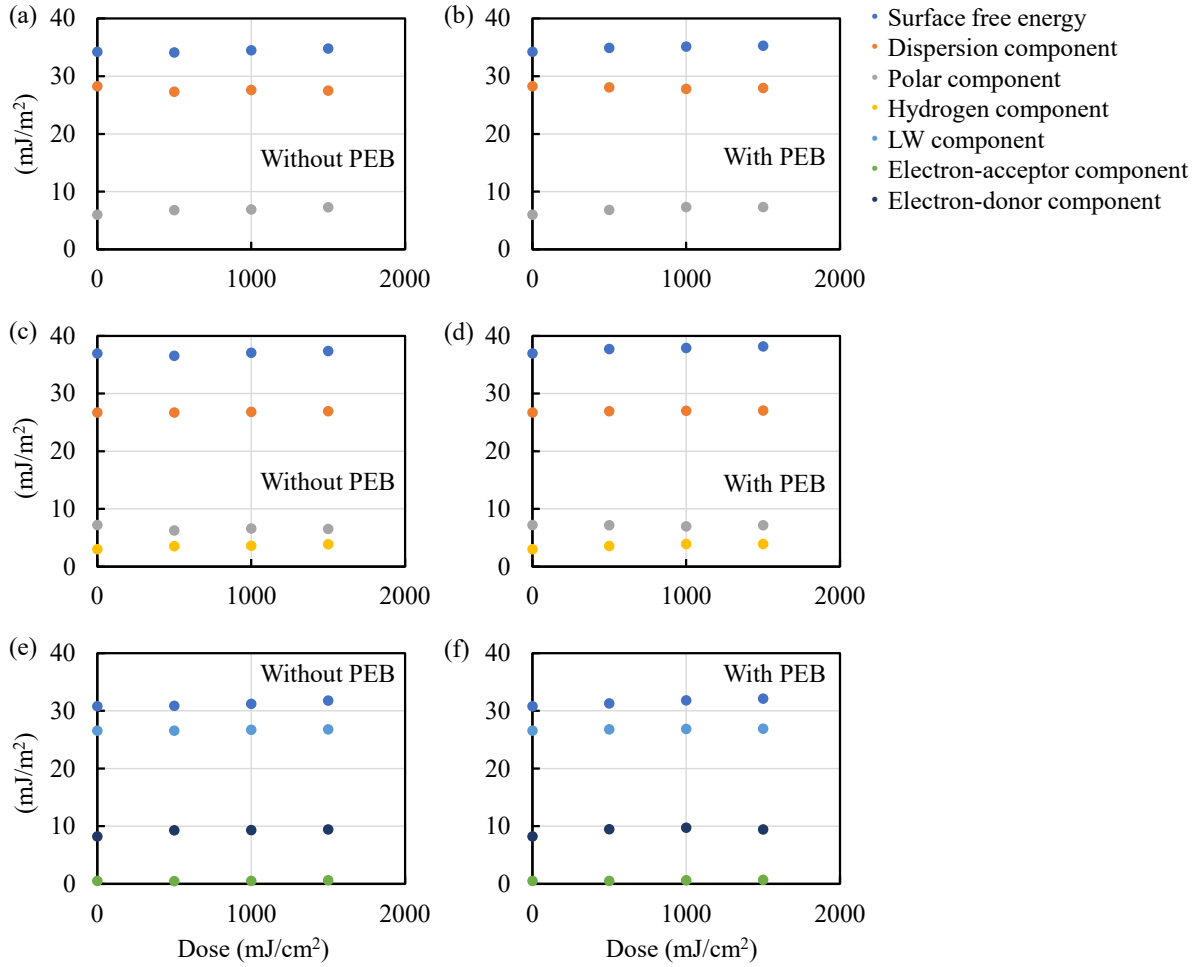

Fig. 4-6. Dependence of surface free energy and its components on UV exposure dose for ZrO_2-MAA films calculated by (a), (b) OWRK, (c), (d) Kitazaki-Hata, and (e), (f) acid–base methods. (a), (c), (e) The samples were not subjected to PEB. (b), (d), (f) The samples were subjected to PEB. The contact angles were measured 6 s after the landing of probe liquid droplets on ZrO_2-MAA films. The probe liquids were water and diiodomethane for the OWRK method, water, diiodomethane, and hexadecane for the Kitazaki-Hata method, and water, hexadecane, and ethylene glycol for the acid–base method.

4-4. Conclusion

The dissolution dynamics of ZrO_2-MAA films was investigated using the QCM method. The ZrO_2-MAA films showed characteristic dissolution dynamics. After the immersion into developers, the acetates slowly infiltrated into ZrO_2-MAA films (a slow decrease in Δf) without the softening of films (no increase in ΔZ) and then rapidly dissolved with the softening of resist film (a sudden increase in ΔZ). The time required for complete dissolution increased with the alkyl chain length of acetates mainly due to the increase in the viscosity of acetates. Compared with normal alkyl chain, the branch at the 2nd position is considered to hinder the 2-methylbutyl acetate in infiltrating the ZrO_2-MAA film. However, the dissolution rate in 3-methylbutyl acetate was higher than that in amyl acetate at the exposure dose lower than 1200 mJ cm^{-2} owing to its low viscosity, while the solubility is considered to be decreased at the exposure dose higher than 1500 mJ cm^{-2} owing to its high polarity of 3-methylbutyl acetate. The onset of dissolution became early by applying to PEB probably owing to the decomposition of bridging ligands.

References

1) T. Itani, P. A. Gargini, P. P. Naulleau, and K. G. Ronse, Proc. SPIE **11147**, 1114701 (2019).
2) J. Schoot et al., Proc. SPIE **11323**, 1132307 (2020).
3) I. Lee, J.-H. Franke, V. Philipsen, K. Ronse, S. D. Gendt, and E. Hendrickx, Proc. SPIE **12494**, 1249405 (2023).
4) A. Develioglu, M. Vockenhuber, L. Lent-Protasova, I. Mochi, Y. Ekinci, and D. Kazazis, Proc. SPIE **12750**, 1275008 (2023).
5) S. T. Meyers et al., Proc. SPIE **11609**, 116090K (2021).
6) J. Haitjema, Y. Zhang, M. Vockenhuber, D. Kazazis, Y. Ekinci, and A. M. Brouwer, J. Micro/Nanolith. MEMS MOEMS **16**, 033510 (2017).
7) I. Bespalov, Y. Zhang, J. Haitjema, R. M. Tromp, S. J. Molen, A. M. Brouwer, J. Jobst, and S. Castellanos, ACS Appl. Mater. Interfaces **12**, 9881 (2020).
8) Y. Zhang, J. Haitjema, X. Liu, F. Johansson, A. Lindblad, S. Castellanos, N. Ottosson, and A. M. Brouwer, J. Micro/Nanolith. MEMS MOEMS **16**, 023510 (2017).
9) Y. Yamashita, T. Chikyow, J. J. Santillan, and T. Itani, Jpn. J. Appl. Phys. **58**, SDDC01 (2019).
10) J. J. Santillan and T. Itani, J. Photopolym. Sci. Technol. **31**, 663 (2018).

11) M. Toriumi, T. Kawasaki, T. Imai, K. Tsukiyama, J. J. Santillan, and T. Itani, Proc. SPIE **10586**, 105860E (2018).
12) M. Toriumi, Y. Sato, M. Koshino, K. Suenaga, and T. Itani, Appl. Phys. Express **9**, 031601 (2016).
13) T. Kozawa, J. J. Santillan, and T. Itani, Jpn. J. Appl. Phys. **57**, 026501 (2018).
14) T. Kozawa, A. Nakajima, T. Yamada, Y. Muroya, J. J. Santillan, and T. Itani, Jpn. J. Appl. Phys. **58**, 036501 (2019).
15) T. Yamada, S. Ishihara, Y. Muroya, J. J. Santillan, S. Yamashita, T. Itani, and T. Kozawa, Jpn. J. Appl. Phys. **58**, 036503 (2019).
16) T. Yamada, Y. Muroya, S. Yamashita, Y. Komuro, D. Kawana, A. Yamazaki, and T. Kozawa, Jpn. J. Appl. Phys. **58**, 096504 (2019).
17) K. Ikeuchi, Y. Muroya, T. Ikeda, Y. Komuro, D. Kawana, and T. Kozawa, Jpn. J. Appl. Phys. **60**, 076503 (2021).
18) T. Otsuka, Y. Muroya, T. Ikeda, Y. Komuro, D. Kawana, and T. Kozawa, Jpn. J. Appl. Phys. **61**, 036503 (2022).
19) T. Otsuka, Y. Muroya, T. Ikeda, Y. Komuro, D. Kawana, and T. Kozawa, Jpn. J. Appl. Phys. **61**, 086508 (2022).
20) J. J. Santillan and T. Itani, Proc. SPIE **10586**, 105860F (2018).
21) H. Wang and H. R. Brown, Macromol. Rapid Commun. **25**, 1095 (2004).
22) O. Loebich, Gold Bull. **5**, 2 (1972).
23) A. Sekiguchi, J. Photopolym. Sci. Technol. **23**, 421 (2010).
24) M. A. Green, Sol. Energy Mater. Sol. Cells **92**, 1305 (2008).
25) *CRC Handbook of Chemistry and Physics*, W. M. Haynes (ed.) (CRC Press Inc., Boca Raton, FL, 2016–2017) 97th ed., p. 6–243.
26) S. L. Oswal, P. Oswal, and R. P. Phalak, Int. J. Thermophsics **17**, 1255 (1996).
27) H. Djojoputro and S. Ismadji, J. Chem. Eng. Data **50**, 727 (2005).
28) H. Betsumiya, Y. T. Ito, T. Kozawa, K. Sakamoto, and M. Muramatsu, Jpn. J. Appl. Phys. **62**, 036503 (2023).
29) W.-H. Fang and X.-Z. You, Int. J. Quantum Chem. **56**, 43 (1995).
30) J. Haitjema, L. Wu, A. Giuliani, L. Nahon, S. Castellanos, and A. M. Brouwer, Phys. Chem. Chem. Phys. **23**, 20909 (2021).
31) D. K. Owens and R. C. Wendt, J. Appl. Polym. Sci. **13**, 1741 (1969).
32) D. H. Kaelble, J. Adhes. **2**, 66 (1970).
33) Y. Kitazaki and T. Hata, Nippon Setchaku Kyoukaishi **8**, 131 (1972).
34) C. J. van Oss, Colloids Surf. A **78**, 1 (1993).

Conclusion

In Chapter 1, the dissolution kinetics of poly(4-hydroxystyrene) (PHS) film in tetramethylammonium hydroxide (TMAH) aqueous solution was investigated using a quartz crystal microbalance (QCM) method. The maximum PHS concentration achievable during development approximately corresponded to the TMAH concentration independently of the film thickness. Dissolution rate decreased due to the decrease in pH during development and the suppression of PHS diffusion caused by the increase in the viscosity of the developing solution. Furthermore, the relationships of surface free energy with swelling and dissolution kinetics were investigated using PHS film with triphenylsulfonium-nonaflate (TPS-nf). Developers were water and 0.26N TMAH aqueous solution. The water intake and dissolution of PHS film with TPS-nf became fast with increasing UV exposure dose. It was found that the increase in the polar components (particularly, the hydrogen bonding component) and the decrease in the dispersion component of surface free energy underlie the fast water intake and dissolution.

In Chapter 2, the dissolution kinetics of PHS films in alkali aqueous solution different from TMAH were investigated using a QCM method. In Section 2-1, the swelling and dissolution kinetics of PHS films in tetrabutylammonium hydroxide (TBAH) aqueous solutions were investigated. The swelling and dissolution kinetics of PHS were observed by changing the protection ratio of the hydroxyl groups of PHS and the alkaline concentration in developers. Not only the dissolution rate but also the dissolution mode changed as the alkyl chains of the tetraalkylammonium cations became longer. For polymer matrices with strong hydrogen bond networks such as PHS, the penetration of tetrabutylammonium cations is considered to be strongly suppressed by their long alkyl chains. In Section 2-2, the dissolution dynamics of PHS in potassium hydroxide (KOH) and sodium hydroxide (NaOH) aqueous solutions were investigated to clarify the effects of small alkaline cations. The temporal changes in the frequency and impedance of QCM substrates during development were measured. The maximum impedance reachable during development significantly exceeded that of the developer saturated with PHS, unlike the case of tetramethylammonium cation. This means that the

PHS matrix near the surface was swollen by decreasing the size of the alkaline cation. By either increasing or decreasing the size of the alkaline cation from tetramethylammonium cation, the transient swelling layer became thick.

In Chapter 3, the author focused on the dissolution dynamics of resists in organic developer. The dissolution dynamics of partially protected PHS in organic developer was investigated using a QCM method to clarify the effects of nonpolar interactions and hydrogen bonding between PHS molecules and solvents. The dissolution dynamics in the solvents, in which the phenolic hydroxyl groups are hardly dissociated, was measured. In a 50 vol% methanol aqueous developer, a large swelling was observed. By decreasing the polarity of the developer, the dissolution dynamics was significantly changed. In the hexyl acetate, the dissolution kinetics of PHS films became similar to that in TMAH aqueous developer although the dissolution mechanism is different.

In Chapter 4, the dissolution dynamics of metal oxide resists (MORs) was investigated using a QCM method. The MORs are promising materials for the high numerical aperture extreme ultraviolet lithography. In this study, zirconia nanocluster resist was used. The ligand was methacrylate. The developers used were ethyl, butyl, amyl, hexyl, 2-methylbutyl, and 3-methylbutyl acetates. The zirconia nanocluster resist showed characteristic dissolution dynamics. After the immersion into developers, the frequency slowly decreased with approximately constant impedance (no viscosity change of the film) for a while and then rapidly dissolved with the softening of resist film. The dependences of dissolution dynamics on the molecular structures of acetates and post exposure baking were clarified. The effect of branched structure at the third position of butyl was, in particular, remarkable.

In summary, this study has deepened our knowledge of the dissolution kinetics of resist materials in various developers by clarifying the meaning of the information contained in the impedance data of the QCM method, which has not been utilized to date. Unlike the solubility, not only electrostatic interaction but also the molecular size, molecular structure, and viscosity of developer and the free

volume of polymer film strongly affect the dissolution dynamics. The dissolution rate, amount of swelling, and mode of dissolution can be controlled by changing the molecular structure, viscosity, and polarity of the developer. In the future, it is expected that material design guidelines will be established based on the findings of this study, and new resist materials and developer solutions will be developed.

List of publications

1. Relationship between poly(4-hydroxystyrene) (PHS) and tetramethylammonium hydroxide (TMAH) concentrations during the development of PHS films in TMAH aqueous solution studied by a quartz crystal microbalance (QCM) method

   Yuko Tsutsui Ito, Kyoko Watanabe, Yuqing Jin, Takahiro Kozawa, Kazuo Sakamoto, and Makoto Muramatsu

   Jpn. J. Appl. Phys. **63**, 018002 (2024)

   DOI: 10.35848/1347-4065/ad17dd

2. Relationship between surface free energy and development process (swelling and dissolution kinetics) of poly(4-hydroxystyrene) film in water and 2.38 wt% tetramethylammonium hydroxide aqueous solution

   Yuko Tsutsui Ito and Takahiro Kozawa

   Jpn. J. Appl. Phys. **61**, 016502 (2022)

   DOI: 10.35848/1347-4065/ac3d42

3. Swelling and dissolution kinetics of poly(4-hydroxystyrene) in tetrabutylammonium hydroxide (TBAH) aqueous solutions studied by quartz crystal microbalance (QCM) method—in comparison with tetramethylammonium hydroxide (TMAH) aqueous solutions

   Yuko Tsutsui Ito, Hitomi Betsumiya, Takahiro Kozawa, Kazuo Sakamoto, and Makoto Muramatsu

   Jpn. J. Appl. Phys. **61**, 066506 (2022)

   DOI: 10.35848/1347-4065/ac6c11

4. Dissolution dynamics of poly(4-hydroxystyrene) in potassium hydroxide (KOH) and sodium hydroxide (NaOH) aqueous solutions investigated by quartz crystal microbalance (QCM) method

   Yuko Tsutsui Ito, Kyoko Watanabe, Takahiro Kozawa, Kazuo Sakamoto, and Makoto Muramatsu

   Jpn. J. Appl. Phys. **63**, 046502 (2024)

   DOI: 10.35848/1347-4065/ad3373

5. Dissolution dynamics of partially protected poly(4-hydroxystyrene) in organic developers investigated by quartz crystal microbalance (QCM) method

   Yuko Tsutsui Ito, Kyoko Watanabe, Takahiro Kozawa, Kazuo Sakamoto, and Makoto Muramatsu

   Jpn. J. Appl. Phys. **63** 076506 (2024)

   DOI: 10.35848/1347-4065/ad5e27

6. Dissolution dynamics of zirconia nanocluster resist

   Yuko Tsutsui Ito, Takahiro Kozawa, Kazuo Sakamoto, and Makoto Muramatsu

   Jpn. J. Appl. Phys. **63**, 046501 (2024)

   DOI: 10.35848/1347-4065/ad313f

Acknowledgements

This study has been carried out under the guidance of Professor Takahiro Kozawa at the Department of Beam Material Science, SANKEN, Osaka University. I would like to express my deepest appreciation to Professor Takahiro Kozawa for his continuous support, constructive suggestions, and warm encouragement throughout this work. Without his guidance and persistent help this dissertation would not have been possible.

I would like to also express my gratitude to Professor Hiroshi Uyama and Professor Akinori Saeki at the Department of Applied Chemistry, Graduate School of Engineering, Osaka University, for reviewing this thesis and giving their valuable comments and suggestions.

I would like to express my gratitude to Mr. Makoto Muramatsu, Mr. Kazuo Sakamoto, and Mr. Takashi Hasebe of Tokyo Electron Kyushu Ltd. for many invaluable discussions.

A special gratitude I give to my former student mentor, Dr. Kazuo Kobayashi, for his enthusiastic guidance. From him I learned how to approach my research. He warmly accepted me when I returned to the Kozawa Lab., and I was able to spend a fulfilling research life.

I would also like to express my appreciation to the staff members of Kozawa Lab., Associate Professor Yusa Muroya, Assistant Professor Kazumasa Okamoto, Mr. Akihiro Konda, Ms. Kyoko Watanabe, Ms. Mikiko Kozawa, Ms. Kinuko Watanabe, Ms. Yuki Ishimaru, Ms. Yukiko Sasaki, Ms. Kyoko Matsuoka, and Ms. Arisa Matsuo for supporting my research. I gained many insights through our daily discussions.

I would like to thank the students of Kozawa Lab; Mr. Azumagawa, Mr. Ikeuchi, Ms. Otsuka, Mr. Tanaka, Ms. Jin, Ms. Takata, Ms. Betsumiya, Mr. Iwashige, Mr. Wang, Ms. Tsuda, Mr. Nishimoto, Mr. Kaneba, Mr. Hashimoto, Mr. Fuku, and Mr. Masuda. Through their humble attitude toward learning, I was reminded of my original intention. I hope that their future is full of success and happiness.

Finally, I express great gratitude to my family, Soichi, Akifumi, Tetsuya, and Chizuru for Understanding, encouragement, and lots of support.

This study was partly supported by Tokyo Electron Kyushu Ltd.